oERDC/CHL Draft Final Report

Coastal and Hydraulics Laboratory

US Army Corps of Engineers®
Engineer Research and Development Center

Long Wave Modeling for South San Francisco Bay Shoreline Study: without Project Conditions

Joseph V. Letter, Jr. and Anne K. Sturm

Draft

5 July 2010

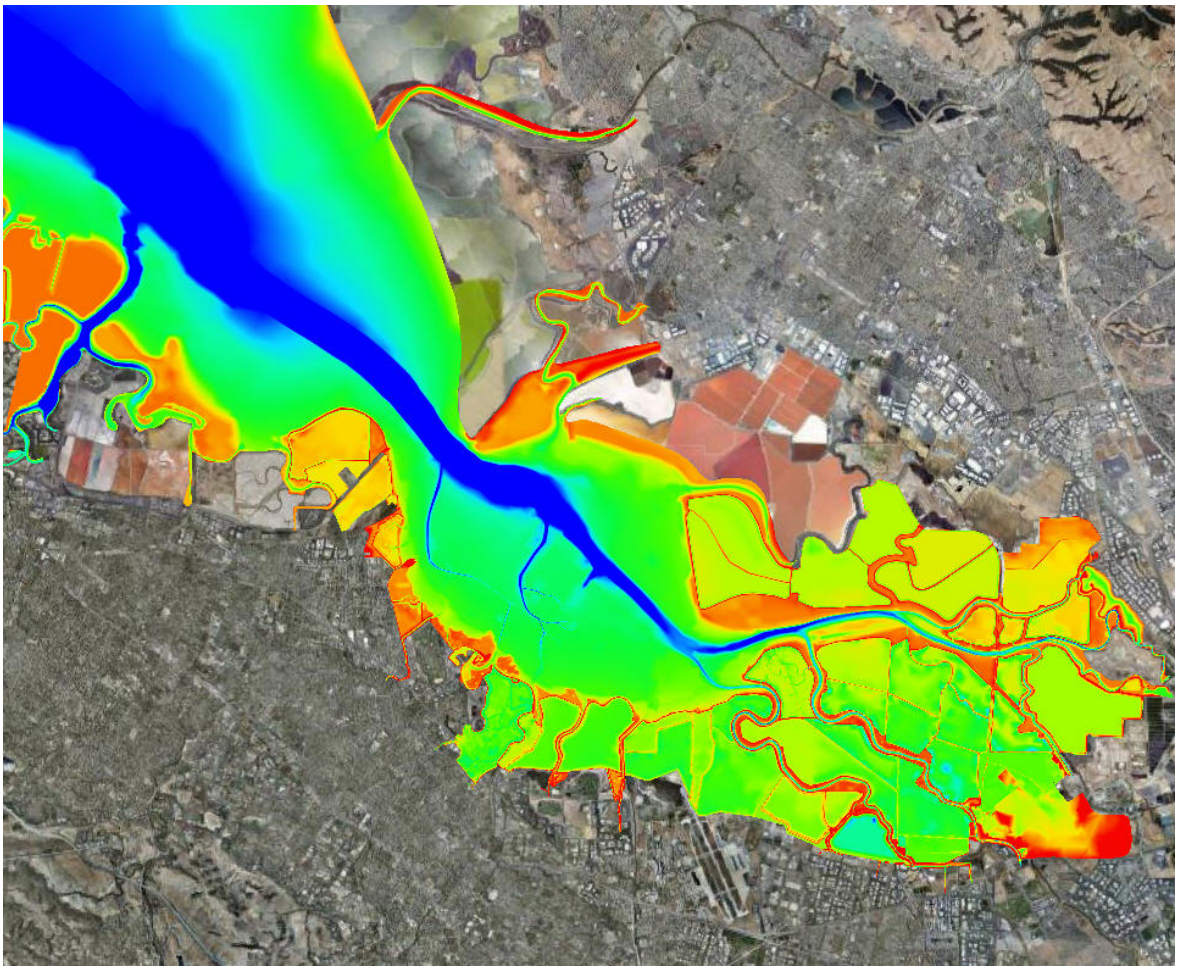

Approved for public release; distribution is unlimited.

ERDC/CHL DRAFT
July 2010

Long Wave Modeling for South San Francisco Bay Shoreline Study: without Project Conditions

Joseph V. Letter, Jr.

U.S. Army Engineer Research and Development Center
Coastal and Hydraulics Laboratory
3909 Halls Ferry Road
Vicksburg, MS 39180-6199, USA

Anne K. Sturm
San Francisco District
U.S. Army Corps of Engineer
1455 Market Street
San Francisco, CA 94103-1398, USA

Draft report

Approved for review

Prepared for U.S. Army Corps of Engineers, San Francisco District
1455 Market Street
San Francisco, CA 94103-1398

Under South San Francisco Bay Shoreline Study

Monitored by Coastal and Hydraulics Laboratory
U.S. Army Engineer Research and Development Center
3909 Halls Ferry Road, Vicksburg, MS 39180-6199

Abstract: This report describes the long-wave modeling for the South San Francisco Bay Shoreline Study to support the development of flooding estimates that incorporate the potential of levee breaching and estimation of uncertainty in the predicted flood levels. The modeling effort used the RMA-2 hydrodynamic model, a component of the TABS-MD numerical modeling system of the Corps. The model was verified to basic tidal propagation and to historical storm events. The model geometry was configured for the cases of with and without levee breaches and a series of simulations conducted that support a database of varying astronomical tide level, storm surge magnitude and wind conditions for use in the statistical treatment of flood levels. The testing program was conducted for the Year 0 geometry and the year 50 geometry, both for without project conditions.

DISCLAIMER: The contents of this report are not to be used for advertising, publication, or promotional purposes. Citation of trade names does not constitute an official endorsement or approval of the use of such commercial products. All product names and trademarks cited are the property of their respective owners. The findings of this report are not to be construed as an official Department of the Army position unless so designated by other authorized documents.

Contents

Preface iv

Unit Conversion Factors v

1 Introduction 1

Background 1
Description of Project Site 2
Salt Ponds 5
Overall Technical Approach 11
Scope 12

2 Model Development 13

Modeling Approach 13
Required Model Features 14
Model Domain 14
Ponds Included in Long Wave Model 14
Coordinate System and Datum 15
Bathymetric and Topographic Data Sources 15
Resolution versus Features 20
Model Mesh 20

3 Boundary Condition Development 35

Astronomical Tides 35
Subtidal Surges 39
Winds 39
Tributary Inflows 40
Tidal Boundary Conditions 40

4 Model Verification 44

Model Coefficient Specification 44
Tidal Propagation 50
Storm Events 50
Sensitivity Simulations 52

5 Design of Model Production Runs 85

Conditional Sampling 85
Selection of Storms 85
Levee Breaching 86

6 Year 0 Results 92

General Circulation 92
Model Response Database for Year 0 92

7 Year 50 Results 109

Model Response Database for NRC Curve I Year 50 109
Sensitivity of Year 50 Long Wave Model to Bathymetric Projection 109

9 Summary 128

References 129

Appendix A; TheTABS-MDS System 132

Report Documentation Page

Preface

The South San Francisco Bay Shoreline Study long-wave modeling was performed in cooperation with and in support of the San Francisco District, U.S. Army Corps of Engineers. The purpose of the effort was to develop and apply a long-wave model to estimate coastal flood levels along the shoreline of extreme South San Francisco Bay. This report summarizes the development and application of that model.

This report was prepared by Joseph V. Letter, Jr., Estuarine Engineering Branch of ERDC-CHL, and Anne K. Sturm, Engineering Division, San Francisco District, U. S. Army Corps of Engineers. Mr. Letter worked under the supervision of Robert McAdory, Chief of Coastal Processes Branch, Bruce Ebersole, Chief of Flood and Storm Protection Division, Rose Kress, Deputy Director of CHL, and William Martin, Director of CHL. COL Gary E. Johnston was Commander and Executive Director of ERDC, and Dr. James R. Houston was ERDC Director. Ms. Sturm worked under the supervision of Janice Lera-Chan, Chief of the Water Resources Section, John H. Jacobson, Chief, Engineering and Technical Services Division, Arijs Rakstins, Deputy for Project Management, Major Adam T. Edwards, Deputy Commander and LTC Laurence M. Ferrell, Commander, San Francisco District, U. S. Army Corps of Engineers.

Unit Conversion Factors, Non-SI to SI Units of Measurement

Multiply	By	To Obtain
cubic feet	0.02831	cubic meters
cubic yards	0.7645549	cubic meters
feet	0.3048	meters
inches	0.0254	meters
miles (nautical)	1,852	meters
miles (U.S. statute)	1,609.347	meters
square miles (U.S. statute)	2.59	square kilometers
mbar	1.00	hPa

1 Introduction

Background

The US Army Engineer Research and Development Center (ERDC) and the U. S. Army Engineer District, San Francisco (CESPN) have collaborated in the development of a technical approach for the hydrology and hydraulics, including coastal engineering (H&H&C, Task 2 of the Project Management Plan) to support the South San Francisco Bay Shoreline Study (SSFBSS) located in the extreme southern end of San Francisco Bay (see Figure 1-1). The project is a complex flood control project to update the level of protection along the shoreline of the extreme southern shoreline of South Bay within San Francisco Bay, including tidal and fluvial damage reduction for the counties of San Mateo, Santa Clara and Alameda, California (see Figure 1-2). The current project will update the previous flood frequency analysis performed by the Corps (USACE, 1984). That earlier analysis was reanalyzed by Knuuti (1995) for the Presidio station. This report addresses the efforts within the first phase of the SSFBSS that evaluates the protection for Santa Clara County and Southern Alameda County.

The flooding analysis developed for the SSFBSS has two components. First, the probability of various flood levels to be exceeded needs to be estimated for each of the food basins located within the study area. These probabilities can then be converted to expected flood levels for specified return periods. Secondly, the uncertainty of those return period flood level estimates needs to be evaluated quantitatively. The uncertainty of the flooding probabilities at a specific location will be a function of the uncertainty in the forcing variables and the uncertainties inherent in the analysis methods themselves.

The development of uncertainties is required for the SSFBSS in order to support the risk analysis for the project. Corps of Engineers policy (USACE, 2006) requires that uncertainties in the level of flood protection be quantitatively evaluated so that the risks associated with the performance of project design features can also be estimated.

Description of the Project Site

The project area is traversed by numerous creeks that drain into tidal sloughs which connect with the bay. The primary tidal sloughs are (see Figure 1-3): Mud Slough in Alameda County; Coyote Slough, Guadalupe Slough, Alviso Slough, Charleston Slough, Mayfield Slough, Mountain View Slough and Whisman Slough (Stevens Creek) in Santa Clara County. Most of the creeks draining to the sloughs are relatively steep and the extent of tidal influence is limited to the lower 5 to 10 miles of the streams (see Figure 1-3).

The tides are amplified in the extreme South Bay relative to tides at San Francisco and exhibit some standing wave characteristics, with amplification of greater than 50 percent for diurnal tides and limited phase difference along the main axis of South Bay. Tides in the bay are mixed with a strong spring-neap variation in the tidal characteristics.

The shoreline of the study area has been buffered from coastal storm damage by the presence of salt ponds (see Figure 1-2). These ponds have been maintained for decades by Cargill, Inc. for salt production. The outboard (bayside) levees have provided partial protection from most storms. Some of these ponds have been turned over to the US Fish and Wildlife Service as a wildlife refuge with some of the ponds being restored to tidal marsh. Historical levels of maintenance of these levees may not be continued over the current project life, potentially increasing the flooding risk.

The project involves a combination of food damage reduction and environmental restoration. The flood control component of the study will involve the alternative alignment of an engineered levee. The zone of potential project protection is also shown in Figure 1-2.

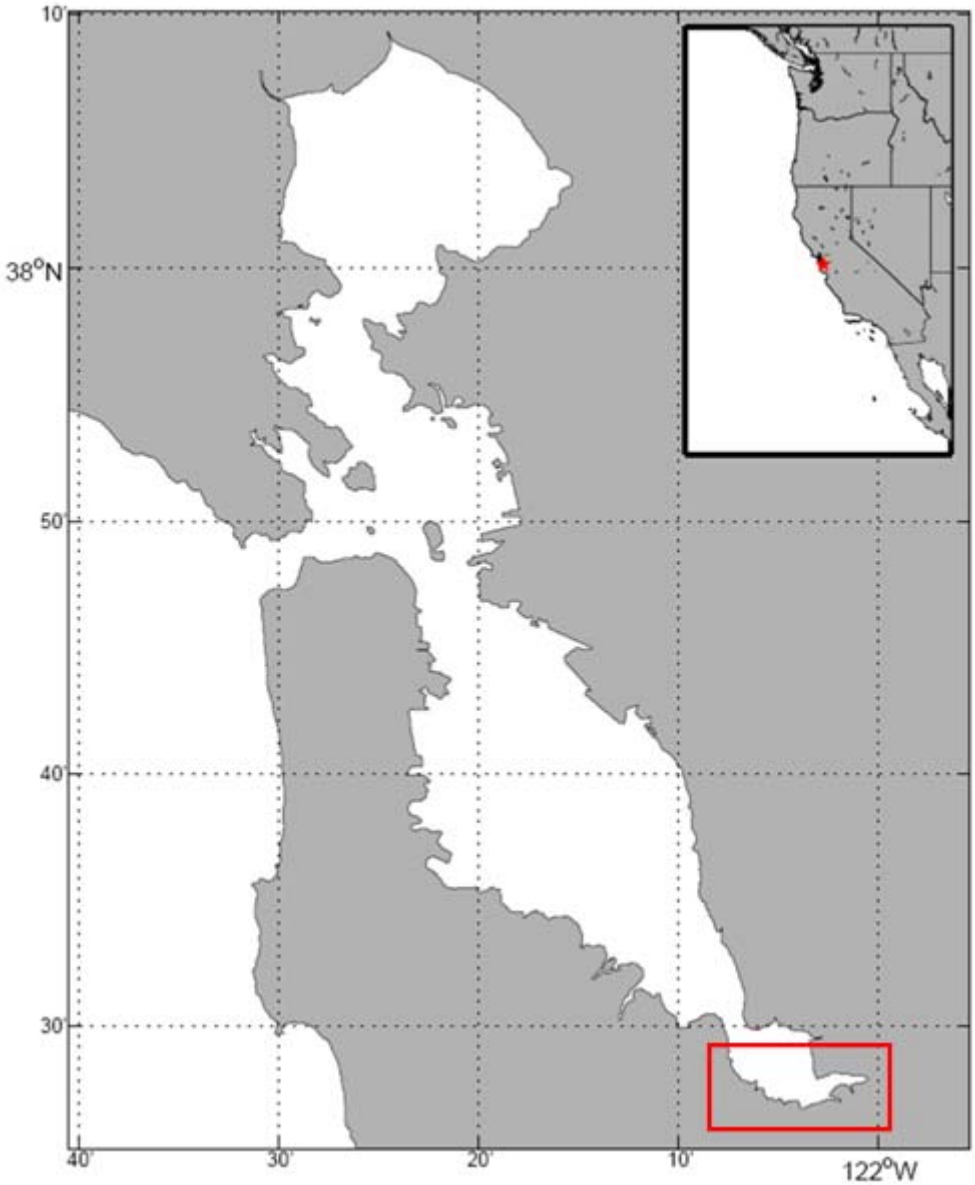

Figure 1-1. Project location.

Figure 1-2. Project area showing salt ponds (shaded green) and limits of the shoreline study (orange polygon)

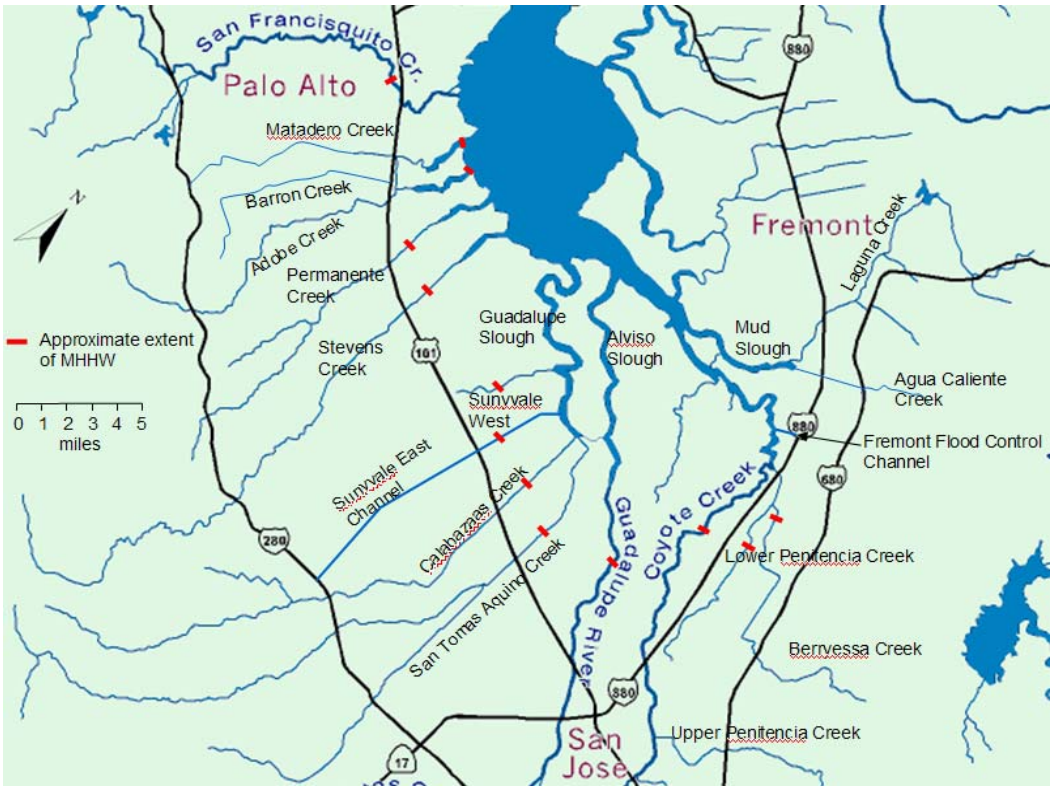

Figure 1-3. Tributaries to extreme South Bay, showing approximate limits of tidal influence

Salt Ponds

The salt ponds were originally constructed for solar evaporation of bay water to produce salt. Water was brought into Pond A1 and then conveyed from pond to pond as it became more saline, eventually reaching ponds used for salt harvesting in Newark, north of the study area. The result was that nearly all of the ponds in the study area were saltier than bay water.

In 2003 the Alviso pond complex in the study area and two other pond complexes in the South Bay were purchased from Cargill Corporation by the Federal and State governments. The Alviso pond complex is now owned and managed by the U.S. Fish and Wildlife Service. Current management of most of the ponds (the "system ponds") is geared towards circulating water through the ponds via short loops that allow relatively short residence times and which minimize the opportunity for large salinity increases which could create problems. Several ponds are managed as seasonal wetlands and are allowed to dry out in summer.

The winter operational plan for the salt ponds developed for Phase 1 of the South Bay Salt Ponds Restoration Project (SBSPRP) Initial Stewardship Plan (ISP) is summarized in Figures 1-4 through 1-6. The winter operational plan was used in the study because the majority of severe coastal storms occur during the winter months.

The primary features of the ISP are the breaching of ponds A6, A19, A20 and A21 and the establishment of weir flow into Pond A8. Flow pathways have generally been altered to be in one primary direction through each pond.

The westernmost Alviso ponds (A1, A2W, AB1, A2E, AB2, A3W, A3E and A4) are operated to create a net flow toward the east, to keep the salinity levels from becoming too high. Pond A3N, however, is planned for operation as a high salinity pond.

Pond A6 is surrounded by external salt pond levees. The external salt pond levee system extends southward from both sides of Pond A6, between Pond A7 and Alviso Slough, and Pond A5 and Guadalupe Slough. No water control structures connect Pond A6 to adjacent sloughs or ponds. However, the ISP calls for four breaches in the external levee on each side of the pond to restore it to a tidal wetland. The plan also calls for numerous internal levee breaches and landscape changes to enhance tidal circulation.

External salt pond levees have been constructed adjacent to Pond A8 along Alviso and Guadalupe sloughs. These levees were originally constructed to protect Pond A8 from fluvial flooding; therefore, crest elevations are on average 12.3 feet (3.75 m) NAVD, which is 4.8 feet (1.5 m) above MHHW and 1.3 foot (0.4 m) above the 1-percent water level, except at the location of the engineered weir. While a levee of this elevation would protect Pond A8 from tidal overtopping, it is likely that the 1-percent water level would cause overtopping because of wave run-up and wind set-up. Internal salt pond levees separate Pond A8 from Ponds A5 and A7. The levee between Pond A8 and Ponds A7 and A5 is on average 4.3 feet (1.3 m) NAVD. The internal levee dividing Pond A8 is on average 3.4 feet (1.0 m) NAVD.

Ponds A5 and A7 are presently managed to maintain tidal circulation via two sets of 48-inch gates located at the northwest and northeast corners of Ponds A5 and A7, respectively. Because of a broken structure at Pond A7, pond operations have been recently modified to intake and discharge through both structures. A 24-inch control gate through the levee between Ponds A7 and A8 remains closed under normal operating conditions. The USFWS occasionally operates a 4,000 gallon-per-minute (gpm) pump to convey water from Pond A7 to Pond A8 when flow through the 24-inch control gate is insufficient. Additionally, the SCVWD operates a pump that conveys water from Pond A4 to Pond A5 via a siphon under Guadalupe Slough.

As part of the Lower Guadalupe River Project, the SCVWD installed a weir between Alviso Slough and Pond A8 to allow overflow from Alviso Slough during 10-percent storm events or greater (>8,600 cfs) to enter Pond A8. During significant flood overflows, water levels in Pond A8 may overtop the levees between Pond A8 and Ponds A5 and A7, and between Ponds A5 and A7 and Pond A6. Flood water retained in the ponds is pumped out via the 4,000 gpm pump connecting Pond A8 to Ponds A7 and A11. The entire Alviso System A7 has a flood control capacity of 13,200 acre-feet (Schaaf and Wheeler, 2004).

Pond A16 is surrounded by external and internal salt pond levees. The external salt pond levee extends along the eastern side of Pond A16 adjacent to Artesian Slough and then along the western perimeter of the pond adjacent to the New Chicago Marsh drainage ditch. The average elevation of the external salt pond levee is 10.7 feet (3.25 m) NAVD (3.2 feet or 1.0 m above MHHW and 0.3 foot or 0.1 m below the 1-percent water level). The internal salt pond levee along the southern perimeter of

Pond A16 separates Pond A16 from New Chicago Marsh. The average elevation of this levee is 9.8 feet (3.0 m) NAVD (2.3 feet or 0.7 m above MHHW).

Pond A17 is hydraulically connected to Coyote Creek via a 48-inch culvert with an adjustable tidal gate, located in the northeast corner of the pond. Pond A16 is connected to Artesian Slough through a 48-inch culvert with an adjustable tidal gate located in the southeastern corner of the pond, just upstream from the Pond A18 south intake/outlet structure (USFWS, 2006). Water within Alviso System A16 flows between the two ponds through an existing gap in both the Pond A16 and Pond A17 levees. A siphon exists between Ponds A17 and A18 that is planned to be plugged and closed (Morris pers. comm., 2006; USFWS, 2006).

During summer operations in 2006, the gates on both the Pond A16 and Pond A17 water control structures were opened to allow muted tidal exchange between Pond A16 and Artesian Slough, and between Pond A17 and Coyote Creek, to manage dissolved oxygen (DO) levels (Mruz pers. comm., 2006). During winter operations, Pond System A16 is operated to take in water from Artesian Slough and discharge to Coyote Creek through Pond A17 to avoid the entrainment of fish in Coyote Creek.

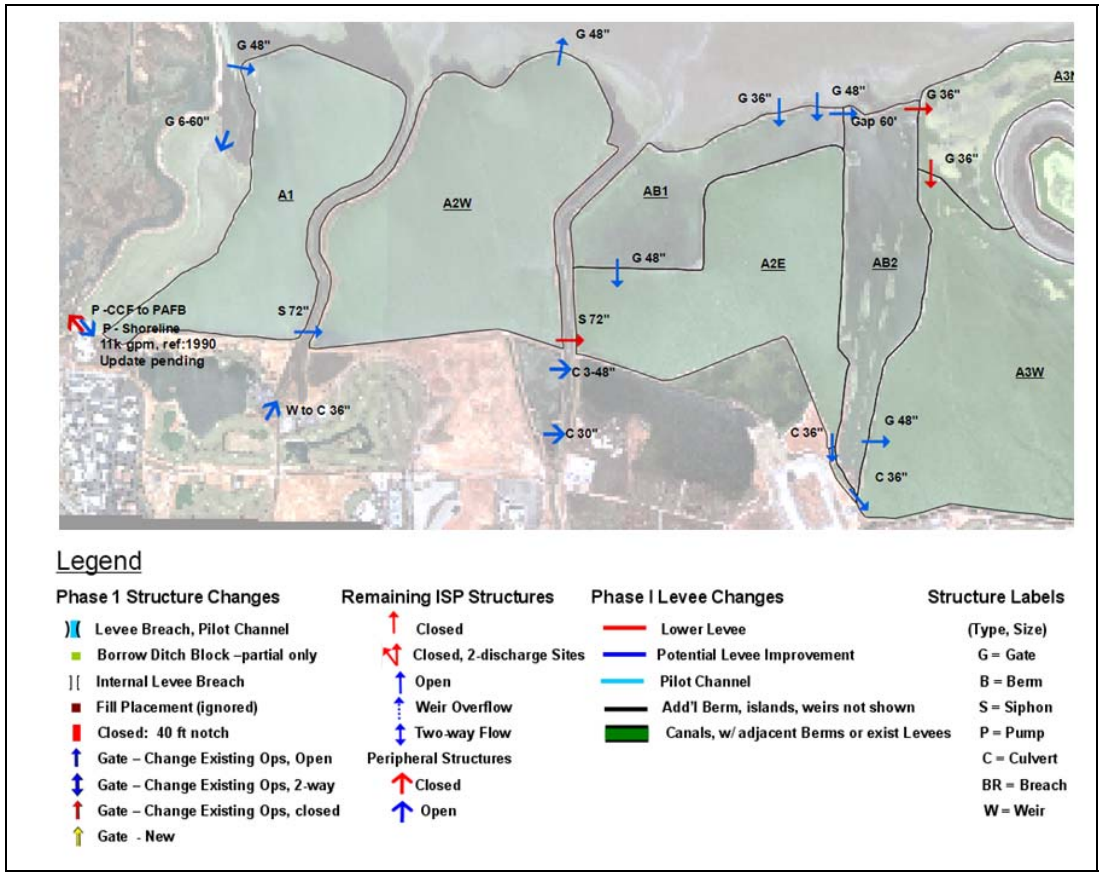

Figure 1-4. Operational changes for Phase 1 of South Bay Salt Ponds Restoration Project for winter conditions; westernmost Alviso ponds

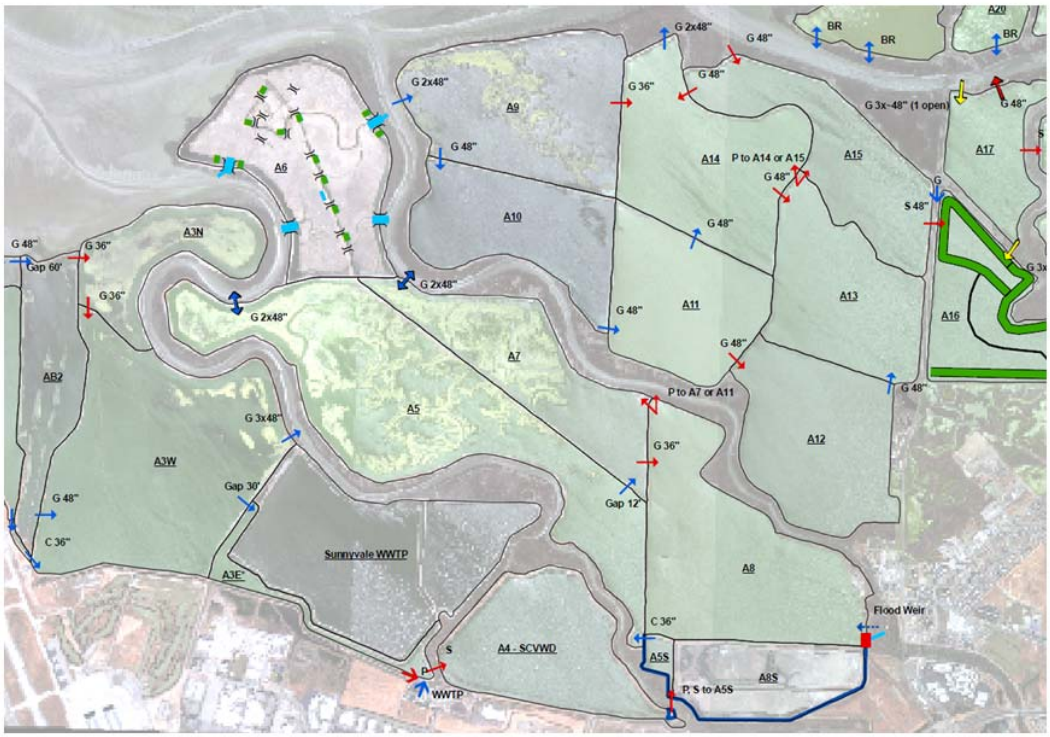

Figure 1-5. Operational changes for Phase 1 of South Bay Salt Ponds Restoration Project for winter conditions; central Alviso ponds. Refer to Figure 1-4 for the legend.

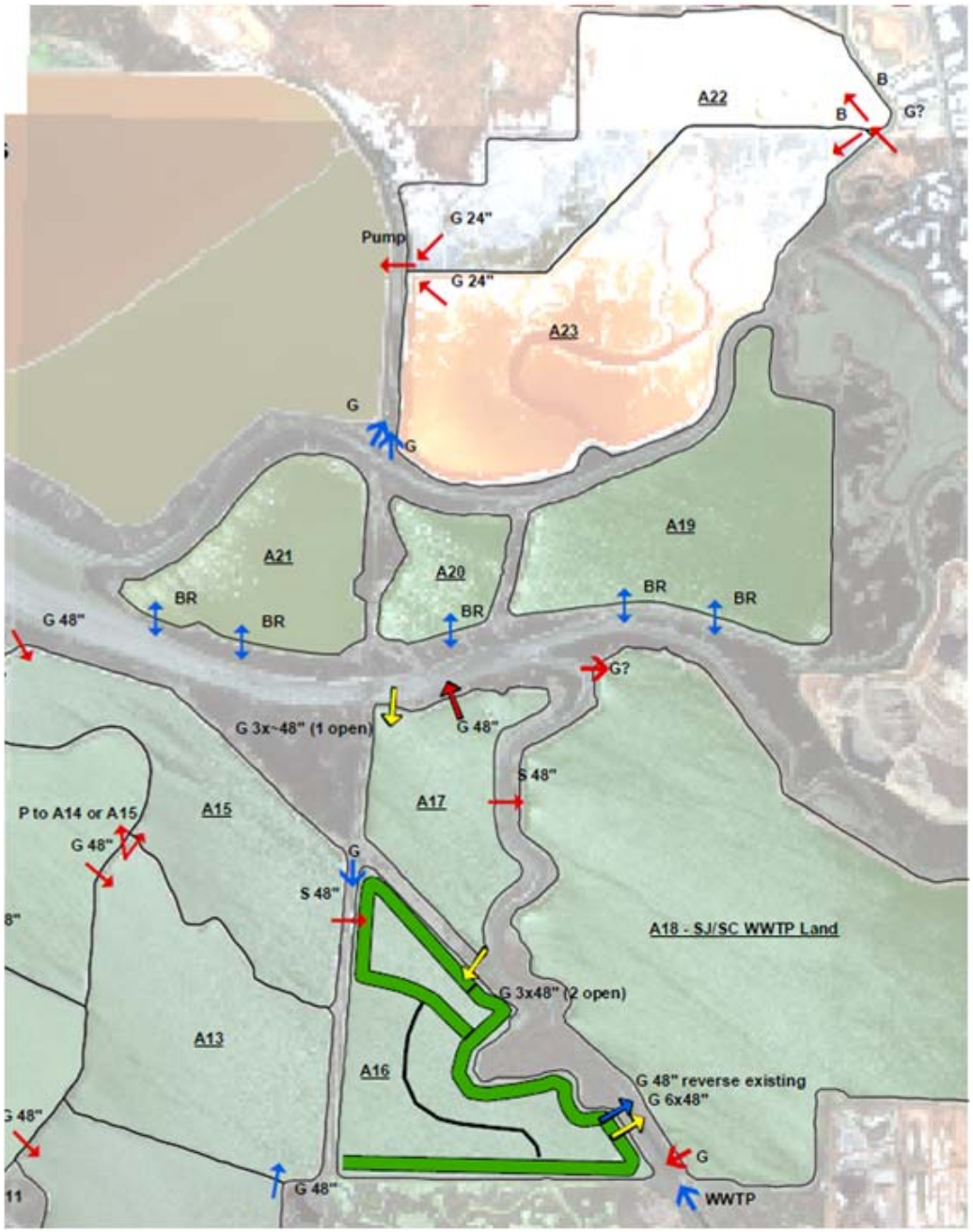

Figure 1-6. Operational changes for Phase 1 of South Bay Salt Ponds Restoration Project for winter conditions; eastern ponds. Refer to Figure 1-4 for the legend.

Overall Technical Approach

The technical challenge of this study has been to apply appropriate technical tools to the processes that affect the flooding in the project area and integrate the effects into an analysis that permits the evaluation of uncertainty without requiring a large degree of iteration among the tools.

The overall approach for the analysis was separated into two major phases. The first was a deterministic processes phase, where specific events were simulated to define the hydrodynamic response and consequences of defined geometric conditions. The second phase was the statistical treatment of the uncertainty of all of the processes and their influence on the uncertainty of flood levels within the project area.

Numerical models developed and the processes they address were:

1. A long wave model (RMA2) to propagate tide levels, including astronomical and residual storm surge from open water in the Pacific Ocean into San Francisco Bay and southward into the study area influenced by local winds. The model predicts peak surge levels at each of the analysis locations. This component of the study is the subject of this report.

2. A short-period wave model (ST-WAVE) to estimate the generation and propagation of locally generated wind waves. The model predicts the wave attack at specific locations along the levees, providing a peak spectral wave period, a significant wave height and direction.

3. A wave runup and levee overtopping model (BOUSS1D) to estimate the volume of water that overtops a series of levee cross sections for specific water level and wave conditions. This model provides the discharges over the levee, the mean and extreme shear stresses on the outer slope of the levee and wave transmission coefficients.

4. Riverine models (HEC-RAS) for defining overtopping of lateral riverine levees within the coastal zone. Each of the riverine models provides the volumes of water for combinations of river discharge and downstream tide level.

5. A levee erosion analysis (Lee, in preparation) that develops a sequencing capability for levee erosion as a function of wave loading (shear stresses and overtopping) and storm duration. The analysis provides probabilities of failure for outer slope erosion and for inner toe erosion failure.

6. Ponding analysis of the resulting flooding extent within the interior flood basin resulting from the volumes of water that pass the inboard levees.

These models provide the capability to estimate the progression of effects of a specific storm event through the project area, predicting flood levels.

The second phase of the study was the application of the modeling and process tools developed in phase 1 in a manner that allows the development of statistical measures of flood levels: expected flood levels for certain return periods and the uncertainties associated with those flood levels. Documentation of other phase 1 modeling tools and the phase 2 uncertainty analysis are documented in separate reports.

Scope

The purpose of this report is to document the development of long wave model that supports the overall project study plan. The model application to the without project conditions is also documented.

2 Model Development

Modeling Approach

The simulation of an area as complex as the extreme South Bay area could be accomplished in a variety of ways. The choice of approach is, in part, a preference of the modeling team. The basic choice is between using a single comprehensive model mesh all the way from the open ocean, through the central bay area and down into the study area and the use of inset model domains. The choice is also a function of the formulation of the model itself. For a structured finite difference model such as DELFT-3D or CH3D the benefits of using inset grids comes from the avoidance of transitioning the detailed resolution in the study area into the rest of the system. Ultimately, the choice relates to the required CPU resources. For unstructured models such as RMA2 or ADH, the meshes are flexible enough to transition the level of resolution coarser as you move away from the study area, while still maintaining sufficient resolution in high energy areas (e.g. Golden Gate).

Another issue with using inset models is the care that must be taken in the location of the interface boundary of the inset mesh. For a system like South Bay, where there is a standing wave phenomenon at play, the correct boundary condition specification can be nontrivial. In addition, if the location of the inset boundaries is such that the alternatives being considered have any impact then the complexity increases.

The choice for the SSFBSS was to use a single comprehensive mesh of the entire system. Another factor in the preference for a global mesh was the level of human intervention required to accomplish an accurate and efficient handoff of information from a global coarse mesh to an inset mesh. The additional computational time required for the global model approach is not significant for an unstructured mesh.

The model chosen for the SSFBSS was RMA2, an unstructured finite element model. It is a component of the Corps TABS-MD modeling system and is capable of including internal control structures (culverts and tide gates). It is a depth-integrated two-dimensional model, which is deemed appropriate for a flooding analysis in the study area, which is not impacted dramatically by vertical density currents.

Required Model Features

The features required for reasonable simulation of the project include:

1. Areas of normal tidal inundation throughout the model domain. These areas are important to getting the overall tidal prism correctly developed for the given tidal forcing.

2. The salt ponds within the extreme South Bay that will either be overtopped or breached, whether deliberately or accidentally, during the project life.

3. Major land features that have a steering effect on the tidal currents, such as islands and bridge constrictions and general shoreline changes.

4. Significant tidal channels that provide influences on the conveyance pathways of tidal currents

Model Domain

The model domain for the comprehensive model mesh includes a portion of the Pacific Ocean, all of Central Bay, San Pablo Bay, Carquinez Strait, Suisun Bay, the Sacramento-San Joaquin Delta, and South Bay all the way into the primary tributaries beyond the head of tide (see Figure 2-1). In addition, the salt ponds around the extreme South Bay which are of significance to the study, were included in the computational domain.

The starting point for the study RMA2 mesh was the previously developed model for the John F. Baldwin channel deepening study. That mesh had 4,748 elements and 13,150 nodes. That model was originally developed for a navigation study in a MLLW vertical reference, which was converted to NAVD88 based on the San Francisco tidal datum.

Ponds included in the long-wave model

The long-wave model did not include all of the ponds in lower South Bay. The focus of this modeling effort will be on the ponds on the southern (western) shore. These are the ponds that are exposed to wave attack and potential breaching. Some of the ponds on the northern (eastern) shore that are not a part of this phase of the flood protection study and are less likely to become breached are not included in the model domain. Figure 2-2 presents the ponds and tidally connected areas that are included. The assumption is implicitly made that those

ponds not included in the model domain are not likely to be breached or if they are breached will have no measurable impact on those ponds that are included in the model domain. Equally important, those ponds are assumed to perform (or not perform) the same for with and without project conditions.

The decision of whether riverine reaches are to be represented as one-dimensional (1D) elements and when to transition to 1D from 2D was based on when the channel, creek or river essentially becomes confined laterally and should be dominated by riverine flows during riverine storms. The 1D formulation was extended upstream to beyond the expected head of tide, allowing for specification of just the river flows as the upstream boundary conditions.

The Sacramento-San Joaquin delta was also schematized as a 1D network of channels to provide the effects of the tidal prism and its overall influence on tidal propagation in the system.

Coordinate System and Datum

The RMA2 model mesh was developed in the California State Plane NAD 83, Zone 3 (0403), in US Survey Feet, as the horizontal coordinate system. The upper portions of the Sacramento-San Joaquin Delta may experience some distortion, but that is acceptable provided the proper general tidal propagation is confirmed. The vertical datum for the mesh development is feet above the NAVD 88. All model boundary conditions and output will be referenced to this datum.

Bathymetric and Topographic Data Sources

The data sources used in the development of the computational mesh for this project were:

1. Navigation charts. - Much of the original mesh (John F. Baldwin Deep Water Ship Channel study) was developed from NOAA navigation charts. The charts used in that development are delineated in Table 2-1.

Table 2-1. NOAA Navigation Charts Used in Global Mesh Development		
Chart Number	Chart Region	Scale
18645	Gulf of Farallones	100,000
18649	Entrance to San Francisco Bay	40,000
18651	San Francisco Bay, Southern part	40,000
18653	San Francisco Bay, Angel Island to Point San Pedro	20,000
18654	San Pablo Bay	40,000
18655	Mare Island Strait	10,000
18656	Suisun Bay	40,000
18657	Carquinez Strait	10,000
18661	Sacramento and San Joaquin Rivers	40,000
18662	Sacramento River, Andrus Island to Sacramento	40,000
18663	San Joaquin River	20,000

2. 2005 USGS South Bay bathymetric survey. These data cover most of the deep water areas south of Coyote Point. Data was collected in a joint effort with NOAA-COOPS, Sea Surveyor, Inc. and Tucker & Associates. The data set used for the modeling was converted from meters above MLLW to feet above NAVD88.

3. Cross sections collected by Moffat and Nichol Engineers (Feb 2005). A set of cross section locations for the lower reaches of Guadalupe Slough, Alviso Slough, Coyote Creek, Coyote Hills Slough, Stevens Creek, Permanente Creek and Redwood Creek were used from a survey conducted by Environmental Data Solutions (Kulpa, 2006) using survey control set by Tucker & Associates (Tucker 3, August 2006).

4. Levee crest elevation survey provided by Moffat and Nichol (July 2005). The crest elevation survey was performed by Tucker & Associates (2004).

5. 2004 LIDAR data from USGS (Foxgrover and Jaffe, 2005). The data set obtained from USGS consisted of high density data, which required extensive

analysis, filtering and quality control in order to make it useable for the modeling effort. While gridded data was available, the need to represent elevation gradients as accurately as possible led to the use of the Bare Earth dataset. Given the high density of the data and the identification of irregular and inaccurate artifacts from the data collection process, significant reprocessing was required. The large data files required special computer power for processing since the tiles could only be loaded one tile at a time on a standard engineering work station. Processing the LIDAR data was performed by Jennifer Wozencraft of the Mobile District (CESAM) under the supervision of Jeff Lillycrop. The processing included thinning of the data sets by defining acceptance criteria based on bathymetric gradients and some filtering to remove oscillations from apparent instrument instability. For the modeling effort, LIDAR data was only used south of the San Mateo Bridge and in locations where alternate elevation data was not available at the time of the LIDAR data reprocessing.

6. Channel cross-sections in the vicinity of Bair Island. A series of 18 channel cross sections in the tidal creeks around Bair Island were used to define the bathymetry of those creeks. Survey was conducted by Philip Williams and Associates (PWA) in 2000 (PWA, 2000, Appendix A).

7. USGS in-pond bathymetric surveys (Takekawa et al. 2005). The bathymetry of a number of the ponds was surveyed by the USGS. Survey was conducted by USGS in 2003 and 2004 with additional survey support from SCVWD in 2005 (Siegel & Leventhal, 2006).

8. ERDC levee transects. In the areas where the ERDC wave runup and overtopping modeling is to be performed, surveys were collected that define the cross-sections of the critical levees.

9. 1998 SCVWD Permanente Creek cross section survey (Choy, 2007). Dataset is the same as that in the SCVWD HEC-RAS model. However, model was not georeferenced and original survey dataset covered a slightly larger area, especially in the vicinity of the Mountain View Tidal Marsh. Cross-sections do not include bathymetry in the tidal portion of the channel.

10. SCVWD Matadero Creek as-built CAD files (Mark Thomas & Company, 2005). Extensive set of AutoCAD files containing 11 April 2003 design plans with as-built edits dated through 16 September 2005. As-builts differed substantially from the original design plans. Located downstream from highway 101, the bypass redirects high flows to a discharge point just north of the municipal work yard.

11. 1999 Towill topographic survey of Palo Alto Flood Basin (Towill, 1999). Photogrammetric survey conducted in 1999 for MacKay and Somps. Work done in conjunction with Schaaf & Wheeler study for SCVWD (Schaaf & Wheeler, 2002). Ground control was provided by MacKay and Somps.

12. 1999 SCVWD Palo Alto Baylands survey (SCVWD, 1999). Topographic survey using aerial mapping with photography flown by Aero-Geodetic. The survey area acquired extends from San Francisquito Creek to the Palo Alto Flood Basin and just west of highway 101.

13. HEC-2 and HEC-RAS model elevation data. The most current HEC-2 or HEC-RAS model for each of the streams in Santa Clara County was acquired from the SCVWD. All models were geo-referenced, as needed, using HEC-RAS. To supplement areas where additional elevation data was not available, the elevation data from each of the models was extracted in ASCII format. Information on each model is provided in Table 2-2. Not all of the data in all the models was used, nor where they used in their original form. Corrections were made based on site visits, new surveys, as-builts, aerial photographs and other resources.

14. 2004 SCVWD topography survey of Alviso Slough (Chung, 2006). Cross-sections surveyed by aerial mapping methods, every 60 meters along length of Alviso Slough.

15. 2005 SCVWD contour map of the Lower Guadalupe River. A contour map and profile of the Lower Guadalupe River Flood Control Project downstream of highway 237 (Dyer, 2006).

16. SCVWD cross-sections of Lower Guadalupe River project. Post construction cross-section drawings dated late 2004 and early 2005 (SCVWD, 2004, 2005). Survey conducted by SCVWD survey section. All drawings are hard copy and were used as reference for flood wall crest elevations.

17. 2007 Bestor / Sea Surveyor riverine survey (Hink, 2007). A new bathymetric and topographic survey was conducted of Stevens Creek, San Tomas Aquino Creek and the east-west portion of Guadalupe Slough. Work was conducted for the USACE, San Francisco District.

Table 2-2 –HEC-2 and HEC-RAS models				
Creek	**Model**	**Model Date**	**Model Author**	**Survey Source Date**
Adobe	HEC-2	July 1977, updated 29 July 1992	GS Nolte & Assoc.	1977
Barron	HEC-2	March 1978, updated 2001?	SCVWD	1989 as-builts
Calabazas	HEC-2	1998	GS Nolte & Assoc.	1998
Coyote	HEC-2	1995, updated March 2003	SCVWD / USACE	As-builts dated 1989, 1994; Surveys dated 1989-1993.
Guadalupe River/ Alviso Slough	HEC-2	2003	Northwest Hydraulics	1996
Guadalupe Slough	HEC-RAS	unknown	SCVWD	Bathymetry: 2002 CH2M Hill; Topography: unknown
Matadero	HEC-2	2002	SCVWD	unknown
Sunnyvale East	HEC-RAS	2007	SCVWD	Aug 2006 SCVWD Survey
Sunnyvale West / Moffatt Channel	HEC-RAS	2007	SCVWD	Aug 2006 SCVWD Survey
Lower Penitencia	HEC-2	Nov 1990	SCVWD	1984 & 1989 as-builts
Permanente	HEC-RAS	unknown	SCVWD	1998 topography only; missing bathymetry in tidal areas

18. City of Mountain View Charleston Slough 2007 Survey. Environmental Data Solutions surveyed a series of cross-section in Inner and Outer Charleston Slough.

19. Multiple site visits in 2007 by CESPN personnel to select locations throughout the ponds and riverine areas were conducted to field check and supplement available elevation data as well as information about planimetric features and hydraulic structures.

Resolution versus Features

An underlying model schematization philosophy was used in development of the model resolution that bears specific mention. The project area and the estuary that it is a component of, is one of the most complex systems in the world. There are innumerable geometric and bathymetric features that influence the system's hydrodynamic behavior. It is beyond the capability of any numerical model to include all of the detailed features. Therefore, some compromise was needed in the overall computational mesh resolution that was utilized in this study. Once that resolution has been approximated the bathymetry can be "loaded" to the mesh. However, if there are real world features that have spatial undulations at essentially a sub-grid scale then those features should be averaged out in the mesh and not incorporated in the mesh. This is analogous to the temporal discretization of a harmonic signal, which in driving a numerical model it is common convention to have on the order of at least 25 time steps to reasonably resolve the tidal signal. Modeling a temporal feature's period at a 2 ΔT will not give accurate results, and modeling a spatial feature's undulation at a $2\Delta X$ scale will also not give reasonable results. Poor resolution for such features generally results in model instability for the nonlinear terms in the equations. So the philosophy used is that if the resolution necessary to resolve those features adequately is not used, then the features have been smoothed out in the model.

Model Mesh

The overall model mesh domain and resolution are presented in Figure 2-3. The bathymetry is shown in Figure 2-4, with a contour range of -300 ft to 0 ft NAVD88. The offshore boundary is approximately 32 miles from the Golden Gate Bridge. The mesh contains approximately 180,000 nodes and 67,000 elements. Details of the mesh resolution and bathymetry are shown in Figures 2-5 through 2-14, with varying color contour ranges to illustrate bathymetric details.

Figure 2-1. Overall comprehensive model domain.

Figure 2-2. Ponds included in the long wave model shaded in yellow. Note the ponds on the north (east) shore that are not included.

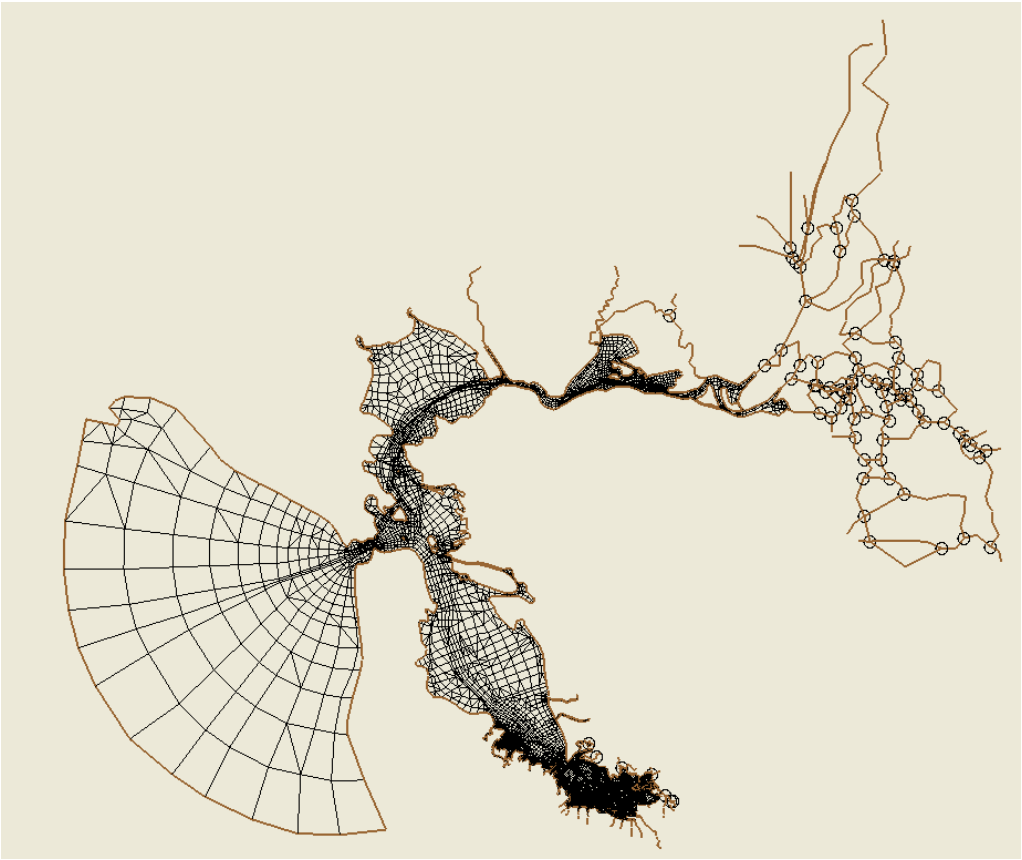

Figure 2-3. The RMA2 model overall mesh domain and resolution

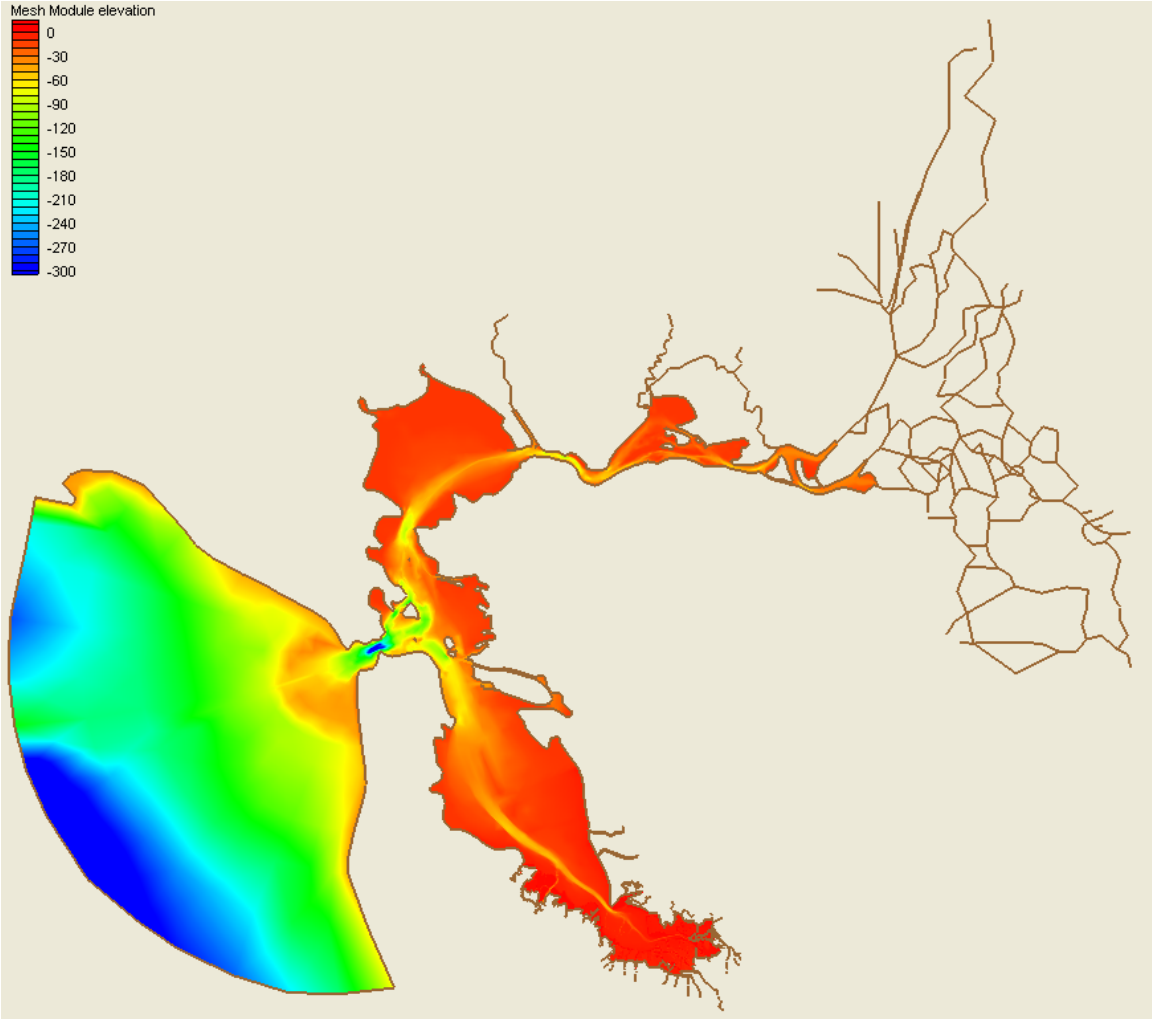

Figure 2-4. SSFBSS RMA2 Mesh bathymetry (elevation contour scale from -300 to 0 ft NAVD)

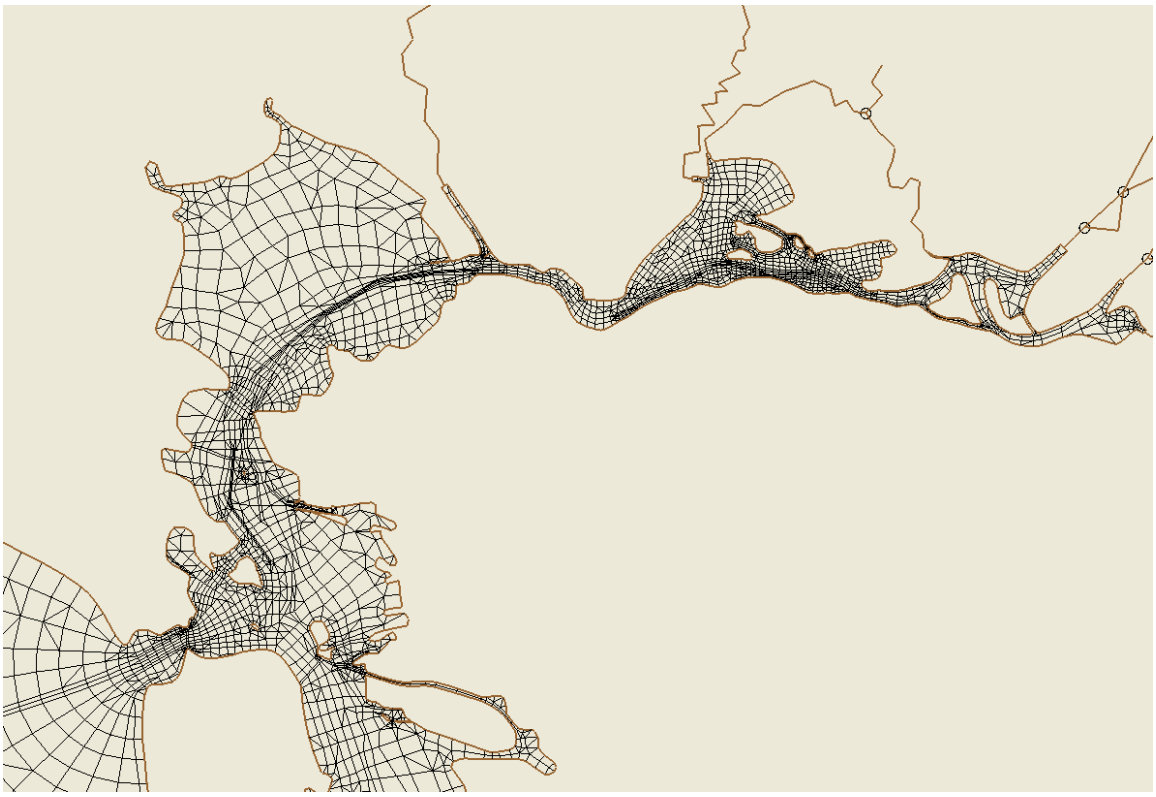

Figure 2-5. Details of model mesh resolution in central and northern bays

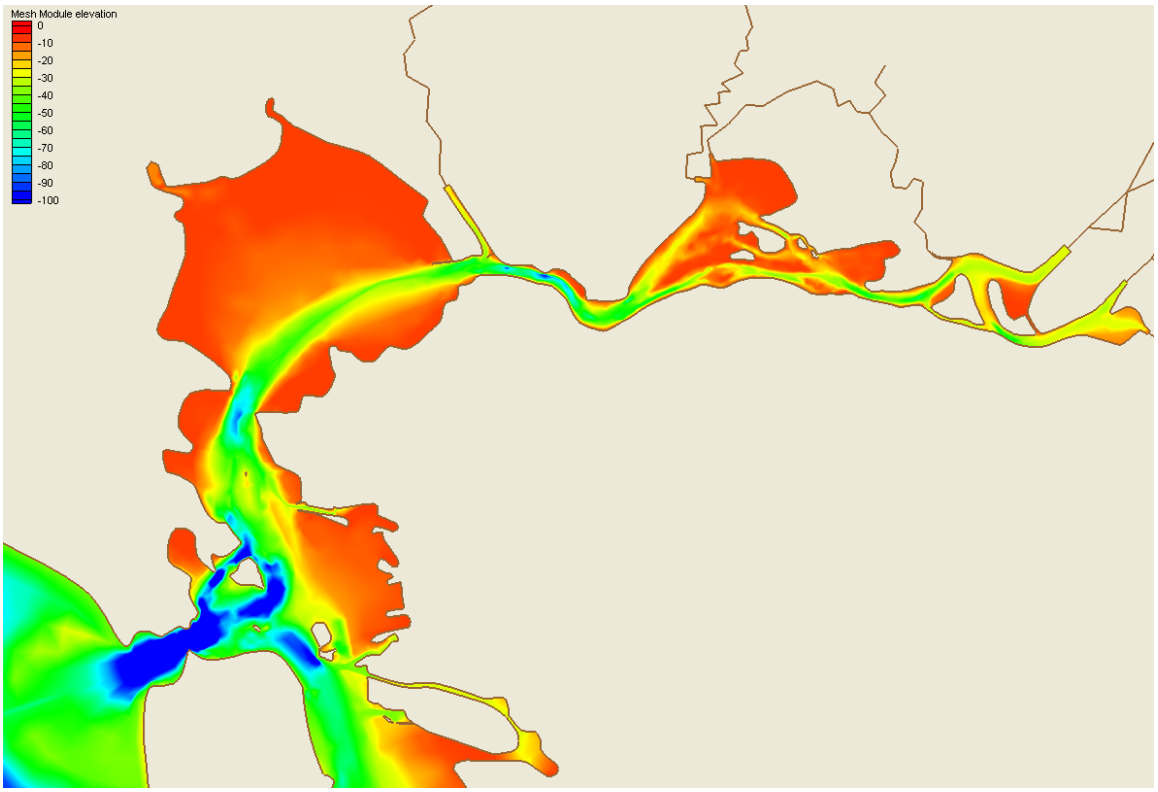

Figure 2-6. Mesh elevations in the central and northern portions of the numerical model (elevation contours from -100 ft to 0 ft NAVD)

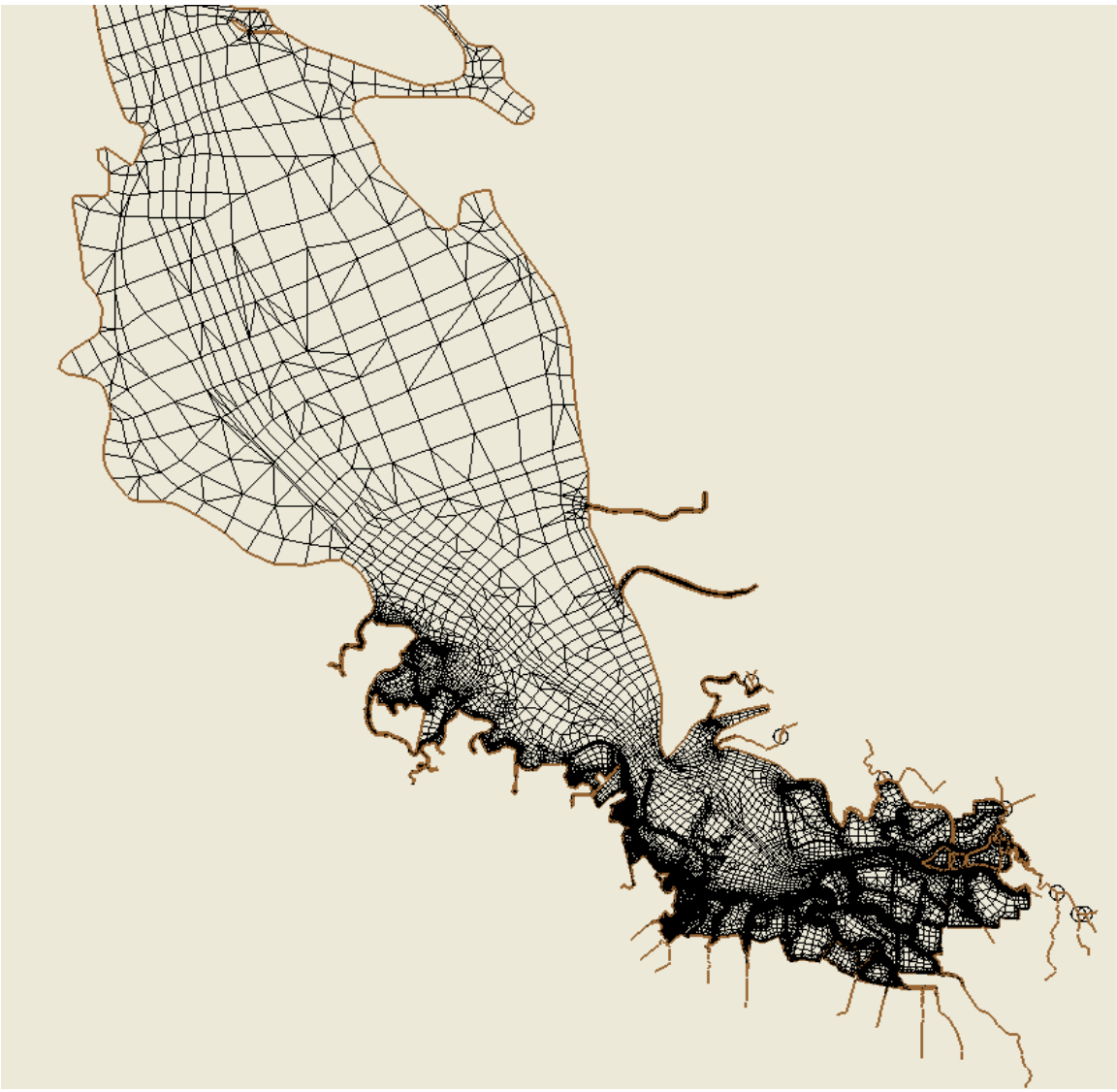

Figure 2-7. Detail of mesh resolution in South Bay

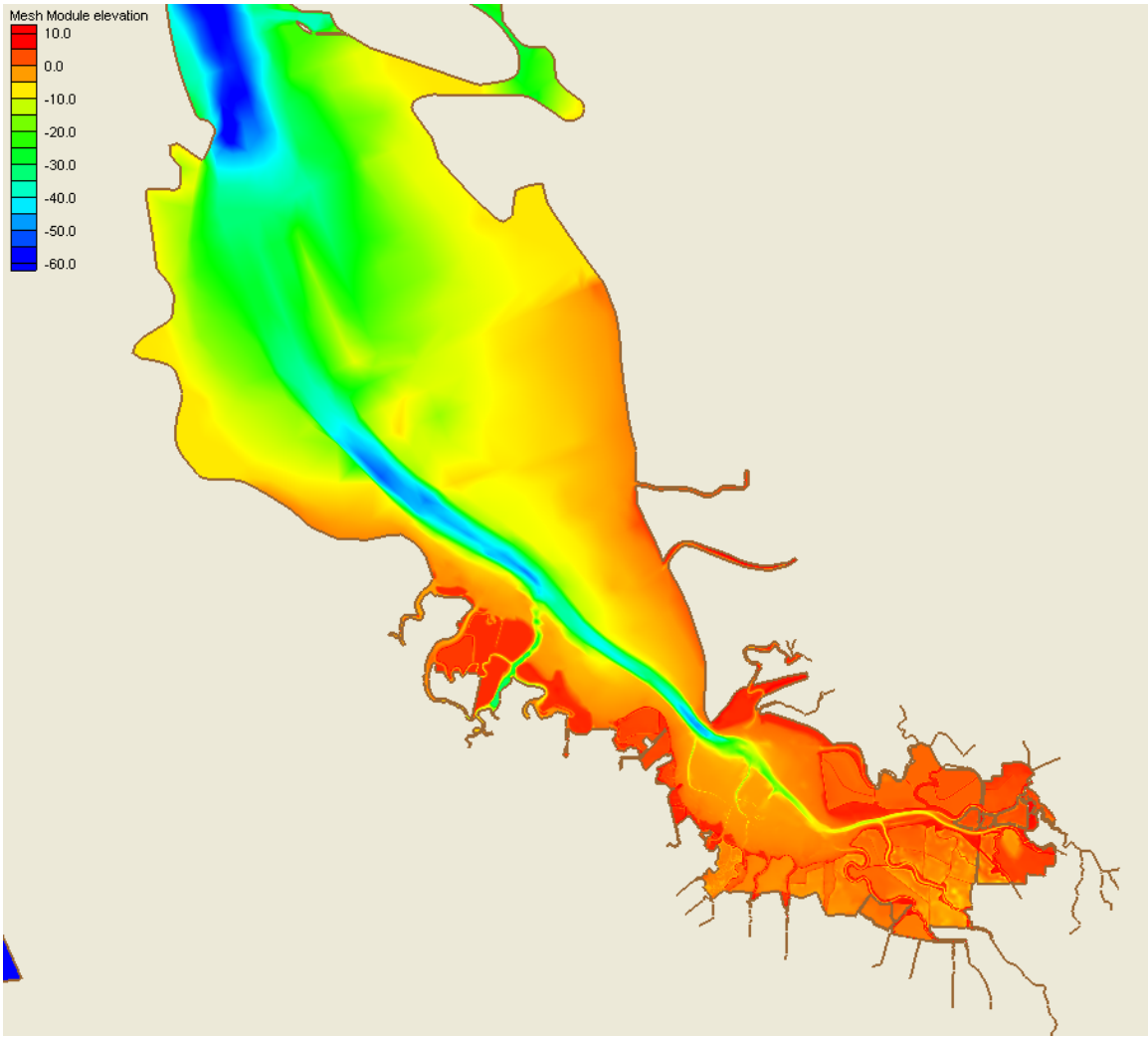

Figure 2-8. Bathymetry of numerical model in South Bay (elevation contours from -60ft to +10 ft NAVD)

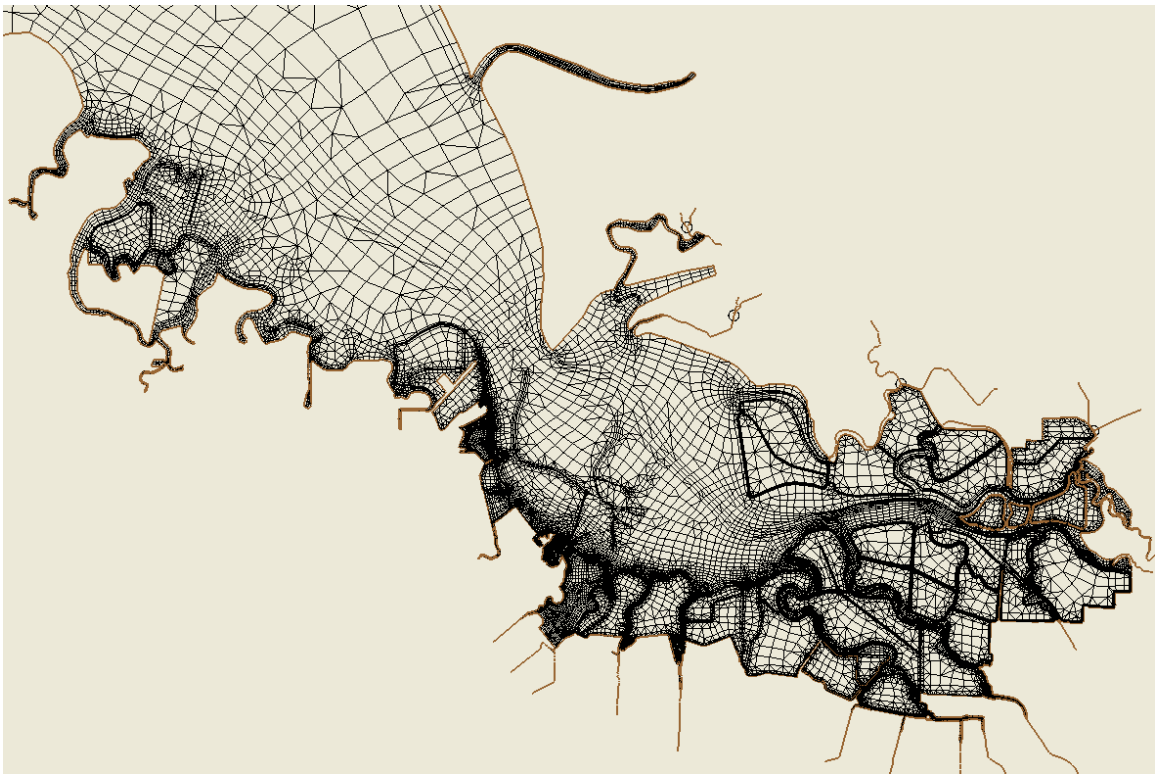

Figure 2-9. Mesh resolution in far South Bay

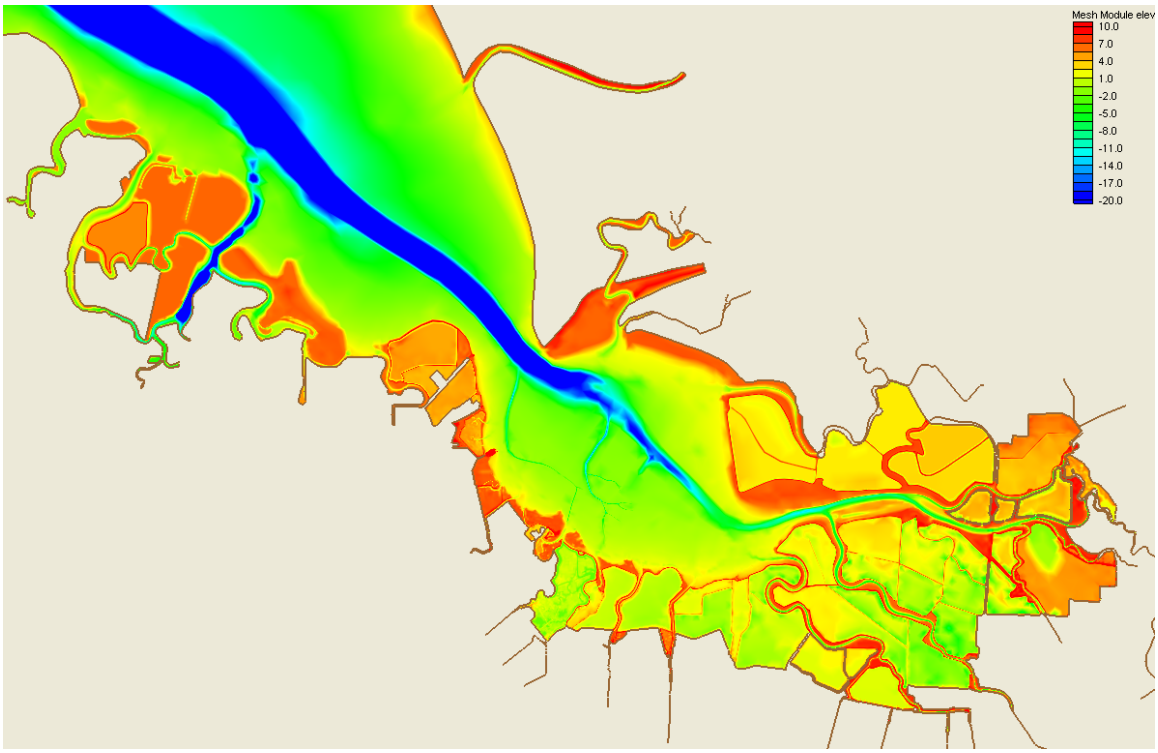

Figure 2-10. Mesh elevations in far South Bay (elevation contours from -60ft to +10 ft NAVD)

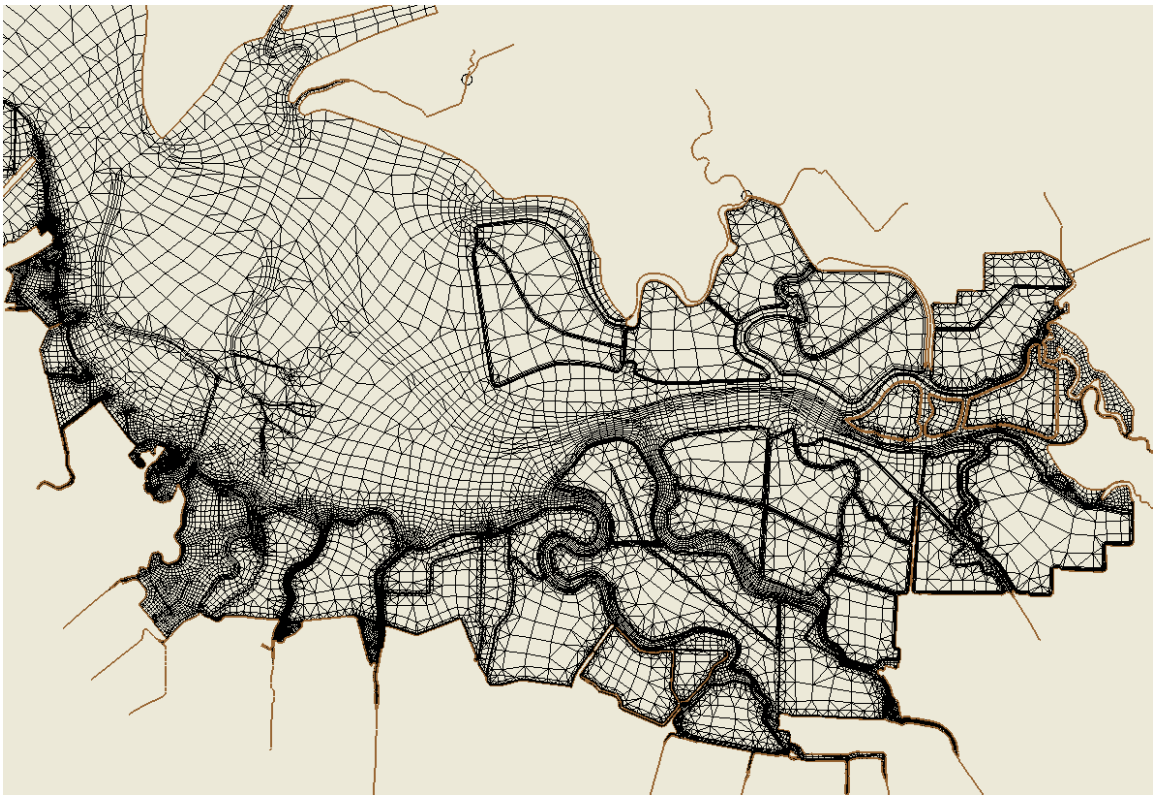

Figure 2-11. Mesh resolution below Dumbarton Bridge

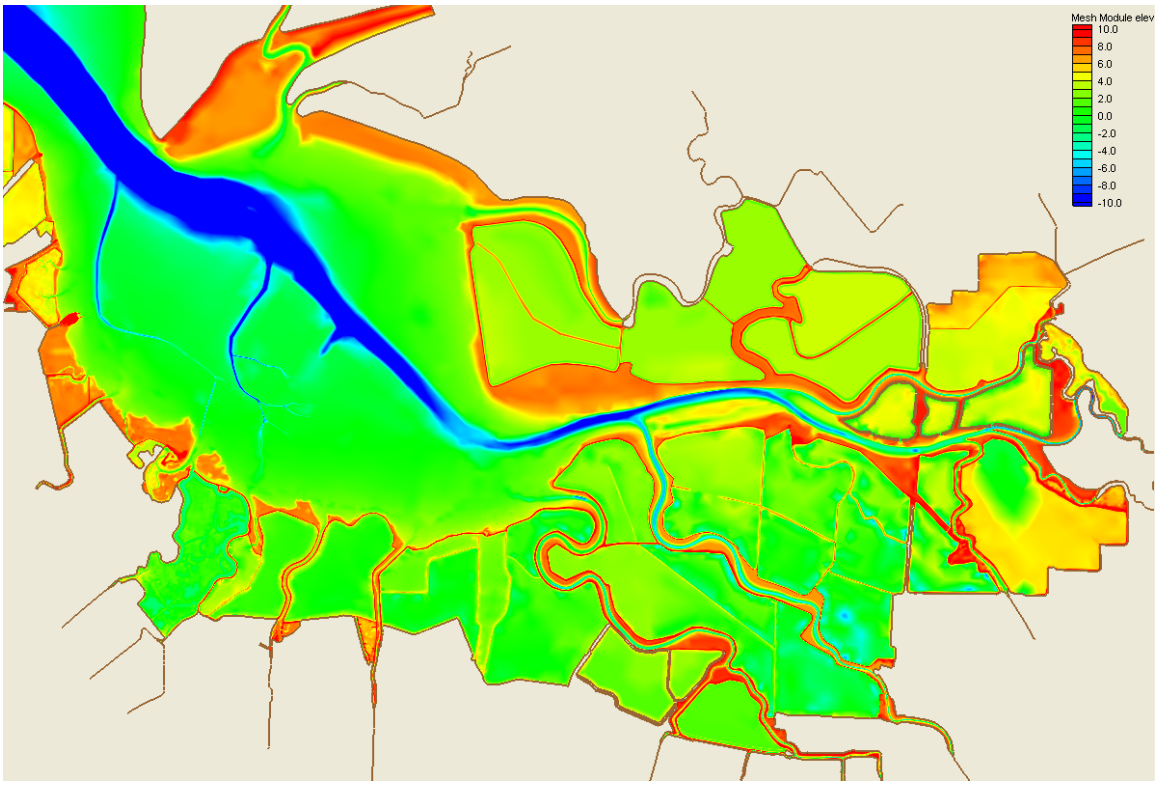

Figure 2-12. Mesh elevations in far South Bay below Dumbarton Bridge (elevation contours from -10ft to +10 ft NAVD)

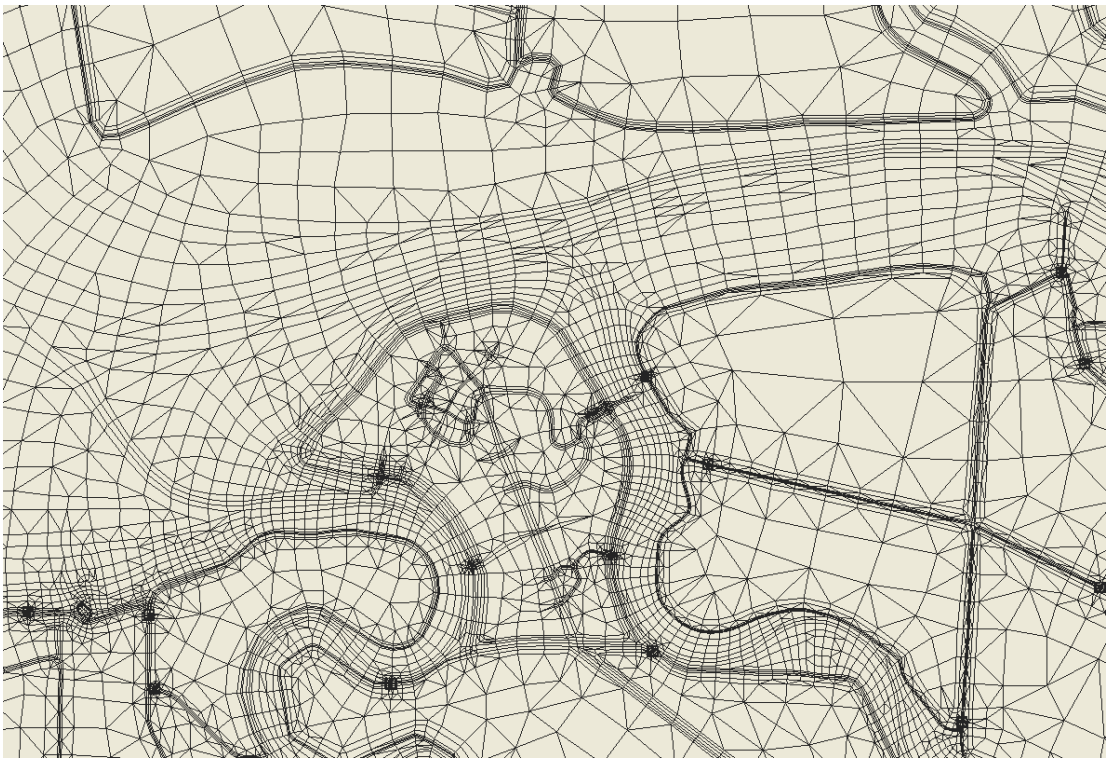

Figure 2-13. Mesh resolution around Pond A6, with breaches in place

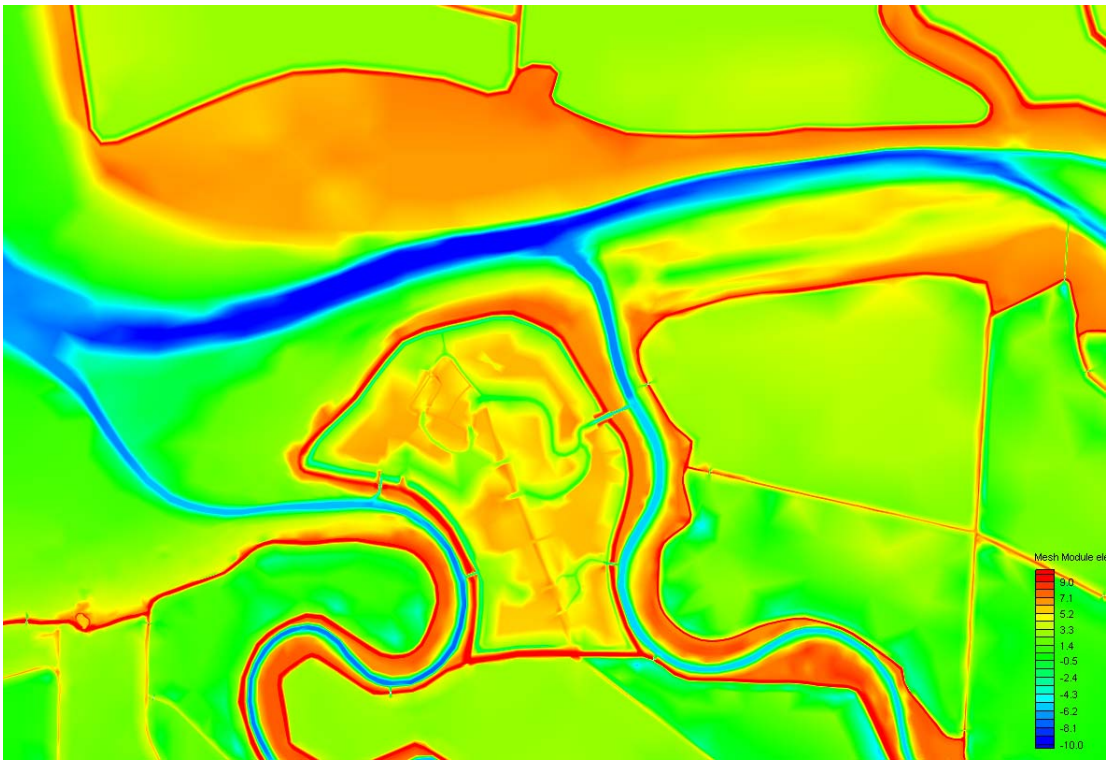

Figure 2-14. Mesh elevations around Pond A6 (elevation contours from -10ft to +10 ft NAVD)

3 Boundary Condition Development

This section describes the procedures used in developing the time-series boundary conditions required to drive the long wave model for a specific storm event.

Astronomical Tides

The tidal harmonics for the primary boundary stations in the vicinity of San Francisco are presented in Table 3-1. With these tidal components the predicted tides can be reconstituted for any period with the appropriate epoch information. Because the station at Monterey is approximately twice the distance from the mouth of the bay and Point Reyes as the southeastern corner of the model mesh at the shoreline, the harmonic data applied there was taken as the average of the harmonics of Point Reyes and Monterey. These averaged constituent amplitudes and phases were then used to interpolate the harmonic coefficients for each harmonic along the arch of the outer mesh boundary using linear interpolation based on the partial arc lengths.

The development of the astronomical tidal signal along the ocean boundary of the mesh was computed as a function of time, t, as follows:

$$\eta_i(t) = \sum_{n=1}^{37} f_n a_{ni} \cos(\sigma_n t - \theta_{ni} - \phi_n) \tag{3-1}$$

where η_i = the water surface boundary value at boundary node i

a_{ni} = the amplitude of the n-th harmonic at node i

f_n = the mid-year nodal factor for harmonic n

σ_n = angular frequency of the n-th harmonic

θ_{ni} = the local phase for the n-th harmonic at node i

ϕ_n = the equilibrium arguments for the n-th harmonic

The node factors and the equilibrium arguments are different for each year, and were obtained from NOAA. The node factors correct for the variation in harmonic amplitudes over the 19-year epoch, and the equilibrium arguments are phase corrections for each harmonic for the year within the epoch.

The numerical model was simulated with the boundary conditions developed by Equation 1, using appropriate friction coefficients for the offshore ocean area. After iteration with friction the harmonic amplitudes throughout the boundary were further adjusted by a universal correction factor of 0.9095. With that adjustment the tidal signal was reasonably replicated at The Presidio. It was considered that the harmonics from near shore stations may have some slight amplification over what is in deep water along the model boundary. The final harmonic coefficients used in the model are presented in Table 3-2.

Table 3-1 Tidal harmonics at key boundary stations

			San Francisco		Point Reyes		Monterey	
Constituent Number	Name	Speed (degrees/hr)	Amplitude (ft)	Phase (degrees)	Amplitude (ft)	Phase (degrees)	Amplitude (ft)	Phase (degrees)
1	M2	28.9841	1.903	338.7	1.818	319.4	1.616	309.2
2	S2	30	0.449	338.4	0.449	316.8	0.428	300.2
3	N2	28.43973	0.404	317.3	0.407	297	0.368	287
4	K1	15.04107	1.207	106.1	1.26	99.9	1.199	99.4
5	M4	57.96821	0.075	38.2	0	0	0	0
6	O1	13.94304	0.755	98.5	0.774	92.9	0.753	91.8
7	M6	86.95231	0	0	0	0	0	0
8	MK3	44.02517	0.062	136.7	0	0	0	0
9	S4	60	0	0	0	0	0	0
10	MN4	57.42383	0.03	19.9	0	0	0	0
11	NU2	28.51258	0.085	320.1	0.079	303.3	0.072	292.9
12	S6	90	0	0	0	0	0	0
13	MU2	27.96821	0.023	237.1	0.046	261.5	0.041	250.8
14	2N2	27.89535	0.046	295.2	0.046	273	0.044	260.7
15	OO1	16.1391	0.036	131.9	0.043	123	0.036	121
16	LAM2	29.45563	0.02	341.8	0.013	353.8	0.011	305
17	S1	15	0.023	164.8	0.039	214.5	0.033	199.1
18	M1	14.49669	0.036	128.5	0.043	116	0.038	109.9
19	J1	15.58544	0.062	119.1	0.075	109	0.071	108.7
20	MM	0.544375	0	0	0	0	0	0
21	SSA	0.082137	0.128	286.2	0.102	284.6	0.09	283.2
22	SA	0.041069	0.125	221	0.2	217.3	0.157	205.6
23	MSF	1.015896	0	0	0	0	0	0
24	MF	1.098033	0	0	0	0	0	0
25	RHO	13.47151	0.03	94.5	0.026	86.4	0.026	88.8
26	Q1	13.39866	0.131	96	0.141	89.7	0.134	87.9
27	T2	29.95893	0.03	316.9	0.023	309.7	0.022	288.1
28	R2	30.04107	0.003	338.3	0.003	316.5	0.003	299.8
29	2Q1	12.85429	0.013	105.1	0.016	99.3	0.016	96.5
30	P1	14.95893	0.381	103.6	0.394	97.5	0.374	95.9
31	2SM2	31.0159	0	0	0	0	0	0
32	M3	43.47616	0.016	38.9	0	0	0	0
33	L2	29.52848	0.052	349.5	0.033	338.1	0.023	343.9
34	2MK3	42.92714	0.046	113.2	0	0	0	0
35	K2	30.08214	0.131	329.2	0.128	306.6	0.121	291.3
36	M8	115.9364	0	0	0	0	0	0
37	MS4	58.9841	0.033	42.4	0	0	0	0

Table 3-2 Tidal harmonics used for model boundary condition interpolation

			Point Reyes		Southeast corner of mesh	
Constituent Number	Name	Speed (degrees/hr)	Amplitude (ft)	Phase (degrees)	Amplitude (ft)	Phase (degrees)
1	M2	28.9841	1.653	319.4	1.562	314.3
2	S2	30	0.408	316.8	0.399	308.5
3	N2	28.43973	0.37	297	0.352	292
4	K1	15.04107	1.146	99.9	1.118	99.7
5	M4	57.96821	0	0	0	0
6	O1	13.94304	0.704	92.9	0.694	92.4
7	M6	86.95231	0	0	0	0
8	MK3	44.02517	0	0	0	0
9	S4	60	0	0	0	0
10	MN4	57.42383	0	0	0	0
11	NU2	28.51258	0.072	303.3	0.069	298.1
12	S6	90	0	0	0	0
13	MU2	27.96821	0.042	261.5	0.04	256.2
14	2N2	27.89535	0.042	273	0.041	266.9
15	OO1	16.1391	0.039	123	0.036	122
16	LAM2	29.45563	0.012	353.8	0.011	329.4
17	S1	15	0.035	214.5	0.033	206.8
18	M1	14.49669	0.039	116	0.037	113
19	J1	15.58544	0.068	109	0.066	108.9
20	MM	0.544375	0	0	0	0
21	SSA	0.082137	0.093	284.6	0.087	283.9
22	SA	0.041069	0.182	217.3	0.162	211.5
23	MSF	1.015896	0	0	0	0
24	MF	1.098033	0	0	0	0
25	RHO	13.47151	0.024	86.4	0.024	87.6
26	Q1	13.39866	0.128	89.7	0.125	88.8
27	T2	29.95893	0.021	309.7	0.02	298.9
28	R2	30.04107	0.003	316.5	0.003	308.2
29	2Q1	12.85429	0.015	99.3	0.015	97.9
30	P1	14.95893	0.358	97.5	0.349	96.7
31	2SM2	31.0159	0	0	0	0
32	M3	43.47616	0	0	0	0
33	L2	29.52848	0.03	338.1	0.025	341
34	2MK3	42.92714	0	0	0	0
35	K2	30.08214	0.116	306.6	0.113	299
36	M8	115.9364	0	0	0	0
37	MS4	58.9841	0	0	0	0

Subtidal Surges

Subtidal surge time series were developed by subtracting the predicted tides from the verified observed tides at each available tidal signal from the three primary ocean boundary tides. When the data were available for the two offshore stations the same approach of averaging the Point Reyes and Monterey signals to estimate the residual signal at the southern edge of the model boundary was used. The residual tidal signal for the February 1998 storm is presented in Figure 3-1. These residual signals were filtered with a band-pass filter using cut-off frequencies of 9 hours and 1600 hours. This filter primarily removed the high-frequency noise while retaining most of the residual energy at the primary tidal frequencies which may be the result of resonance with the tidal harmonics.

If offshore tidal records were not available for extraction of residual tides then the residual signal at San Francisco was used at the ocean boundary. The approach is based on the observation that the low-frequency component of the residual tidal signal is a regional water level response and the San Francisco residual surge is not significantly different from those observed at Point Reyes and Monterey for the same storm. Figure 3-2 presents the residual tidal signals for Monterey, Point Reyes and San Francisco. The San Francisco residual is in closer agreement with Point Reyes than Monterey, which should be expected.

Winds

Winds were analyzed for a number of meteorological stations around the bay. However, because of the effects of the mountains around the bay and limited data over the open water portions of the bay it was very difficult to develop a reasonable spatially distributed wind field for driving the numerical models. The analysis has been documented by Conner (2006, under review) and the final recommendation as been to use the winds from the San Francisco Airport uniformly over the model domain. The rationale for this approach is that SFO is in South Bay and it is located very near the shoreline and will be more appropriate for over the open waters of the bay. The wind time series were decomposed into the north-south and east-west components prior to also being low-pass filtered at a cut-off period of 6 hours prior to use in the model for each event.

Tributary Inflows

Tributary inflows are not significant into extreme South Bay. The coincident peak 100-year flood levels for all tributaries would be 68,000 cfs. Sensitivity testing on the long wave model with a constant 30,000 cfs combined inflows had only a 0.2 ft impact on flood levels in South Bay in the vicinity of the project. The long wave model was subsequently simulated using the mean discharges on each tributary. This is further justified by the ephemeral nature of the flood flows on the tributaries and the low probability of coincident occurrence. The tributary inflows used in the long wave model are summarized in Table 3-3.

Tidal Boundary Condition

The tidal boundary conditions along the offshore model boundary were generated from the locally interpolated tidal harmonic constants using Equation 1 and added to the locally interpolated tidal residual signal to define a unique time series boundary condition at each computational node along the boundary.

For the specification of specific storm events for Year 50 the net sea level rise is then also added to raise the boundary conditions the appropriate amount.

Table 3-3. Tributary Inflows for tidal propagation verification for RMA2		
Tributary	Inflow, cfs	
Sacramento River	20000	
San Joaquin River	1000	
Redwood Slough	2	
San Francisquito Creek	17	
Permanente Creek	3	
Stevens Creek	13	
Sunnyvale West channel	3	
Sunnyvale East channel	3	
Calabazas Creek	15	
San Tomas Aquino Creek	3	
Guadalupe River	87	
Mallard Slough	3	
Coyote Creek	48	
Penitencia Creek	3	
Berryessa Creek	3	
Calera Creek	3	
Agua Caliente Creek	3	
Laguna Creek	3	
Mowry Slough	6	
Plummer Slough	2	
Newark Slough	3	
Alameda Creek	20	
Old Alameda Creek	13	
Total South Bay	278	

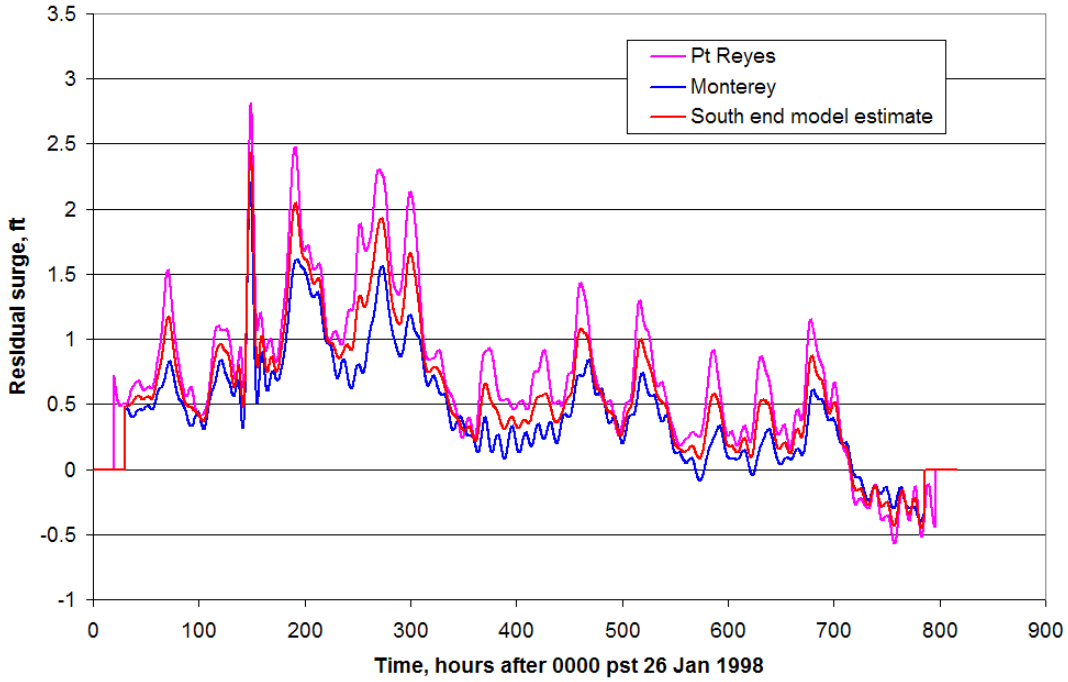

Figure 3-1. Example of the development of the residual tidal signal at the corners of the ocean in the model mesh, for use in interpolation along the mesh boundary.

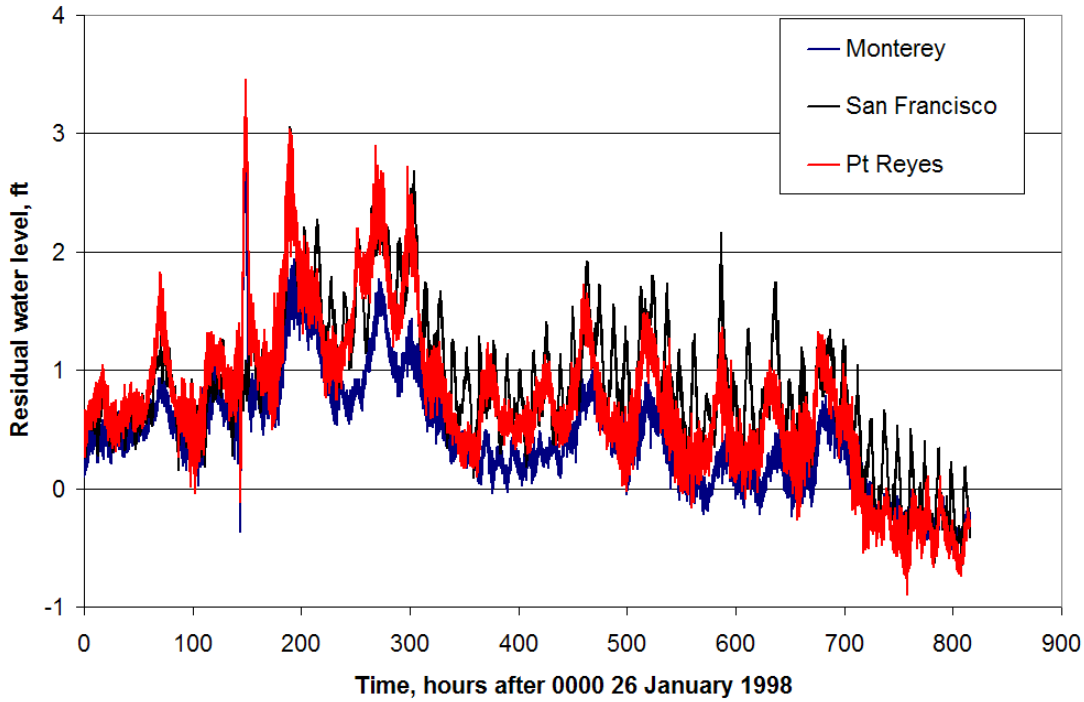

Figure 3-2. Comparison of raw residual water levels at Monterey, Pt. Reyes and San Francisco for February 1998

4 Model Verification

The goal of the long-wave numerical model verification is to provide confidence in its ability to predict tidal storm surge levels in the study area. That confidence is associated with how well the model propagates the time variation in the shape of the flood profile as well as the ability to accurately predict the peak of the surge. The model verification procedures involve the adjustment of the bottom friction, eddy viscosities and marsh porosity parameters until specific events are reasonably replicated in the areas of interest.

Model coefficient specification

The specification of the model RMA2coefficients was made by the use of multiple elemental property layers (a feature in RMA2 version 5.00). This was accomplished by the merging of essentially four GIS layers for coefficient specification: friction, eddy viscosity, marsh porosity and Coriolis.

Friction

The frictional specification for the model was developed in two levels of depth dependence. The friction has been represented successfully in previous modeling within San Francisco Bay as inversely proportional to depth. This application of the model utilized a bottom roughness as a function of water depth (Christensen, 1970 and USA ERDC, 2003) with the functional coefficient varying generally by surface characteristics. The mathematical form of the dependence of the Manning's friction coefficient with depth is

$$n = \frac{n_0}{d^{\alpha}} + n_m e^{-d/d_0} \tag{2}$$

where: n = Mannings n used in model

n_o= reference Mannings n for a depth of 1 ft

d = local water depth, ft

α = depth dependence exponent

n_m = vegetative roughness contribution

d_o = reference depth controlling exponential decay of vegetative friction effect

The model controls for the roughness are through the specification of n_o, n_m, α, and d_o. These coefficients varied throughout the model as illustrated in Figures 4-1 and 4-2 for the material specification layer for friction. The material layers for specification of friction were generally defined based on water depth, due to the natural tendency for vegetation and water conveyance capacity to evolve based on bottom elevation. The coefficients for each material type are shown in Table 4-1. The selection of the coefficients was based on previous modeling experience within San Francisco Bay, which led to the development of the functional development of Equation 2 (Donnell, et al, 2006). The functional effects of water depth for each material specification are illustrated in Figure 4-3. This figure can be somewhat misleading, since for deepwater areas the depth will remain quite large throughout the entire model simulation. These are tied to the local water depth at each computational node in the mesh fro every model time step. Because of the lack of degrees of flexibility in the response for the one-dimensional elements, the depth dependence coefficient is set very small so that the friction is essentially a constant.

Table 4-1. Model frictional function coefficients for equation 1						
Depth Range (ft, NAVD88)		Material Type	n_o	d_o	n_m	α
from	to					
- infinity	-100	2	0.04	2.0	0.04	0.167
-100	-50	3	0.04	2.0	0.04	0.167
-50	-30	4	0.04	2.0	0.04	0.167
-30	-20	5	0.04	2.0	0.04	0.167
-20	-15	6	0.04	2.0	0.04	0.167
-15	-10	7	0.04	2.0	0.04	0.167
-10	-6	8	0.04	2.0	0.04	0.167
-6	-2	9	0.04	2.0	0.04	0.167
-2	0	10	0.04	2.0	0.04	0.167
0	3	11	0.04	2.0	0.04	0.167
3	6	12	0.06	2.0	0.20	0.167
6	8	13	0.04	2.0	0.15	0.167
8	infinity	14	0.04	2.0	0.15	0.167
South Bay 1D		15	0.03	0.4	0.0	0.0
Sacramento delta 1D		16	0.035	2.0	0.0	0.0
		17	0.032	2.0	0.0	0.0
		18	0.020	2.0	0.0	0.0
		19	0.027	2.0	0.0	0.0
		20	0.024	2.0	0.0	0.0

Eddy viscosity

The eddy viscosities were also specified , in part, as a function of water depth. The model has the feature to allow the specification of the eddy viscosity as a function of the Peclet number, defined as

$$P_e = \frac{\rho UL}{E_{xx}} \tag{3}$$

where ρ = the fluid density

U = the fluid velocity

L = element horizontal dimension

E_{xx} = eddy viscosity

The eddy viscosity is determined by specifying the Peclet number and solving for the eddy viscosity as the velocity varies in time.

The eddy viscosity specification in areas of lateral flow separation was handled via a Smagorinski (1963) specification of the form

$$E_{xx} = F * A\left[\left(\frac{\partial u}{\partial x}\right)^2 + \left(\frac{\partial v}{\partial y}\right)^2 + 2\left(\frac{\partial u}{\partial y} + \frac{\partial v}{\partial x}\right)\right] \tag{4}$$

Where A is the area of the element, F a scaling factor and the other terms are the velocity gradients. The scaling factor used for this study was 0.10 and the eddy viscosity had a minimum value of 5.0 lb-sec/ft^2. Figures 4-4 and 4-5 present the spatial variation in the specification of the material properties for the eddy viscosity. Table 4-2 presents the specifications used in the model.

Table 4-2 Material specification of eddy viscosity via Peclet number

Depth Range (ft, NAVD88)		Material Type	Peclet Number
from	to		
- infinity	-100	3	20
-100	-40	4	20
-40	-20	5	20
-20	0	6	20
0	3	7	20
3	6	8	15
6	8	9	1
8	10	10	1
10	infinity	11	0.8

Marsh Porosity

Marsh porosity was developed (Roig, 1995) as a transition method between wet and dry states within RMA2. The partial motivation was to eliminate the severe shocks that occur with conventional wetting and drying which rather arbitrarily

must define elements as either wet or dry. Combine the binary wet/dry state decision with numerical oscillations and the model often becomes unstable while attempting to resolve wet-dry boundaries within the nonlinear iterations for a time step.

The basic intention of the method is that it tries to provide a gradual and continuous variation between the wet and dry states that is both more realistic and more stable numerically. The implementation of the method involves the definition of a fractional wetted area as a function of water surface elevation. The implementation of the method within RMA2 is limited to a four phase variation (see Figure 4-6) for the case of a falling water surface elevation. The first phase at an extremely high relative water level the node is viewed as completely wet, with a fractional wetted area of 1.0. As the water level falls the node enters the transition phase, where the fractional wetted area decreases linearly with falling water level. The third phase is the portion of the vertical distribution where the fractional wetted area takes on a minimum value (AC3 in Figure 4-6). The final phase would be the dry phase when the water level falls below 0.0. In the actual implementation in RMA2 the drying logic will dry the node when the local water depth falls below the drying threshold.

The marsh porosity method is implemented within RMA2 on a nodal basis. This has been the source of considerable confusion in users developing an understanding of the technique. The fractional wetted area is more easily conceptualized on an elemental basis but, in fact, it is actually representative of the local area associated with each node. Mathematically, the influence of the marsh porosity of each node is distributed over each element based on the finite element nodal basis functions of the element. That is just a fancy way of saying that the closer you are to the node the more effective its nodal marsh porosity value is and the farther away the less influence it has.

Ultimately the decision of whether an element is wet or dry comes down to the status of the wet or dry state of each of the nodes in the element. In the conventional wetting and drying approach, without marsh porosity, an element is made dry if a *single* node within the element becomes dry. When marsh porosity is invoked the element becomes dry only after *every* node in the element is dry. This is logical in that if it were the same as the conventional method of wetting and drying then it would not be much of a transition. So by deferring the drying process until all nodes are dry the shock is removed. In the process of deferring drying the remaining wet nodes within the element are passing less and less water due to the restricting effect of reducing the fractional wetted area. The flow

restricting effect is accentuated when the bottom roughness is prescribed as a function of water depth.

The material definitions used for specification of marsh porosity are illustrated in Figure 4-7. Again the variation in the specification was primarily by water depth but with fewer intervals (12 material types). The actual parameters that are defined in Figure4-6 are listed in Table 4-3.

Table 4-3 Marsh Porosity specifications

Depth Range (ft, NAVD88)		Material Type	Parameter		
from	to		AC1	AC2	AC3
- infinity	-3	2	3	2	0.01
-3	-1	3	3	2	0.01
-1	1	4	4	2	0.01
1	3	5	6	2	0.01
3	5	6	8	2	0.01
5	7	7	10	2	0.01
7	9	8	12	2	0.01
9	11	9	14	2	0.01
11	13	10	16	2	0.01
13	15	11	18	2	0.01
15	17	12	20	2	0.01
17	19	13	22	2	0.01
19	21	14	24	2	0.01
21	23	15	26	2	0.01
23	25	16	28	2	0.01
25	27	17	30	2	0.01
27	infinity	18	32	2	0.01

Coriolis

The Coriolis effect was included in all model simulations by specifying the local latitude (37.8 degrees north) as a constant over the model (essentially an *f*-plane model). The row of elements closest to the ocean boundary had the Coriolis

effect turned off to avoid an inconsistency in the tidal boundary specification. The data supporting our boundary conditions is not accurate enough to handle the very sensitive interplay between the Coriolis effect and it's local balance in the water surface gradient along the boundary. The specification spatial distribution is shown in Figure 4-8.

Tidal Propagation

The basic characteristics of the tidal propagation in the system are documented in Figure 4-9. The figure shows the progression of the tidal datum through the system (MLLW, MLW,MHW and MHHW). The model simulations are presented as a series of high and low water progressions for specific tides, rather than long-term tidal means. Also plotted are the predicted high and low water values for several of the active tide stations for the same period as the model simulation.

Storm Events

The model was simulated for the storm events presented in Table 4-4. These events were selected from the conditional sampling of astronomical tidal peaks greater than 5.5 ft and residual surge peak levels greater than 1.5 ft. For the January 1983 simulation, four of the top 39 highest observed peaks occurred.

Table 4-4 Verification storm events simulated

Simulation Number	Starting	Ending	Ranked events
1	1/17/1983	1/31/1983	1,5,16,39
2	12/2/1983	12/9/1983	2
3	2/2/1998	2/9/1998	3,4,12
4	11/25/1997	12/8/1997	17,32
5	12/20/2006	12/28/2006	none

February 1998 storm.

The tidal conditions at San Francisco for the period of the February 1998 storm are shown in Figure 4-10, for the predicted, observed and residual tidal signals.

The model response at San Francisco is presented in Figures 4-11 and 4-12, showing the accuracy with which the model boundary conditions are specified

and propagated through the model ocean area. The model compares very well with the verified tidal observations before and up to the peak of the surge. However, after the peak has passed, the model low waters are lower than the observed tides. This is the result of the flood peak passing through the system, which was not included in the model boundary conditions for this simulation. The model response for stations within the bay where observed tidal adapt were available form NOAA are shown in Figures 4-13 through 4-17.

The model was simulated with and without the storm residual forcing, so that the model response without the surge can be subtracted form the pure tidal simulation response to yield the model tidal residual. This is presented in Figure 4-17 for Redwood City, showing very good comparison. The model simulations presented show the case of a simulation with no wind and one with a constant 20 mph wind. The plot shows that without the wind the model peak surge is as much as a half a foot low. Adding the wind cuts that difference about in half. This shows that he winds are important to getting very precise matches in the water levels, but since the wind fields are unknown it was not warranted to spend excessive time attempting to match the peaks any better.

The response at Redwood City illustrates the highly nonlinear response in far South Bay to the combination of residuals and winds. The strong peak in the residual tides at Redwood City at hour 150 in Figure 4-17 is driven by wind effect. The amplification of the residual tides is difficult to summarize because of wind contributions to the bay setup.

December 2006 storm.

The tidal conditions for the storm that occurred during December 2006, while the SSFBSS wave data collection effort was ongoing are shown in Figure 4-18 for the San Francisco tide gage. The subtidal surge peaked on the 27th, during a neap tide, so the tidal water level was not very high. There was a wind-wave event that is being used in the calibration of the wave model, so the long-wave simulation is important in defining the water levels for the wave model.

The model response at San Francisco is shown in Figure 4-19 for driving the model with the predicted tide with the filtered subtidal surge added, and with and without wind applied. The with wind case used the SFO wind time series applied uniformly over the model. There is essentially no difference between the with and without wind tidal response at the San Francisco gage. The response at Redwood City is presented in Figure 4-20, showing a response to the winds near the peak surge around hour 150. The improvement with the winds was only

about a third of the difference between the without wind simulation and the observed tidal peak.

December 1983 storm.

The tidal conditions at San Francisco for the December 1983 storm are shown in Figure 4-21, when a subtidal surge greater than 2 ft occurred during a spring tide. The tidal surge peaked at 8.77 ft on December 3rd.

The numerical model response at San Francisco is shown in Figure 4-22 for simulations with tidal surge, with and without the SFO uniform winds. Again the winds drive the response closer to the observed tide near the peak of the surge, but not quite the degree required to obtain a match in the peak elevation.

The model response at Redwood City is shown in Figure 4-23. The response is very similar to the response at San Francisco.

January 1983 storm

The tidal conditions at San Francisco for the January 1983 are presented in Figure 4-24. This event was the highest storm in the period of record, with a subtidal surge in excess of 2 ft occurring during a spring tide.

November 1997 storms.

During November through December 1997 several peak surges occurred. These are shown in Figure 4-25. One peak occurred at 7.76 ft on 13 November, a 1 ft subtidal surge during a spring tide. The peak of 7.62 ft on the 26 November occurred with almost a 2 ft surge at a mean tide . Finally, a sure peak at 7.72 ft occurred on the 14 December with a 1 ft surge on a spring tide.

Sensitivity Simulations

Effects of wind stress on tidal surge

The model was tested in both the test mesh and the project mesh for the effects of winds on the tidal storm surge. Because of the unavailability of the spatially varying winds the sensitivity testing to data has been with spatially uniform winds.

The first test for the wind sensitivity were to determine the basic effect of the winds on a static water level with no tides. For these tests the water level was

held at mean tide level (3.17 ft NAVD). The model was then subjected to a series of wind speeds of 20, 30 and 40 mph constant and uniform from the northwest. The response of the system to this forcing is shown in Figure 4-26 for the 40 mph case. The figure shows the evolution of the water level with time at a number of locations within the system. It can be seen that within 19 hours the water level has stabilized.

Figure 4-27 presents the profile of the equilibrium water levels for wind speeds of 20, 30 and 40 mph. This shows tat the maximum wind setup is increases dramatically southward and for the 40 mph test, with the setup on the order of 2 ft at the mouth of Coyote Creek. The maximum setup for the 30 mph run was about 0.6 ft, and for the 20 mph test about 0.25 ft, both at Coyote Creek.

Equilibrium wind tests for the more extreme winds are not realistic for estimating the effects of the extreme events, primarily because the most extreme winds are very short-lived events embedded within a time-series of much lower wind speeds. This effect was illustrated in the effects of adding the time-series winds to the verification events (Figures 4-20).

Effects of tributary inflows on tidal surge

Tests were conducted to see the impacts of extreme bounds on the tributary inflows on the peak surge levels. The results are summarized in Figure 4-28. The discharges from South bay tributaries varied between a low flow of 278 cfs to 30,000 cfs. The net delta outflow was simulated at either 11,000 cfs or 300,000 cfs. Each of these simulations were made with the full tidal forcing, with the residual surge on top of the predicted tide as described above. The peak residual water level at each of the profile stations was determined by subtracting the model response at each station for the predicted tide alone to yield a residual response time series. These simulations presented in Figure 4-28 are summarized in Table 4-5. These tests show that a constant 30 mph wind over the duration of the simulation is an extreme condition. The response to the time-varying SFO winds is closer to the no-wind response than to the constant 30 mph test runs. The impact of the raising of the delta outflow from 11,000 cfs to 300,000 cfs was to raise the water levels far upstream in the northern reaches by approximately one foot. The impact at the extreme end of South Bay at Coyote Creek was to raise the peak residual by only 0.03 ft. The impact of increasing the South Bay inflows from 278 cfs to 30,000 cfs raised the peak residual at the mouth of Coyote Creel by 0.16 ft. The effects of the South Bay flow increase vanishes around Hunter Point.

Period of Record Event

The period of record event occurred during the January-February 1983 storm. The profile of the peak flood level for that simulated period in the numerical model is compared to the peak information from the NOAA data in Figure 4-29. The model profile matches relatively well compared to the NOAA reported peak flood levels.

Table 4-5. Discharge sensitivity tests

Test label in Figure 4-28	Discharges (cfs)		Winds (mph from NW)
	Delta	South Bay	
300KLow	300,000	278	30
300K30K	300,000	30,000	30
11K30K	11,000	30,000	30
11KLow	11,000	278	30
300K30K- Dr	300,000	30,000	30
Time varying SFO winds-300K30K	300,000	30,000	Time-varying
11KLow no wind	11,000	278	0

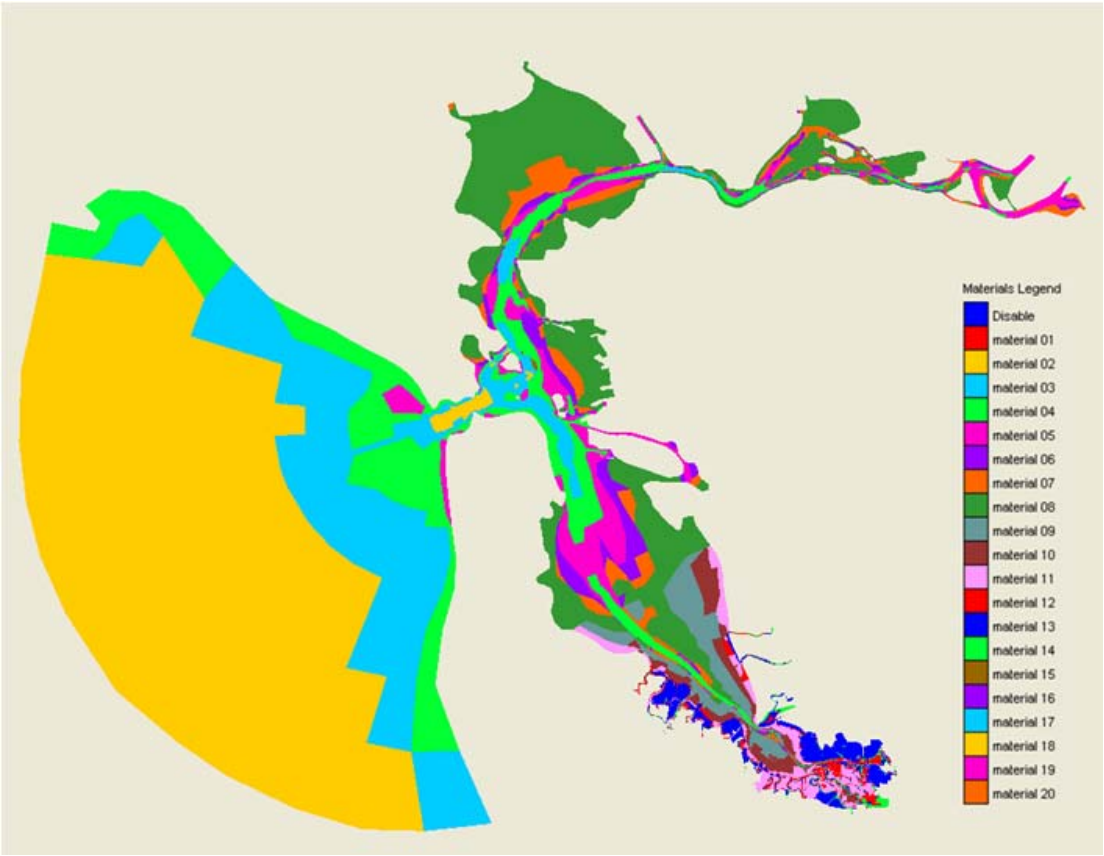

Figure 4-1. Material properties for frictional specification.

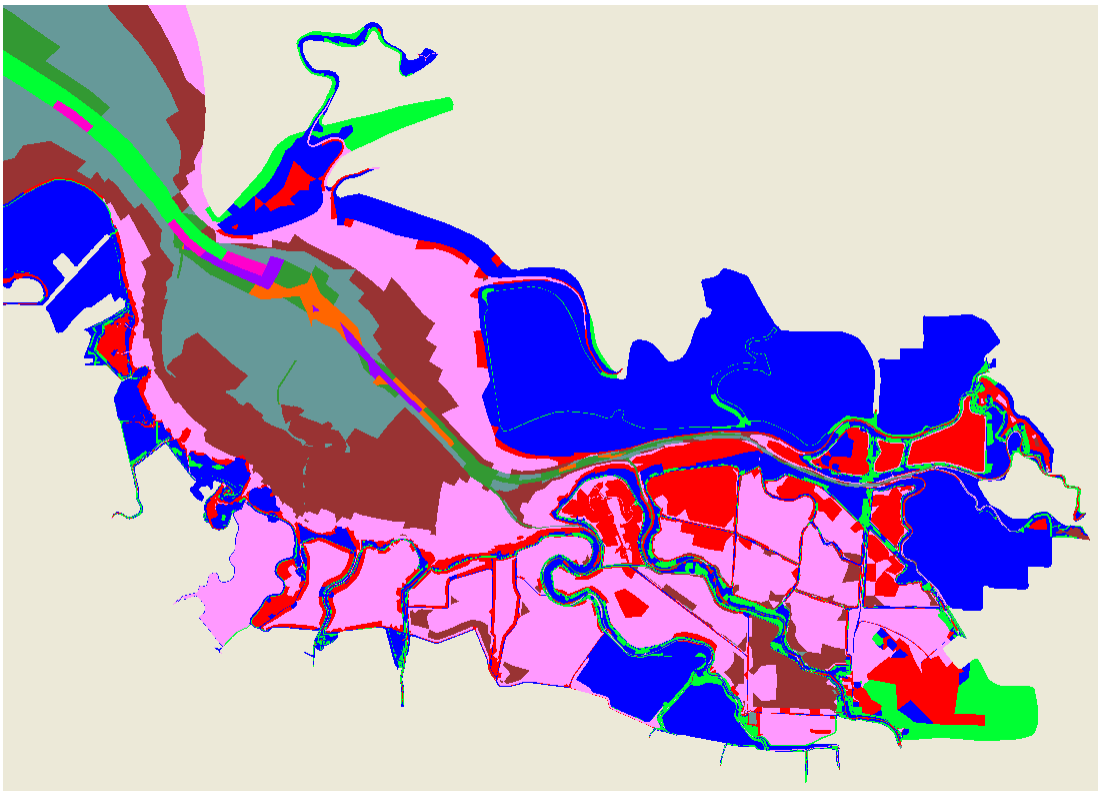

Figure 4-2. Material properties for frictional specification, details in study area. See Figure 4-1 for the legend.

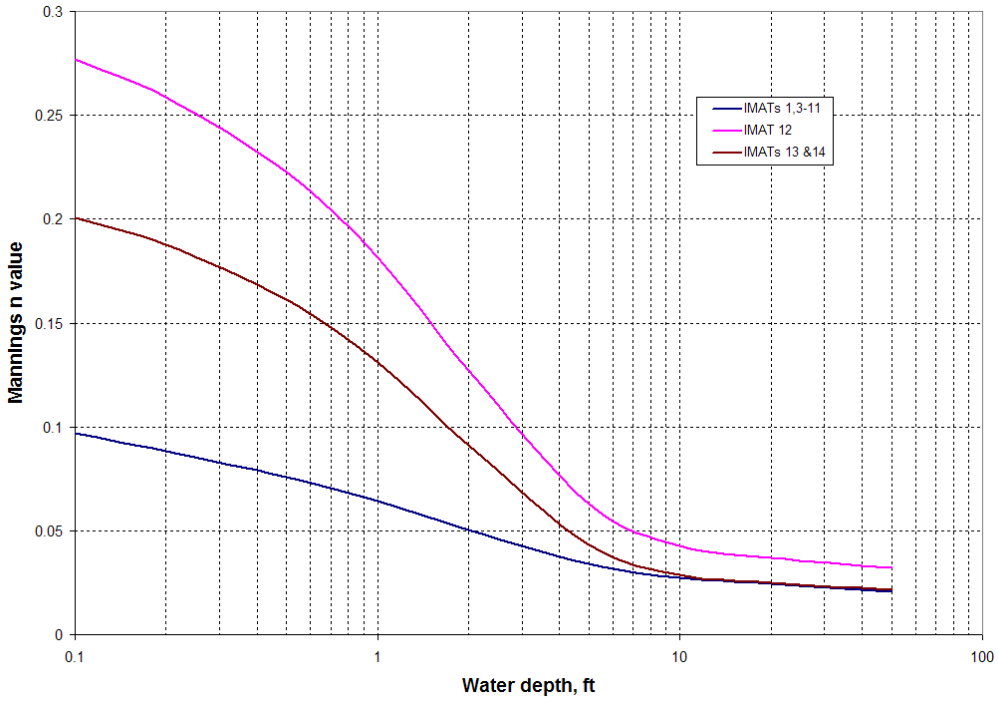

Figure 4-3. Variation in Manning's n friction coefficient with local water depth based on Equation 2 and the coefficients in Table 4-1.

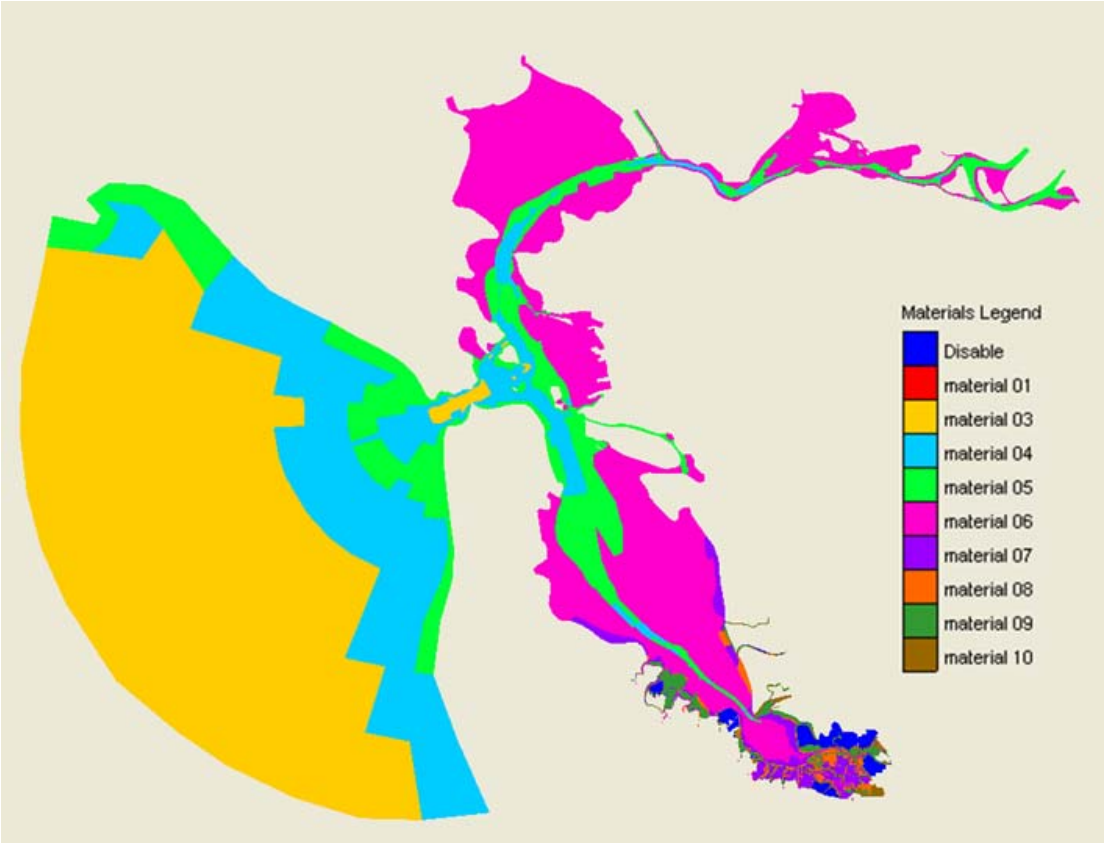

Figure 4-4. Material property specifications for eddy viscosity assignment.

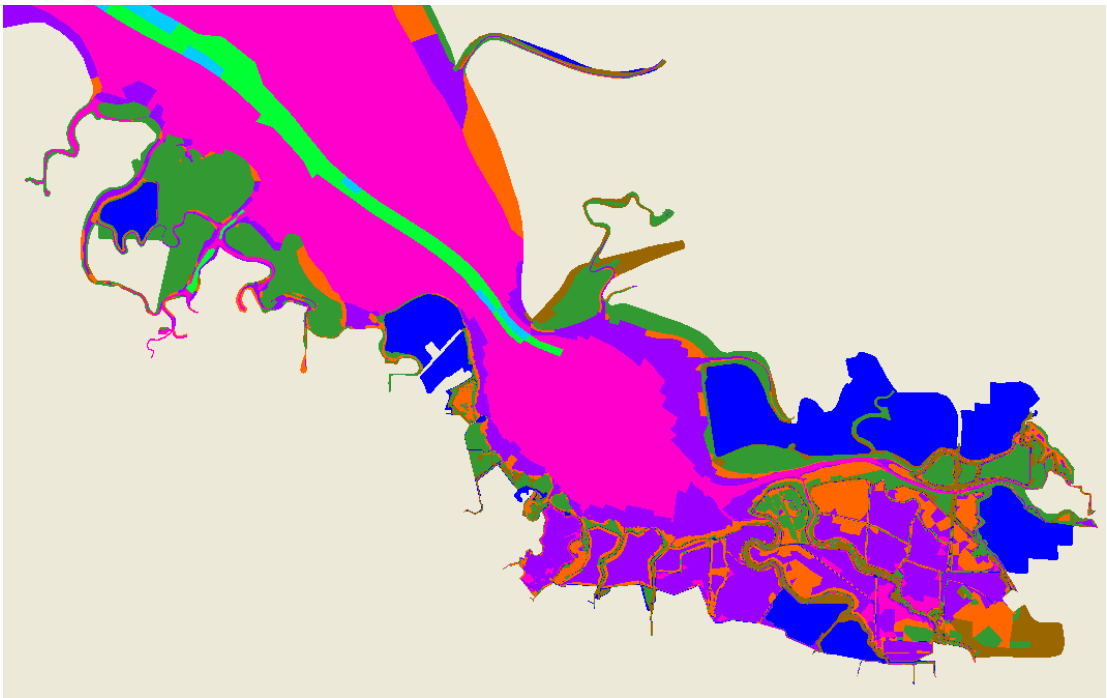

Figure 4-5. Material property specifications for eddy viscosity assignment in far South Bay.

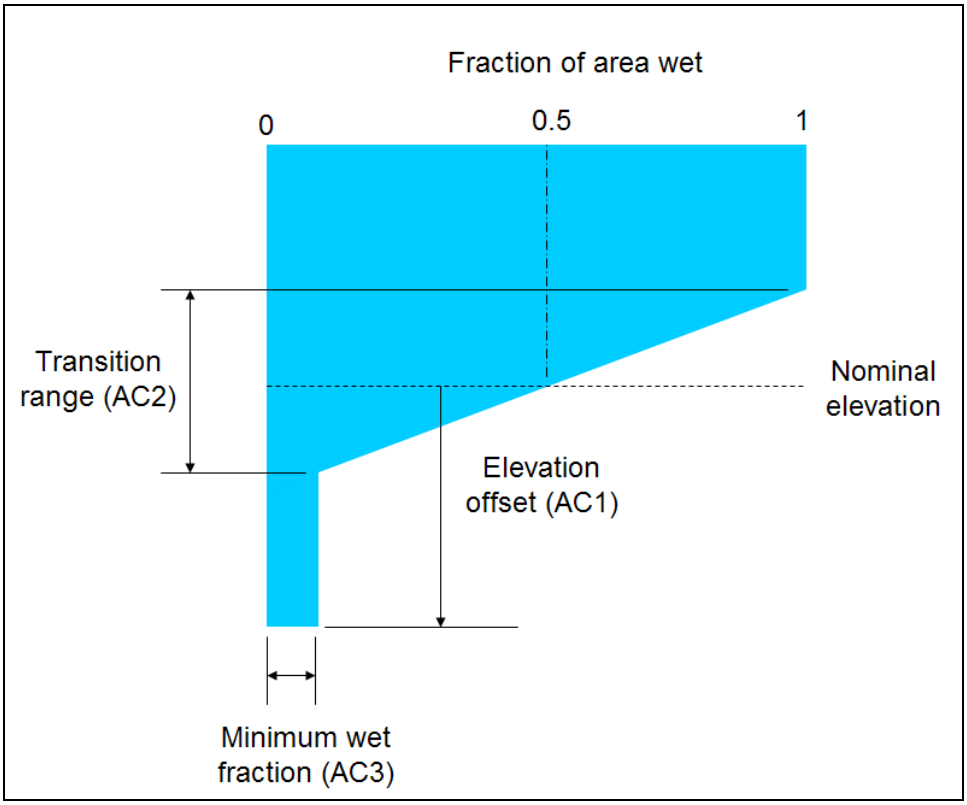

Figure 4-6. Definition sketch for marsh porosity specification

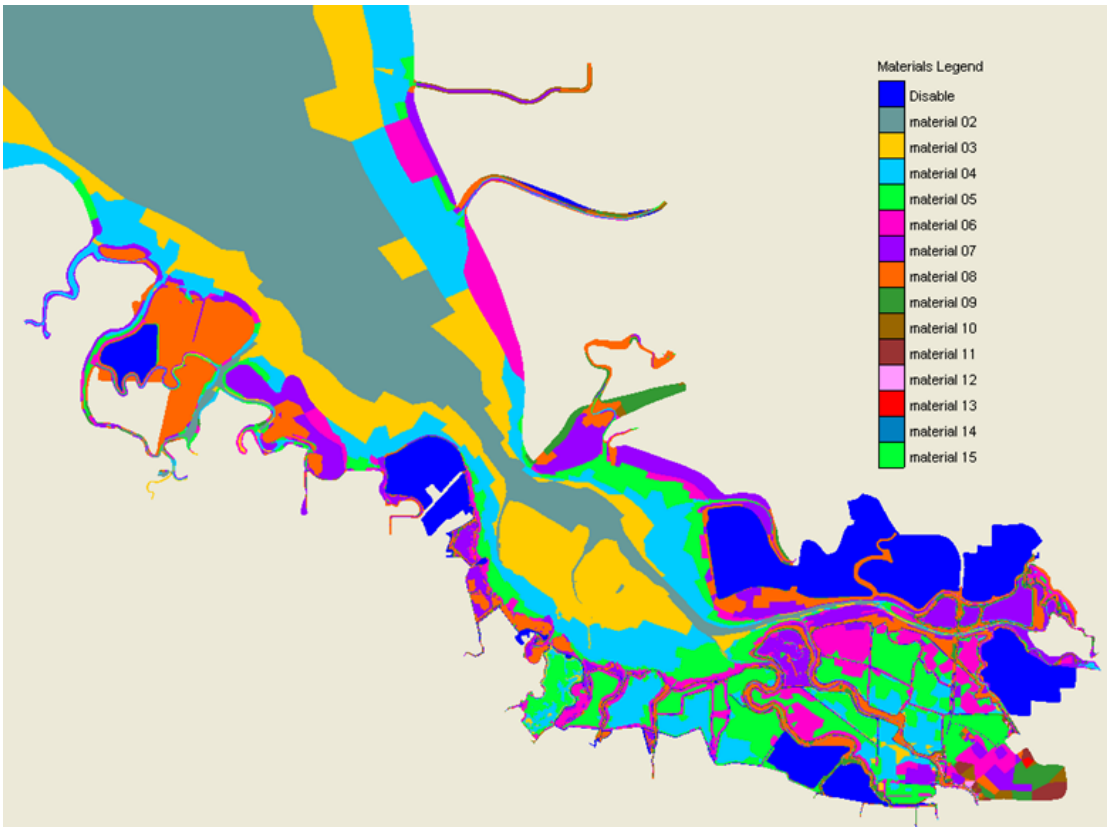

Figure 4-7. Material properties for marsh porosity specification.

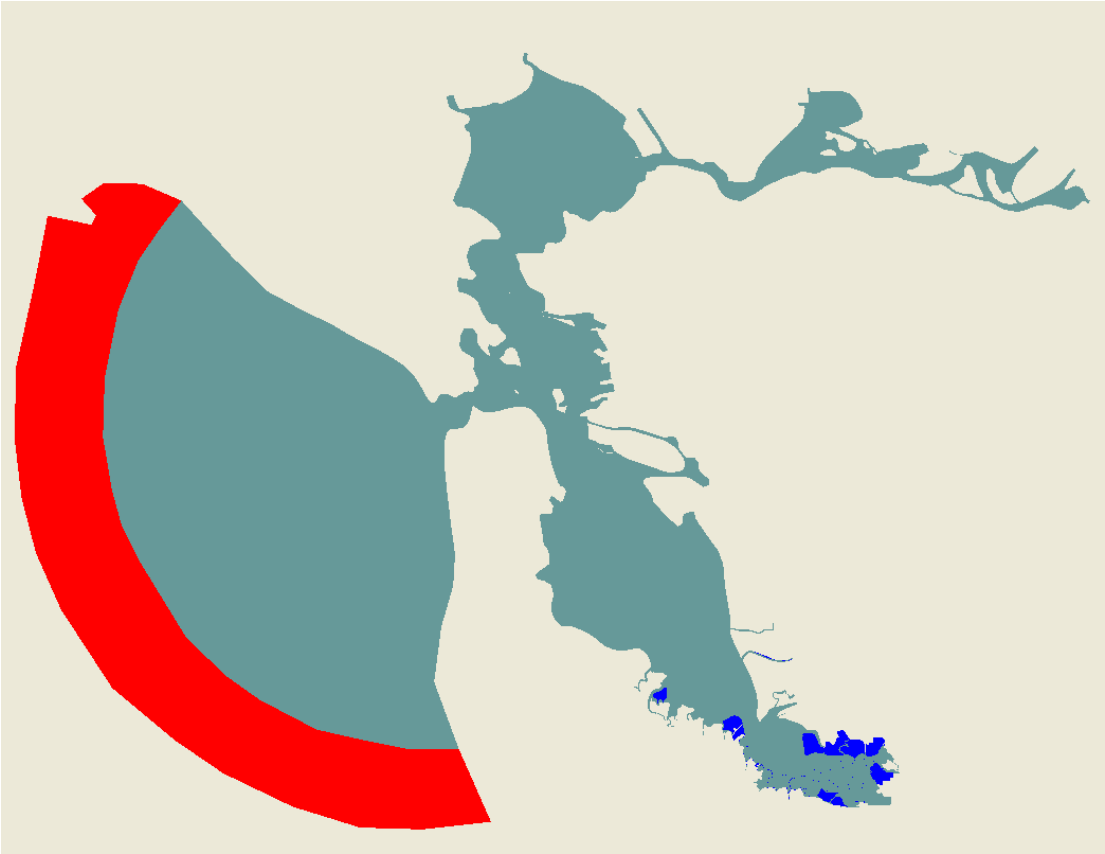

Figure 4-8. Model specification of Coriolis (local latitude)

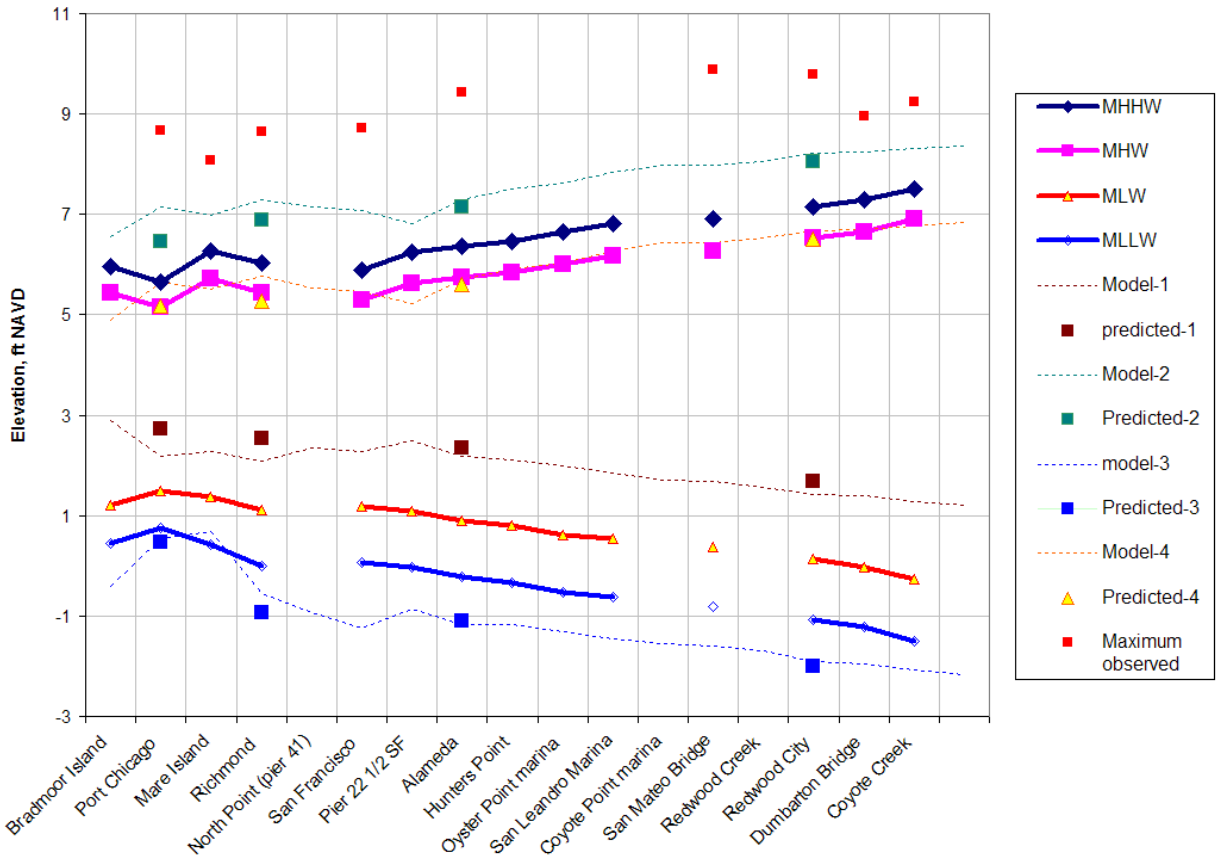

Figure 4-9. Model characteristics of harmonic tidal propagation. MHHW, MHW MLW MLLW are all from the NOAA tidal analysis. The model-*i* and predicted-*i* are the model and predicted harmonic tidal progression of high and low-waters through the system.

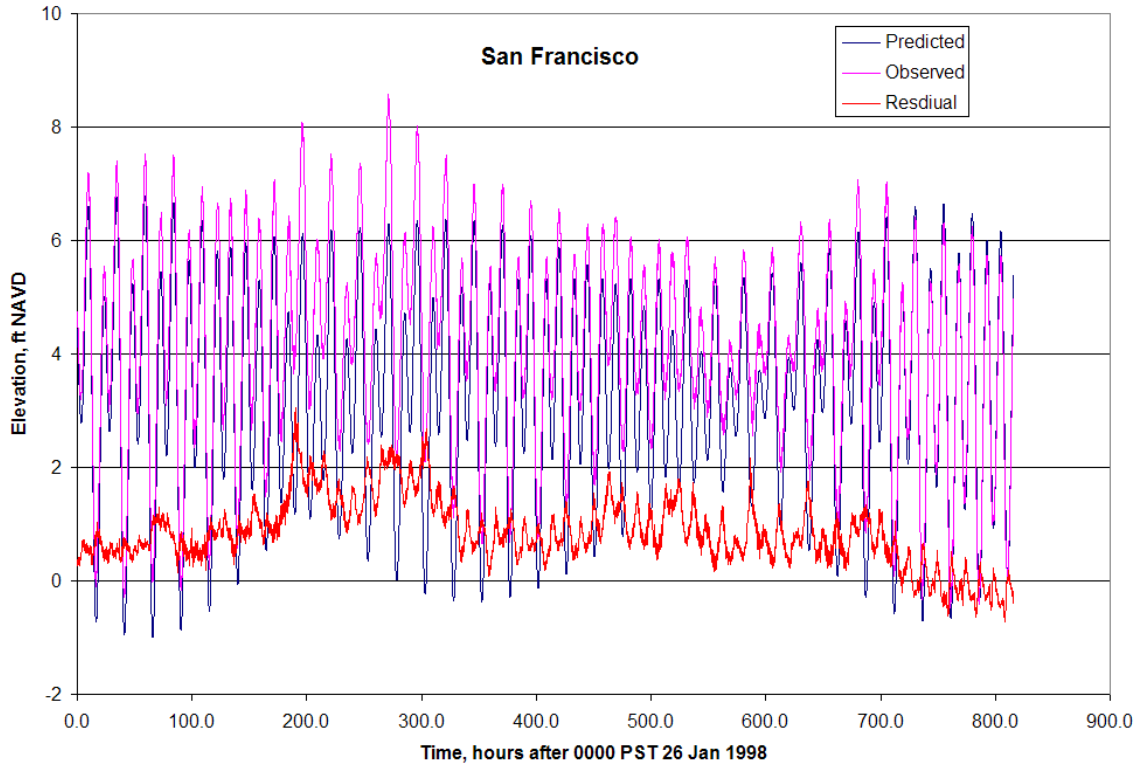

Figure 4-10. The tidal conditions at San Francisco for the February 1998 storm

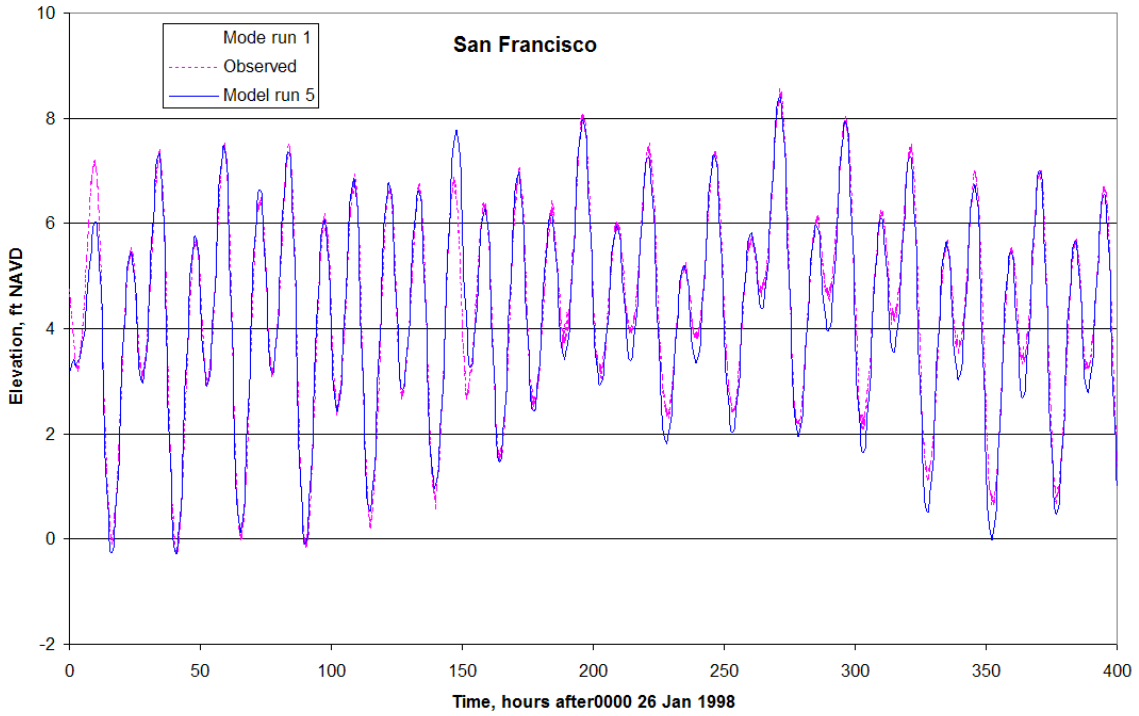

Figure 4-11. Model simulation of February 1998 storm at model control station (San Francisco)

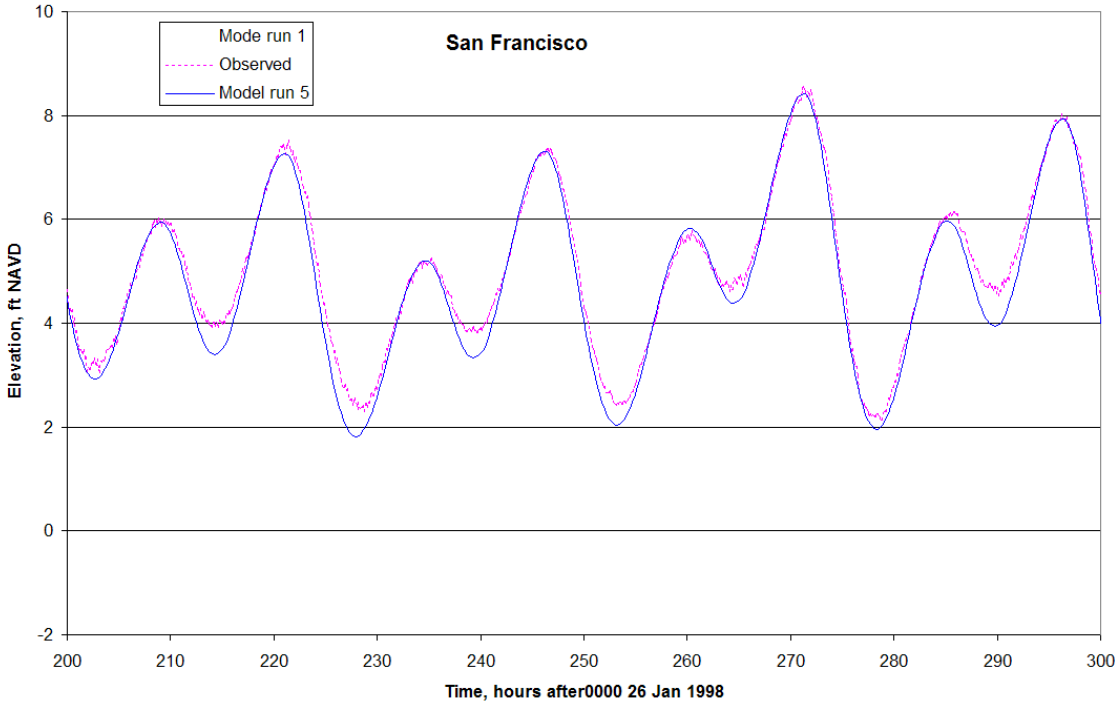

Figure 4-12. Closer detail of storm simulation tidal signal control at San Francisco near peak of storm surge.

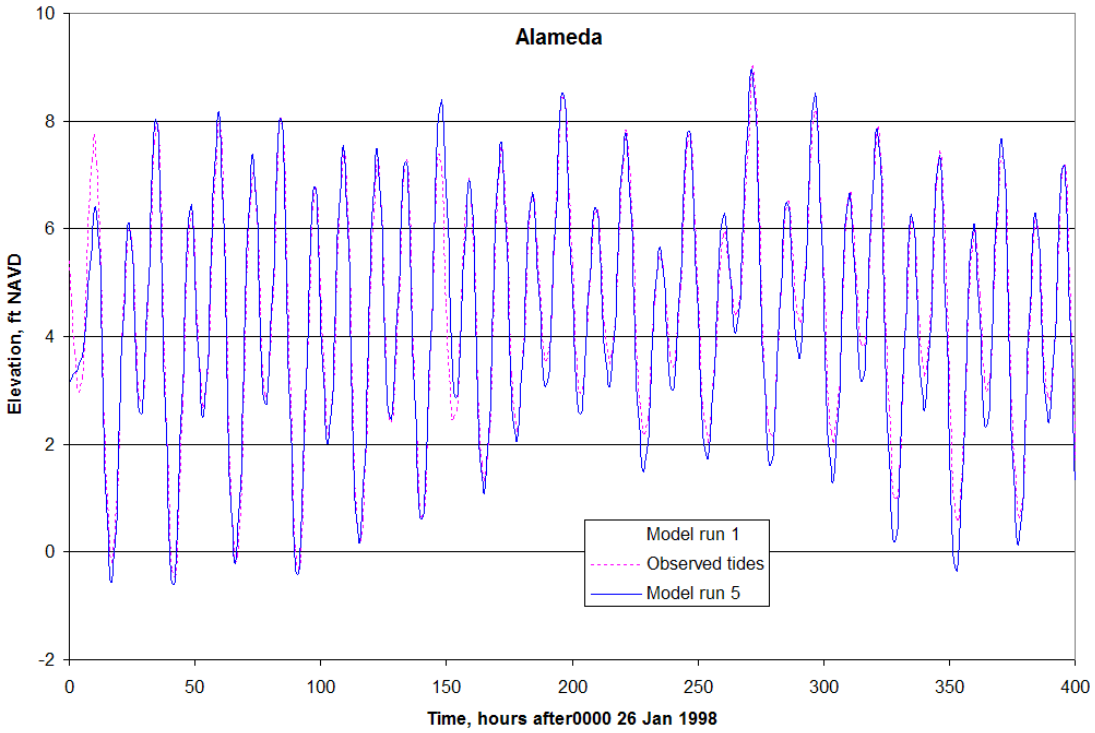

Figure 4-13. Model verification at Alameda for February 1998 storm

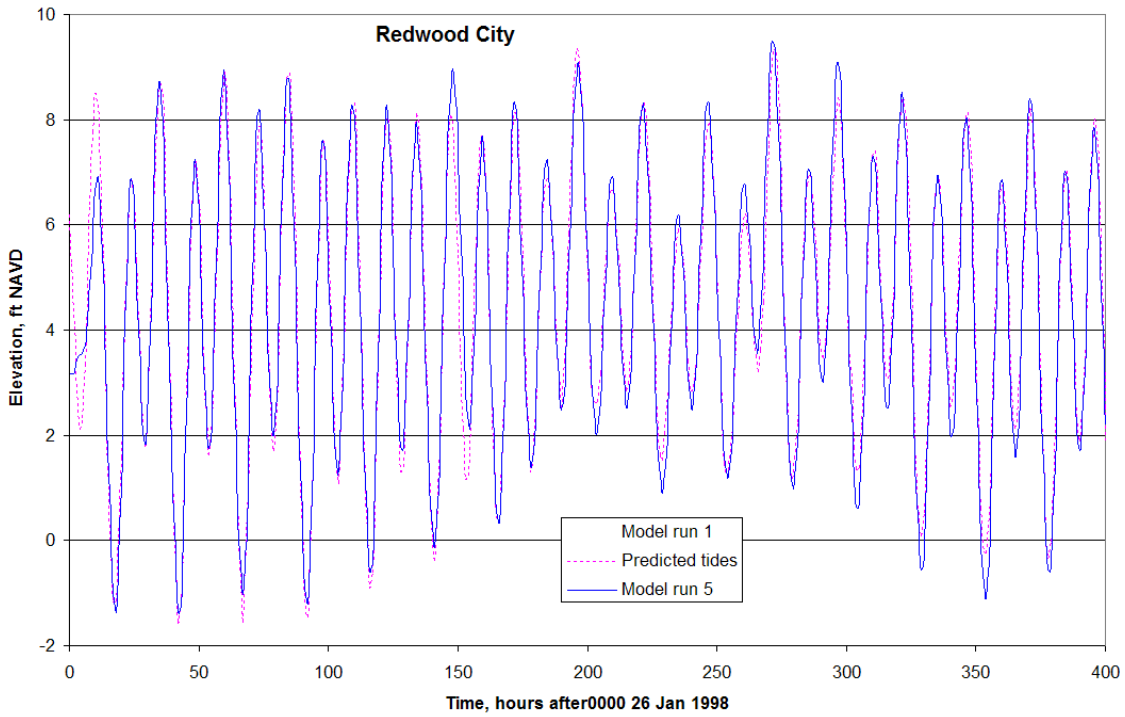

Figure 4-14. Model verification at Redwood City for February 1998 storm

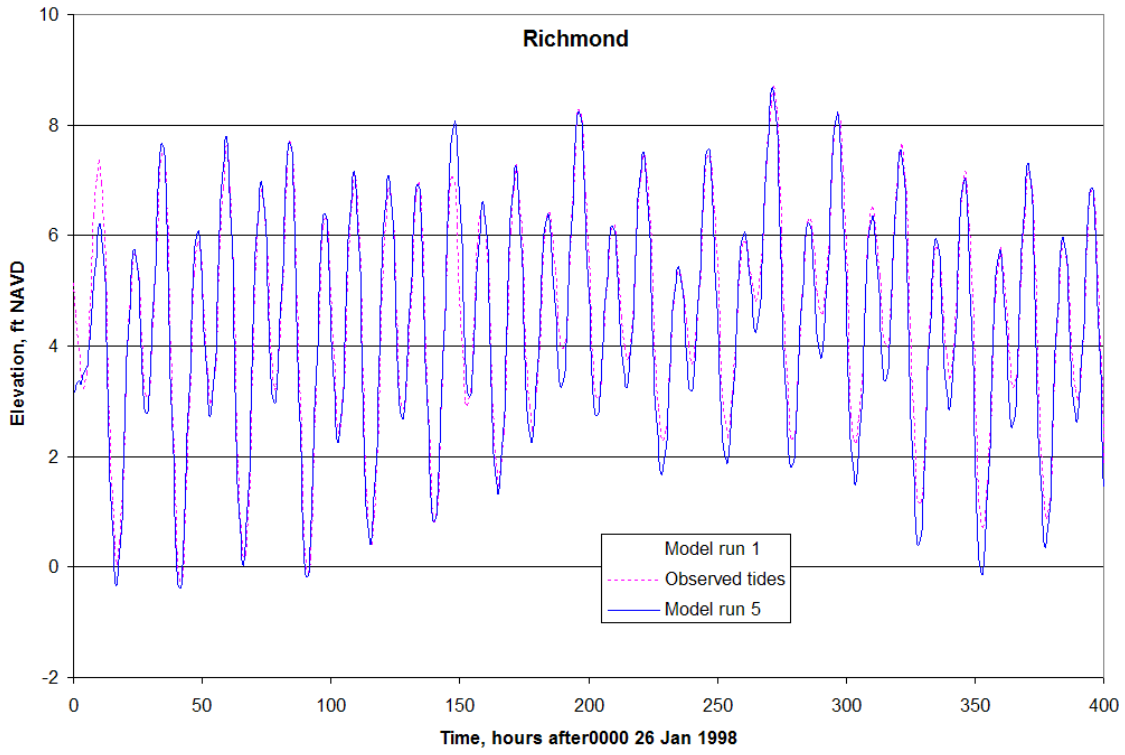

Figure 4-15. Model verification at Richmond for February 1998 storm

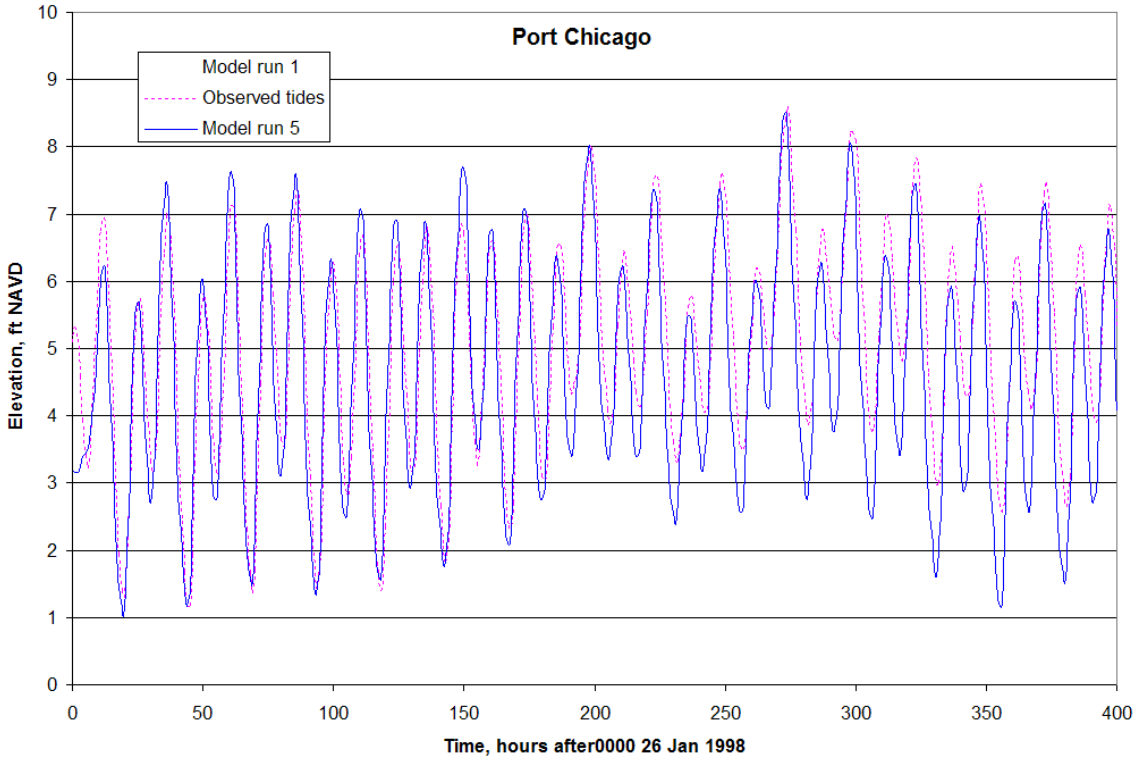

Figure 4-16. Model verification at Port Chicago for February 1998 storm

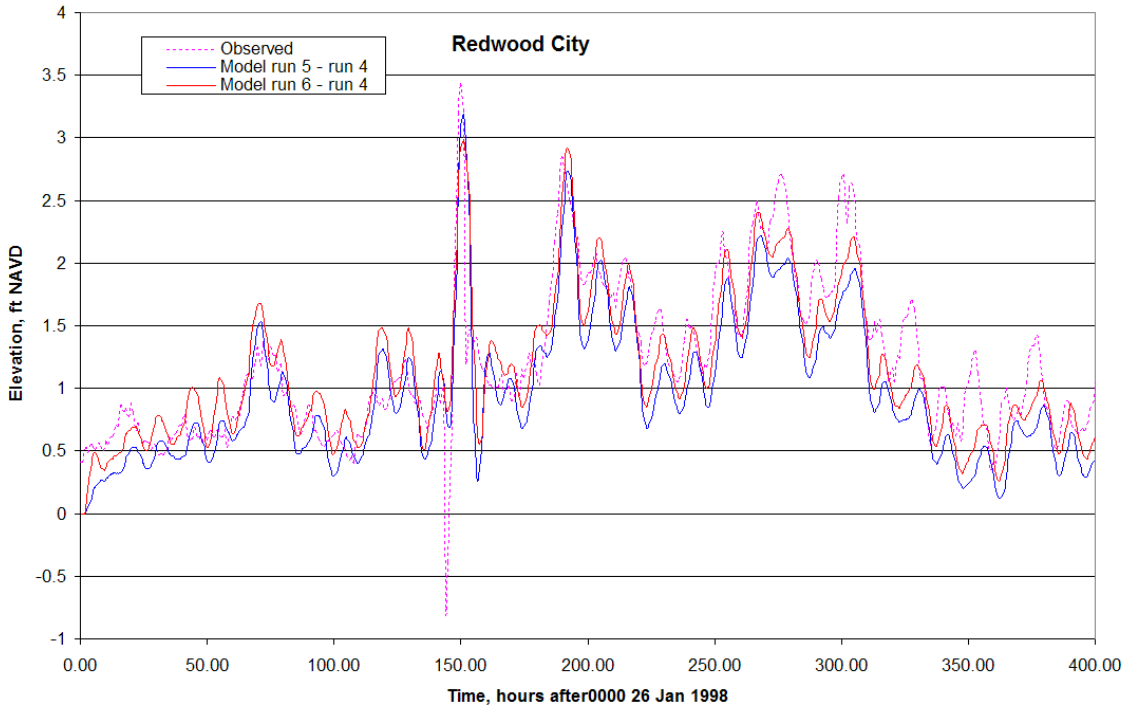

Figure 4-17. Comparison of tidal residual at Redwood City for model results to observed residual from NOAA data. Run 5 was forced with subtidal residual but no wind. Run 6 was the same residual tidal forcing in the ocean, but with a 20 mph uniform constant wind applied.

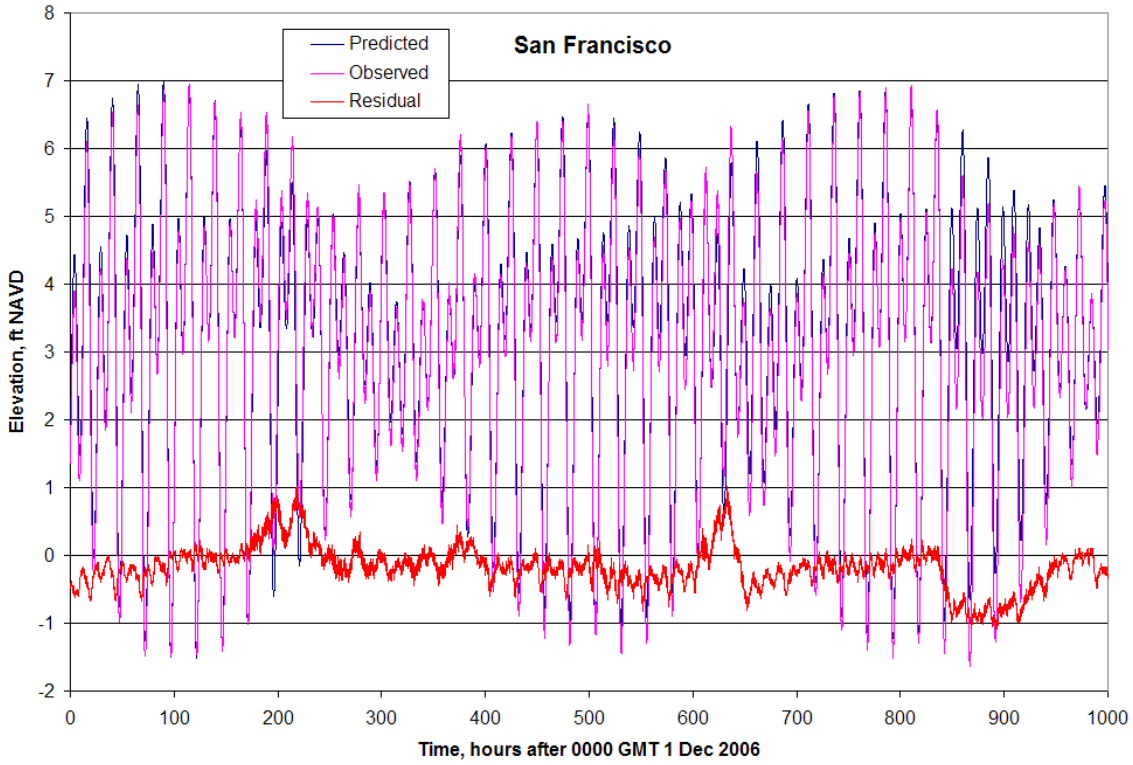

Figure 4-18. The tidal conditions at San Francisco for the December 2006 storm

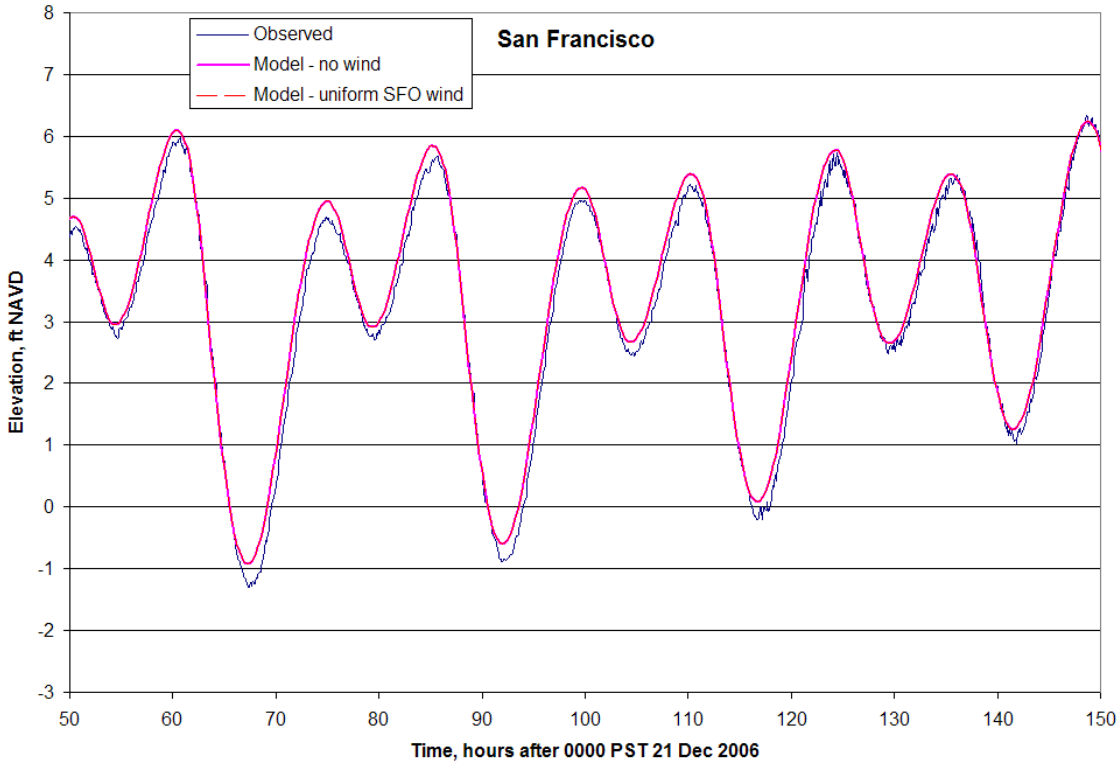

Figure 4-19. Tidal response at San Francisco for the December 2006 storm

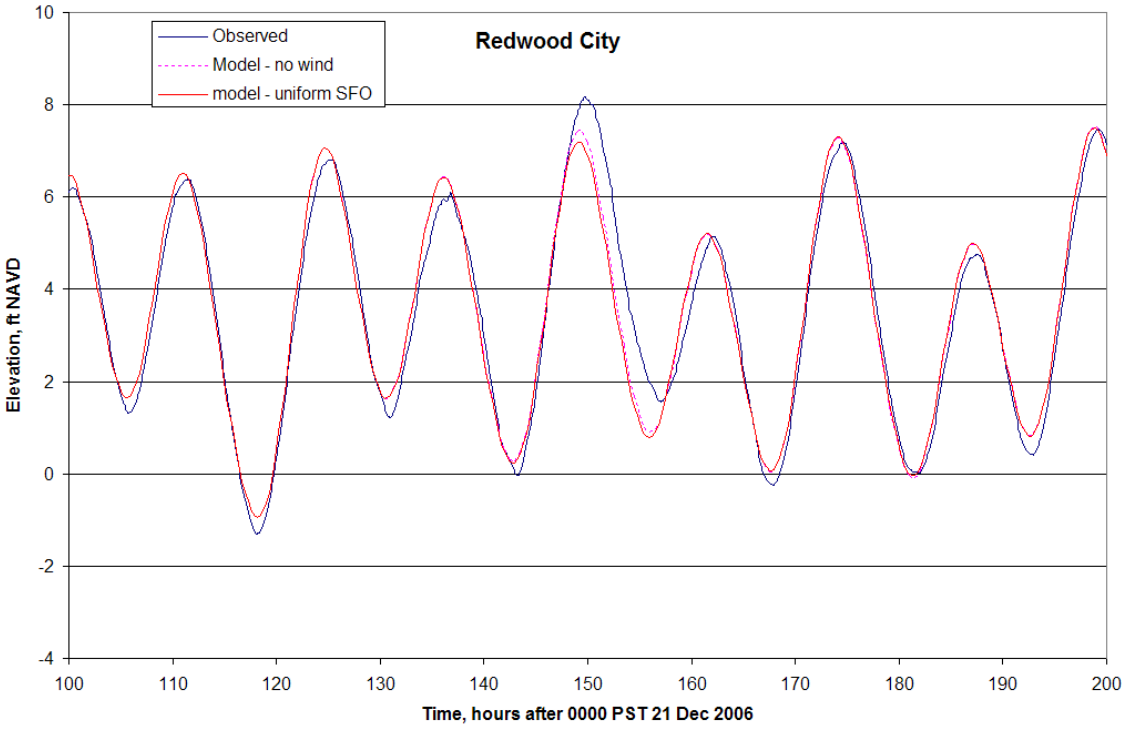

Figure 4-20. Tidal response at Redwood City for the December 2006 storm

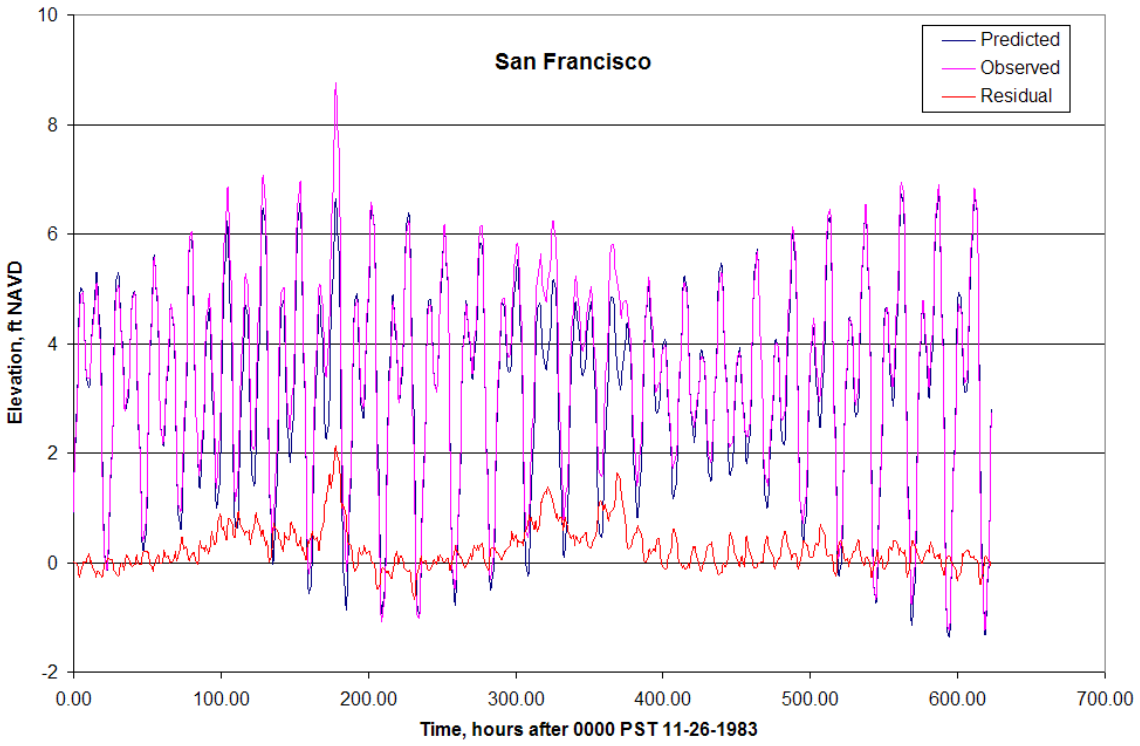

Figure 4-21. The tidal conditions at San Francisco for the December 1983 storm

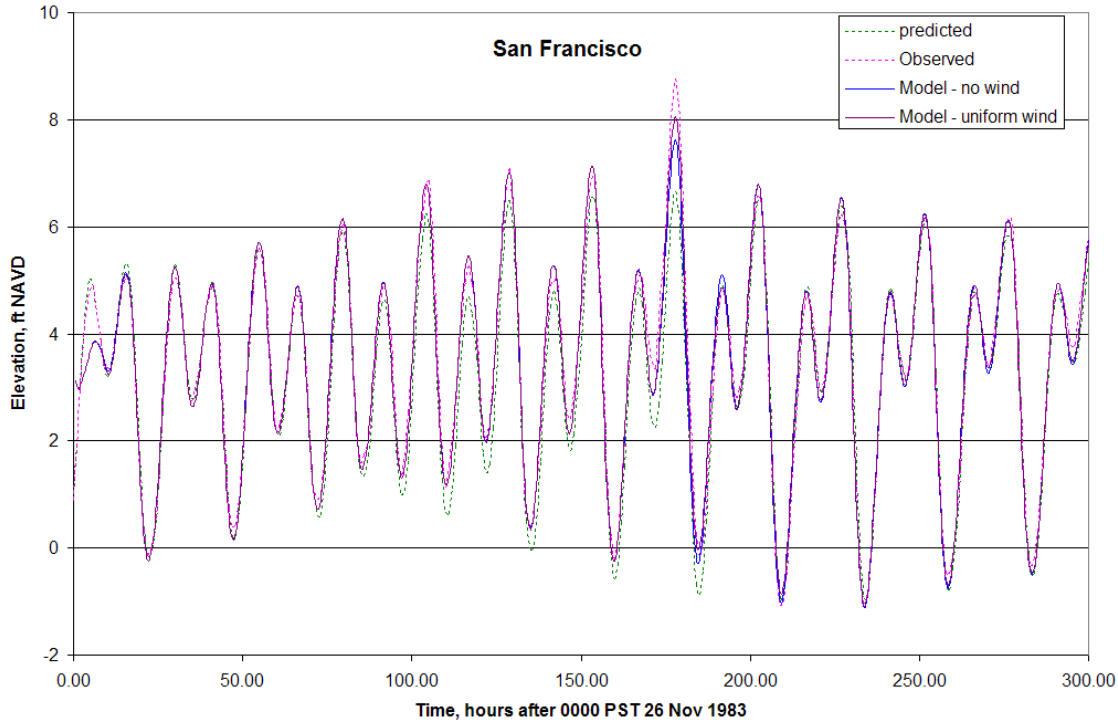

Figure 4-22. The tidal response at San Francisco for the December 1983 storm

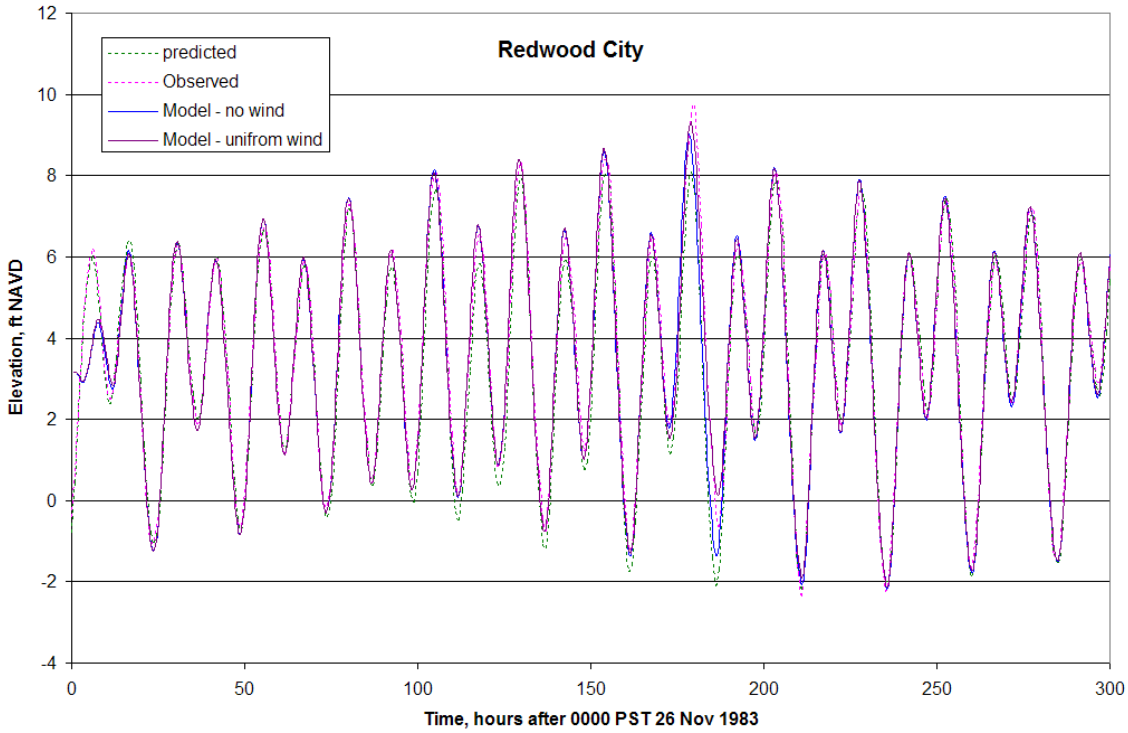

Figure 4-23. The tidal conditions at Redwood City for the December 2006 storm

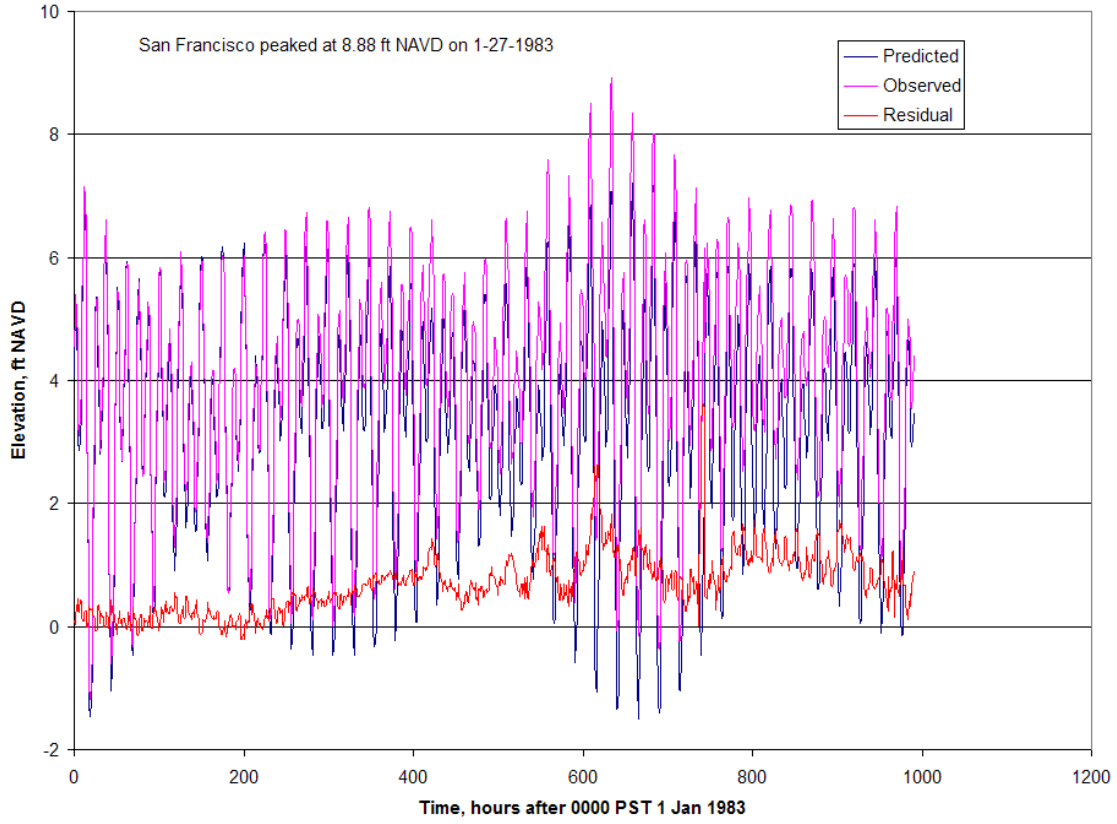

Figure 4-24. The tidal conditions at San Francisco for the January 1983 storm

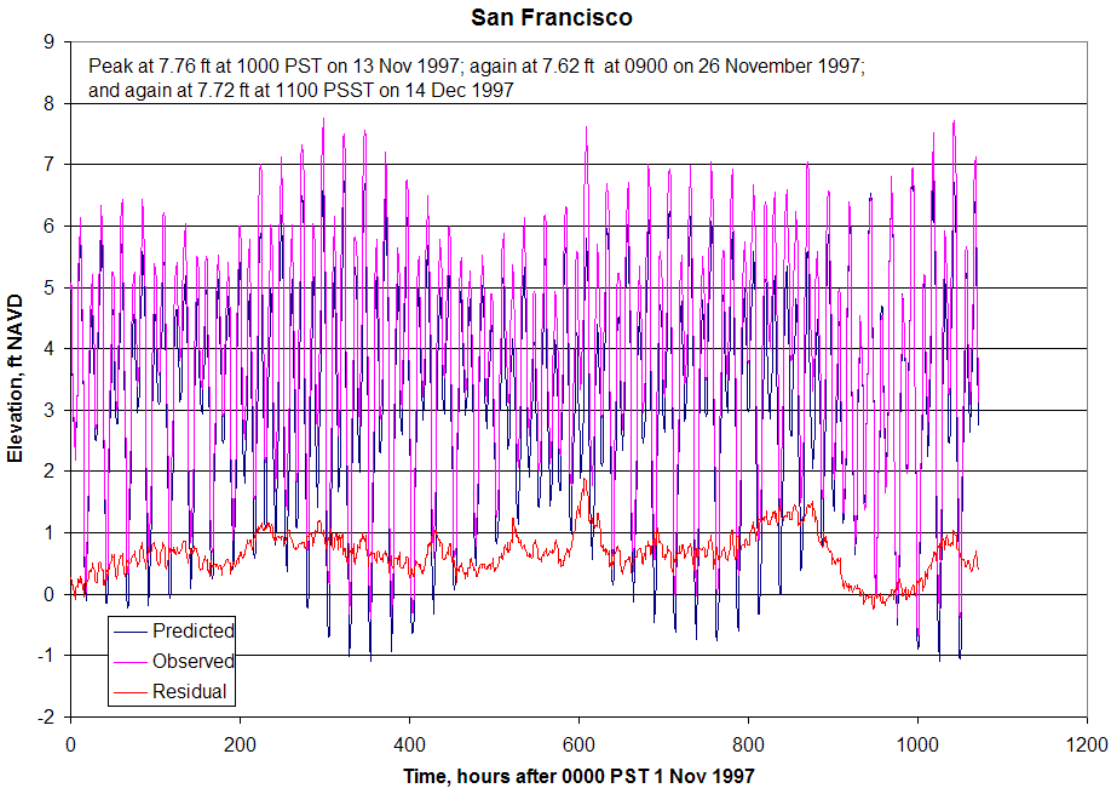

Figure 4-25. The tidal conditions at San Francisco for the November 1997 storm

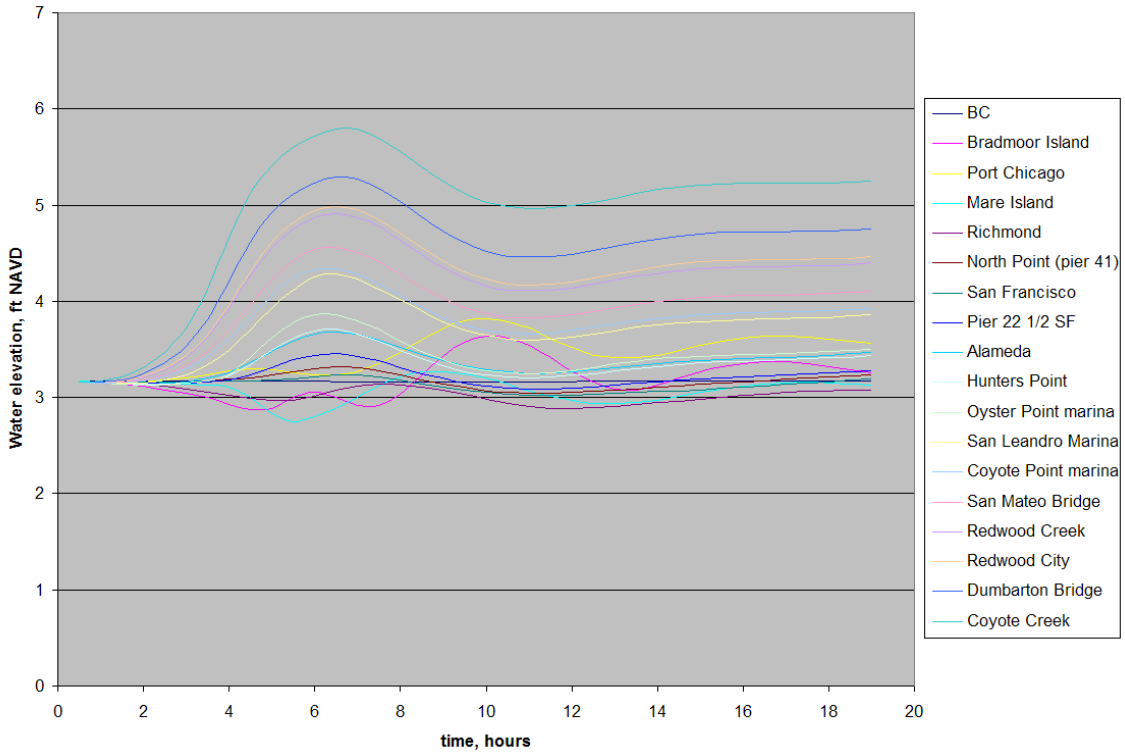

Figure 4-26. Time series evolution of the wind sensitivity tests on the test mesh. 40 mph constant uniform NW wind that ramps up over the first 4 hours. Static water level at the ocean BC of 3.166 ft NAVD

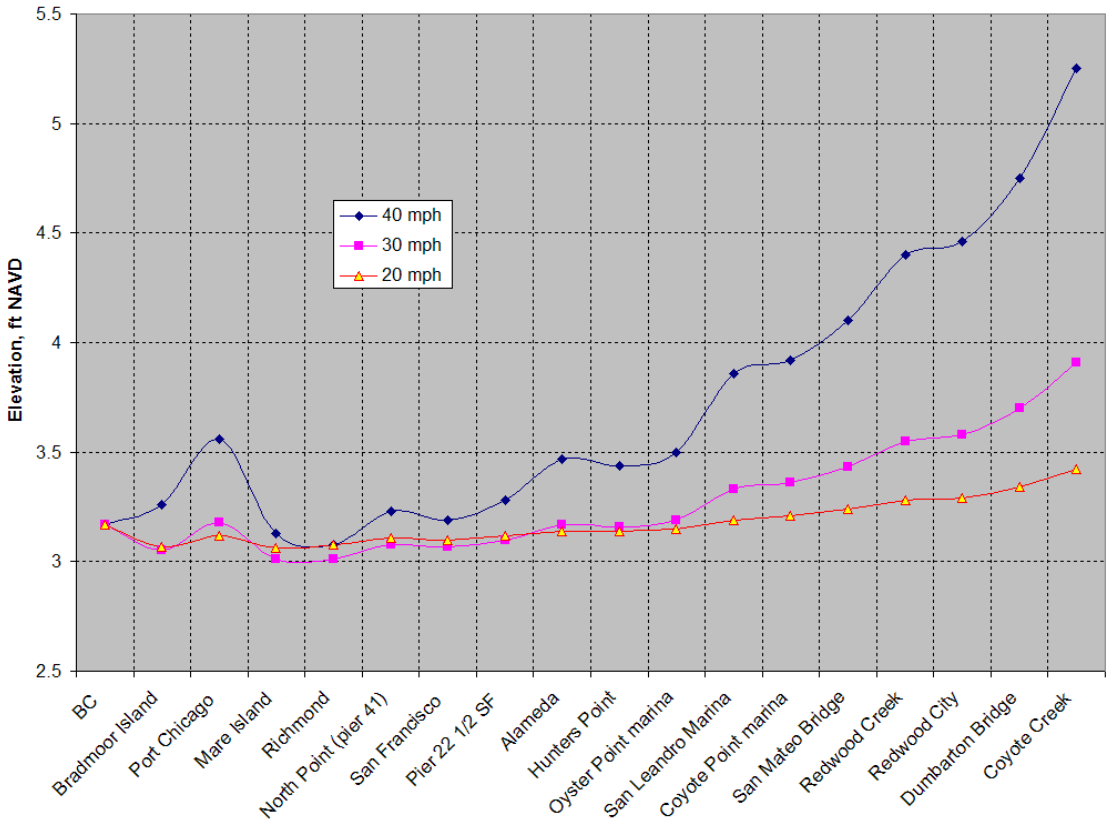

Figure 4-27. Profile of the water surface elevations at hour 19 for 20, 30 and 40 mph uniform NW wind for the static tide level sensitivity tests.

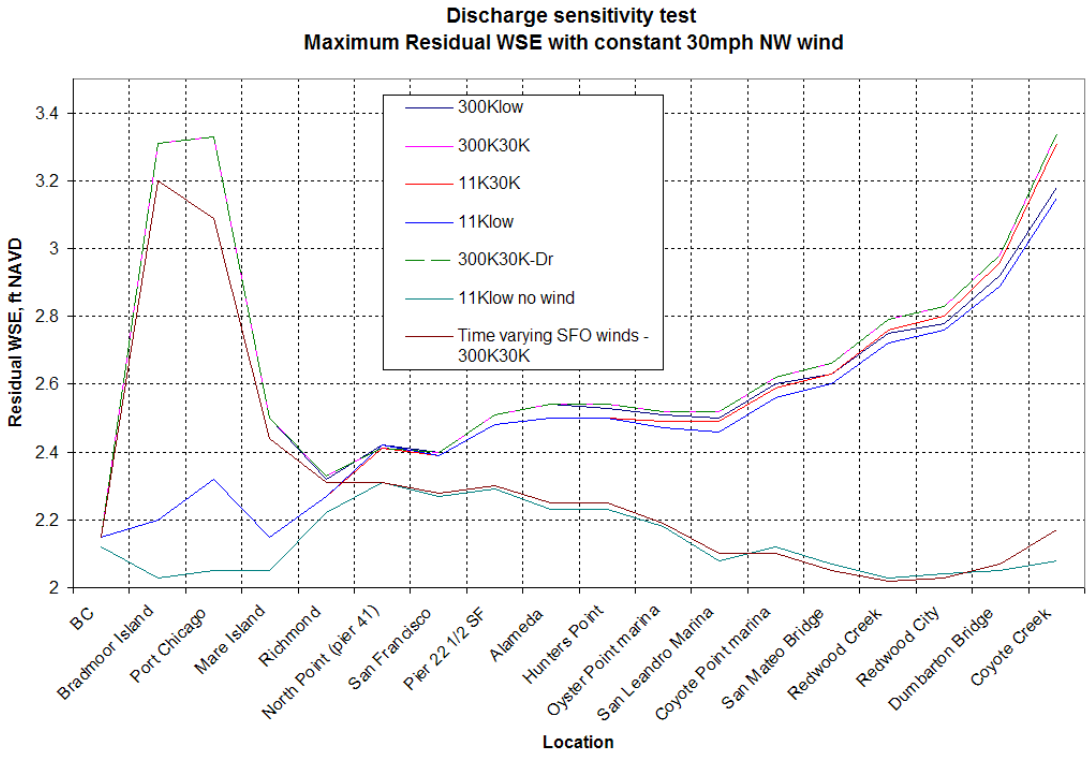

Figure 4-28. Sensitivity results for variation in tributary inflows.

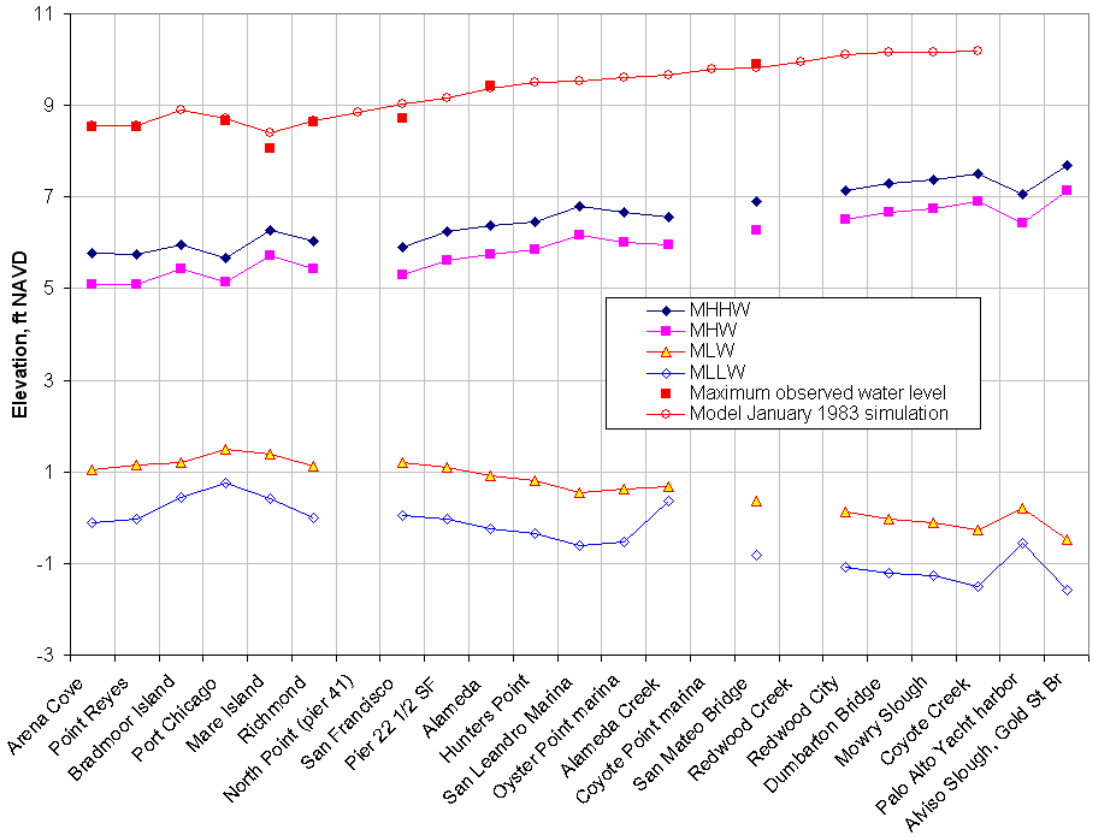

Figure 4-29. Model peak flood profile for the period of record event (January-February 1983).

5 Design of Model Production Runs

Conditional Sampling

The conditional sampling of storm events within the 105 year period of record at San Francisco (Presidio) identified 47 storm events, which had a predicted astronomical tide level greater than 5.5 ft and a peak residual surge level during the storm greater than 1.5 ft. These storm events were evaluated for development of a sequence of simulations that would create a database of events for incorporation into the statistical analysis of flooding potential (uncertainty analysis; Letter, 2009).

Selection of Storms

The long wave model production events are listed in Table 5-1. Many of the events were observed historical events. The earlier events, prior to 1975, had no observed wind data for development of wind forcing. Those events had the winds selected randomly from the observed data CDFs and then fixed. Additional events were simulated (designated by S* in the event column in Table 5-1) which were supplemental events developed to improve interpolation within the state space. These supplemental events were generally created by taking the largest residual surge signal (February 1998. 3.1 ft) and making the peak of the surge coincident with a variety of other observed tidal signals.

The coverage of the selected storms within the predicted tide versus residual tide possible combinations is presented graphically in Figure 5-1.

The total duration of the combined simulations performed for the production database is an extremely small percentage of the total period of record. However, this set of simulations covers the highest storm response events of the period of rec0rd.

The assumption implicitly made is that the impact flooding sensitivity for uncertainty in lower magnitude storm events is much lower than the flooding sensitivity to uncertainty in the largest events. The impact of the smaller events is generally low and the uncertainty in the estimated tidal response for those events will normally not change the fact that there is essentially no flooding impact for most of those events. For the higher magnitude events, when flooding impacts are large, the sensitivity to uncertainty may also be large.

Levee Breaching

The impact of levee breaching within the analysis is that a breach of an outboard levee will allow bay waters to enter the ponds and then attack the inboard levees. The number of possible combinations of breached conditions could not be realistically simulated for this project. Even simulations of single breaches at each critical outboard levee reach would have increased the modeling effort by an order of magnitude. Consequently, an approach was developed that simulated the long wave model with only two breach configurations: no breaches and all levees breached. The breach conditions were developed for each levee section based on the assumption that the breaches are at an equilibrium condition with respect to erodibility of the levee material and the shear stresses created by flow through the breach.

The evaluation of breach equilibrium geometry was made using an analytical model for flow through a tidal inlet and the associated energy loss. This estimated the peak velocity in the breach, which was converted to a shear stress. The dimensions of the breach were treated until the shear stresses in the breach matched the shear strength of the levee material. The development of the equilibrium breach geometry is described more completely in the uncertainty analysis documentation (Letter, 2009, in preparation).

The long-wave tidal model was applied in two modes for a series of production events designed to span the range of tides and wind conditions:

1. Without breaching

2. With breaching of the levees using the breach geometries as estimated by the analysis described above

The locations of the beaches in specific levees are shown in Figure 5-2. An example breach geometry is illustrated in Figure 5-3, for Pond A2W. The locations of the breaches were placed by the local conditions of the levee, the foreshore protection and the wave climate. The precise location of the breaches was not felt to be critical to the water elevations within the breached ponds.

Table 5-1. Production events for long wave model

Storm	Tidal condition		Peak Wind Condition		Historical event period	
	Astronomical Tide (ft NAVD)	Residual surge (ft)	Speed (mph)	Direction (deg N)		
1	6.43	1.63	68	200	1/28/1915	1/31/1915
2	6.24	1.12	31	260	2/1/1915	2/4/1915
3	6.37	1.09	73	135	2/7/1915	2/10/1915
4	5.89	0.9	47	0	1/30/1926	2/2/1926
5	5.35	0.94	46	190	2/2/1926	2/5/1926
6	6.15	1.19	42	270	12/16/1940	12/19/1940
7	6.75	1.39	41	180	12/23/1940	12/26/1940
8	7.06	1.32	32	200	1/15/1973	1/18/1973
9	7.07	1.11	10	160	1/17/1973	1/20/1973
10	5.58	1.16	17	300	1/17/1983	1/20/1983
11	6.26	1.47	29	200	1/22/1983	1/25/1983
12	7.12	1.97	34	200	1/26/1983	1/29/1983
13	7.21	1.27	20	230	1/28/1983	1/31/1983
14	6.65	2.26	48	300	12/2/1983	12/5/1983
15	5.95	1.72	49	255	11/25/1997	11/28/1997
16	5.59	1.5	47	220	12/5/1997	12/8/1997
17	6.16	1.89	23	120	2/2/1998	2/5/1998
18	6.28	2.25	31	200	2/4/1998	2/7/1998
19	6.37	2.16	25	200	2/6/1998	2/9/1998
20	5.58	3.1	39	150	S1	1/17/1983
21	5.58	2.4	51	225	S2	1/17/1983
22	6.65	3.1	37	170	S3	12/5/1983
23	7.21	3.1	47	270	S4	1/28/1983
24	7.21	2.4	60	225	S5	1/28/1983
25	6.65	1.58	54	140	S6	12/5/1983

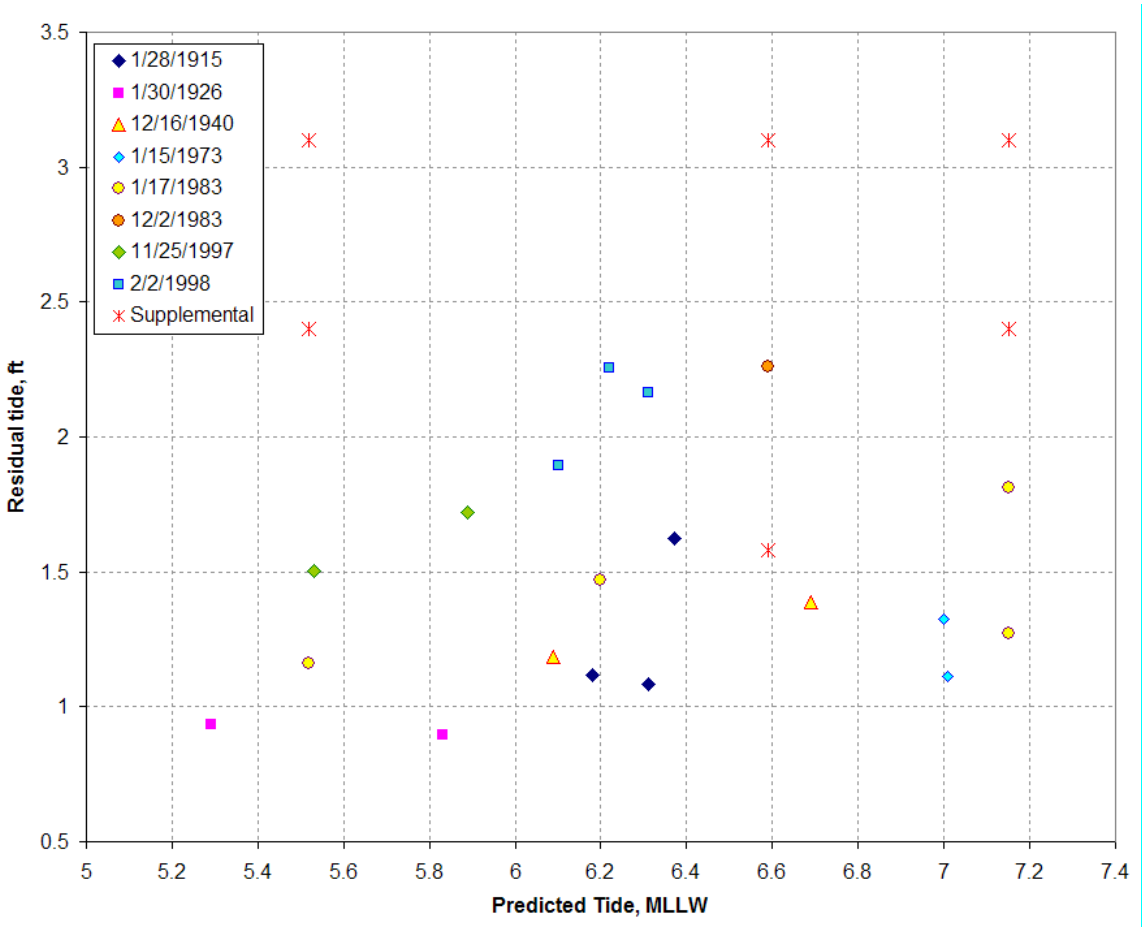

Figure 5-1. Production simulation combinations of predicted tide and residual tidal surge.

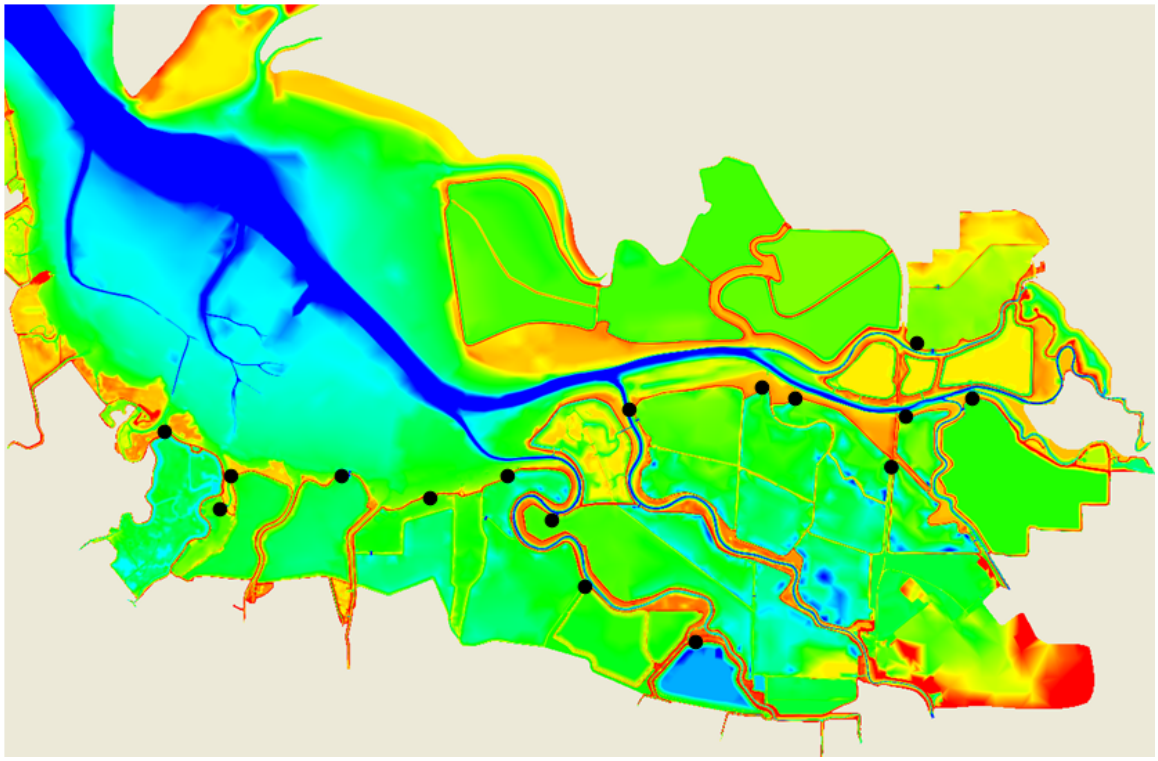

Figure 5-2. Location of levee breaches simulated for the with-breaches simulations.

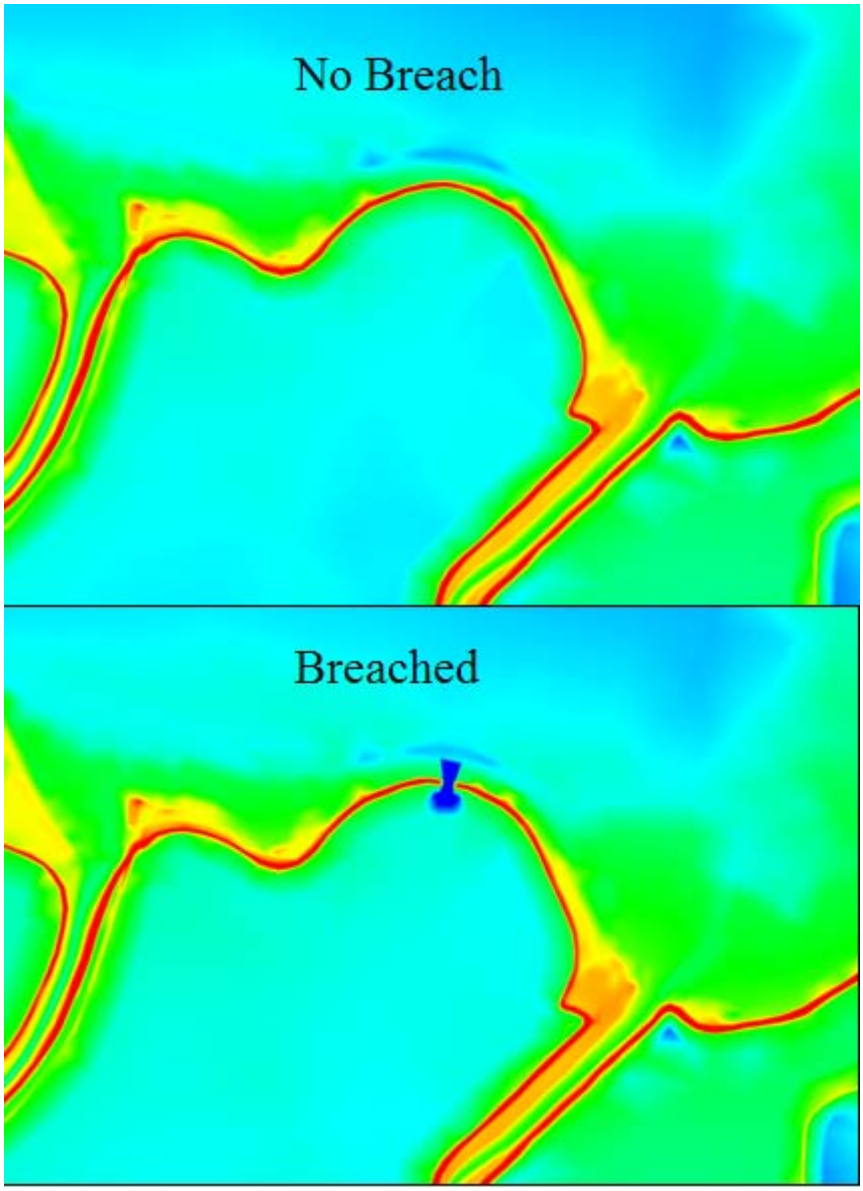

Figure 5-3. Comparison of the breached and no breached geometry in the Pond A2W outboard levee.

6 Year 0 Results

General Circulation

The general model circulation patterns, illustrating the spatial fidelity of the circulation are presented in Figures 6-1 through 6-4. Figure 6-1 presents the velocity magnitude contours with vectors for a flood tide for Central Bay and Northern South Bay, with a portion of the Pacific Ocean. The model flow distribution is largely controlled by the local bathymetry.

Figure 6-2 presents a contour of velocity magnitude for Far South Bay for the breached condition without vectors to illustrate the exchange through the breaches in the salt ponds for an ebb tide condition. The circulation patterns are for a single point in time and the overall circulation is extremely complex with tidal phasing affecting the timing of when each pond exchange peaks.

Figure 6-3 shows the exchange in the vicinity of Pons A6 for the breached condition at an ebb tide. This illustrates the flow patterns within the pond, the other nearby breached ponds and the adjacent tidal sloughs. Figure 6-4 shows the same general circulation in the vicinity of the Alviso ponds.

Model Response Database for Year 0

The simulation results for Year 0 bathymetry were analyzed for peak flood levels at specific locations selected for the statistical uncertainty analysis. Those locations are presented in Figure 6-5. The locations of those analysis stations used for the characterization of the long wave model results are presented in Table 6-1. The data base of responses for the events listed in Table 5-1 are presented in Tables 6-2 and 6-3 for simulations without and with breaches, respectively, for the Year 0 simulations. The event numbers are 1 through 25 for the no-breach conditions and 26 through 50, sequentially for the with beach conditions.

The database for the with breach condition was constructed such that for the forcing at the outboard levees, the flood levels used were the no-breach condition. This was done so that computations of overtopping used the full flood level attack potential. The differences between the breached and no-breach conditions

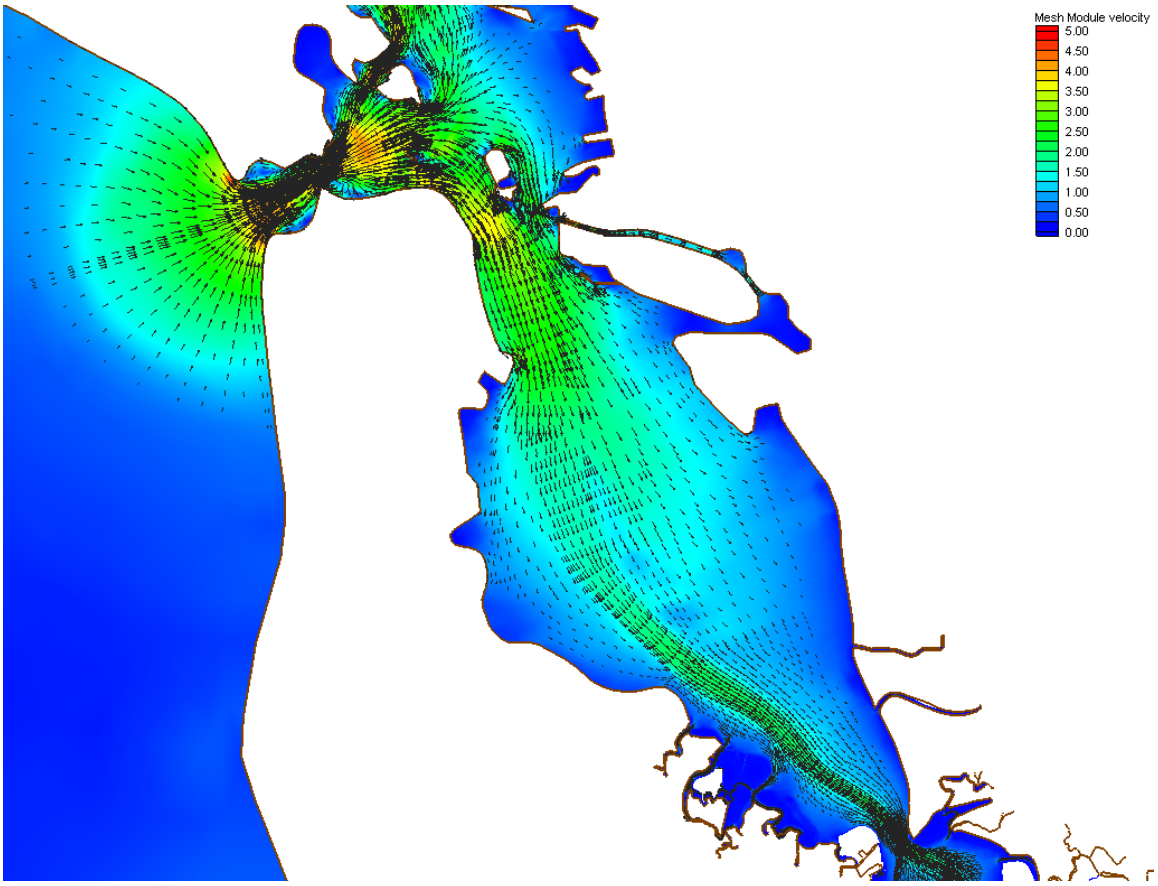

Figure 6-1. Example model circulation patterns in Central Bay and greater South Bay during a flood tide.

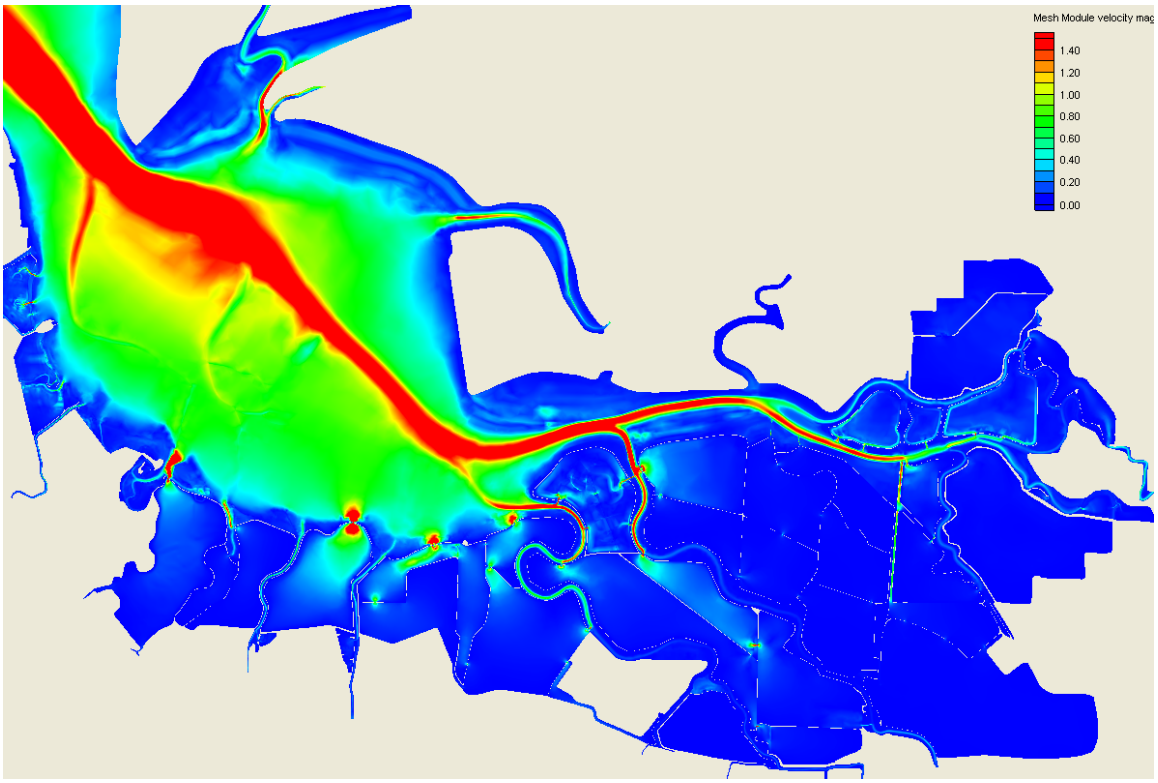

Figure 6-2. Velocity magnitude contours showing exchange with breached ponds during an ebb tide.

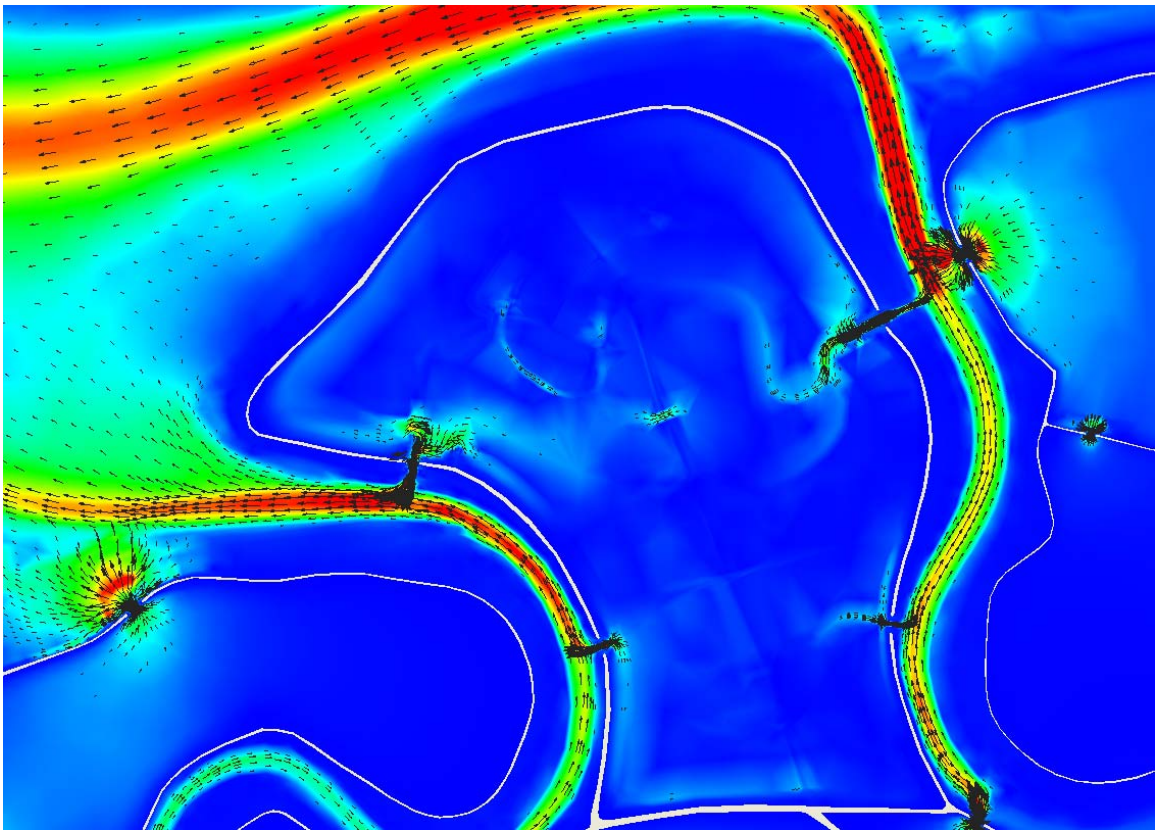

Figure 6-3. Current velocity magnitude contours with velocity vectors in the vicinity of Pond A6 during an ebb tide.

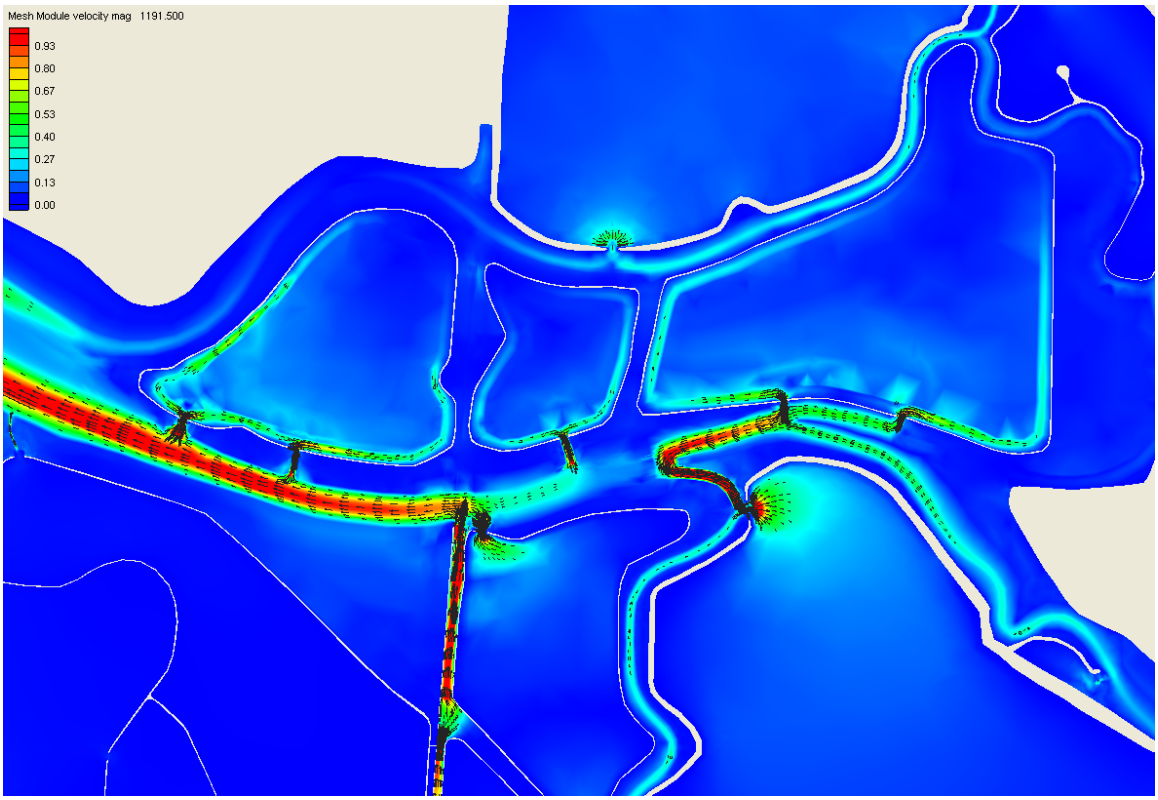

Figure 6-4. Tidal circulation in the vicinity of the Alviso ponds during an ebb tide for the breached condition.

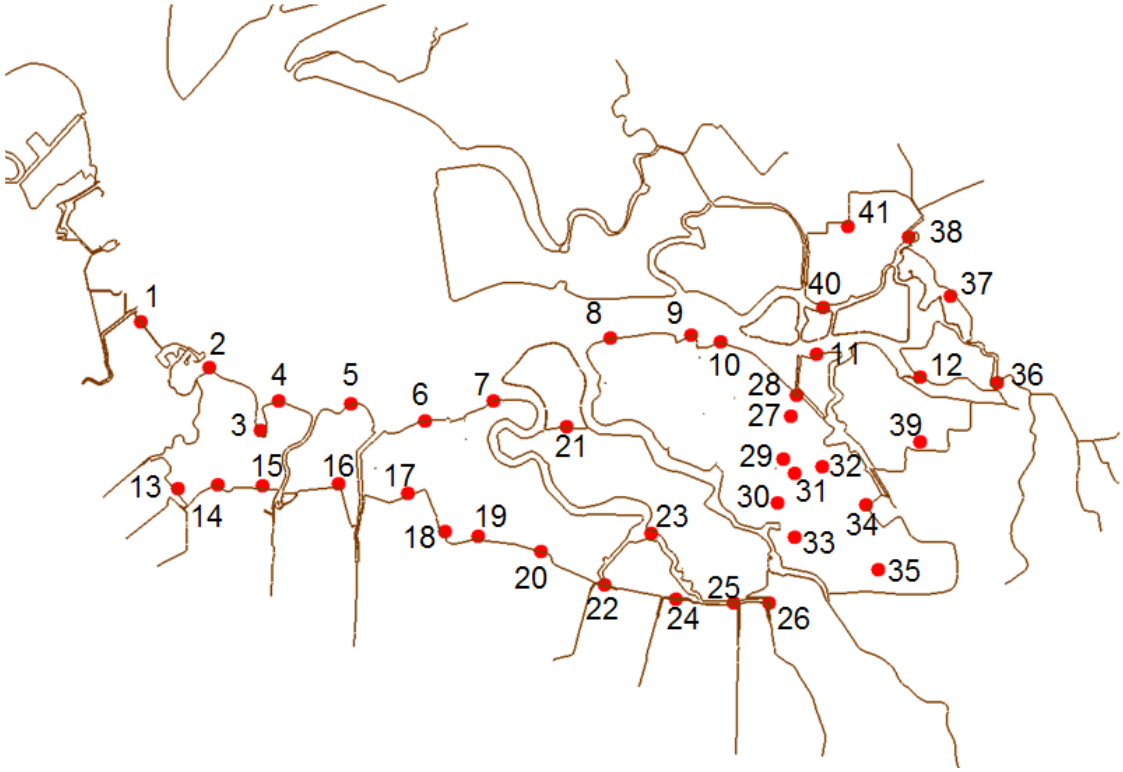

Figure 6-5. Locations of production simulation analysis for statistical database. See Table 6-1 for coordinates

Table 6-1. Long Wave Model station locations

Station ID	State plane NAD83 - CA zone 3 ft	
	Easting	Northing
1	6092774	1995360
2	6097020	1992464
3	6100097	1988699
4	6101317	1990413
5	6105771	1990309
6	6110484	1989257
7	6114638	1990465
8	6121974	1994295
9	6126933	1994503
10	6128790	1994100
11	6134723	1993269
12	6141163	1991841
13	6095021	1984999
14	6097565	1985181
15	6100175	1985090
16	6105121	1985194
17	6109250	1984687
18	6111652	1982376
19	6113768	1982000
20	6117676	1981091
21	6119234	1988894
22	6121558	1979027
23	6124440	1982169
24	6125985	1978157
25	6129569	1977884
26	6131802	1977858
27	6133087	1989452
28	6133490	1990764
29	6132763	1986713
30	6132308	1984012
31	6133386	1985882
32	6135281	1986375
33	6133373	1981974
34	6137917	1986583
35	6138573	1979793
36	6145973	1991556
37	6143117	1996931
38	6140468	2000566
39	6141440	1987950
40	6135195	1996204
41	6136679	2001231

Table 6-2. Long wave model responses for no breach condition for Year 0

Event ID	Breach	Station ID							
		1	2	3	4	5	6	7	8
1	0	7.176	7.187	7.214	7.197	7.208	7.218	7.240	7.261
2	0	7.723	7.735	7.765	7.746	7.758	7.770	7.793	7.816
3	0	7.903	7.916	7.951	7.930	7.943	7.956	7.983	8.009
4	0	8.077	8.089	8.119	8.101	8.112	8.124	8.148	8.171
5	0	8.562	8.577	8.615	8.591	8.606	8.620	8.650	8.679
6	0	8.620	8.635	8.674	8.650	8.665	8.680	8.710	8.740
7	0	8.775	8.790	8.831	8.806	8.822	8.837	8.869	8.900
8	0	8.808	8.822	8.857	8.835	8.849	8.862	8.890	8.917
9	0	8.998	9.014	9.053	9.029	9.044	9.059	9.089	9.119
10	0	8.963	8.975	9.005	8.986	8.998	9.010	9.033	9.056
11	0	9.276	9.291	9.329	9.306	9.320	9.335	9.364	9.393
12	0	9.400	9.416	9.457	9.432	9.448	9.464	9.496	9.527
13	0	9.614	9.632	9.677	9.649	9.667	9.684	9.720	9.755
14	0	9.789	9.808	9.858	9.827	9.846	9.865	9.904	9.942
15	0	9.662	9.679	9.724	9.696	9.713	9.730	9.765	9.799
16	0	9.984	10.004	10.053	10.023	10.042	10.061	10.099	10.137
17	0	10.147	10.167	10.219	10.187	10.207	10.227	10.267	10.306
18	0	9.807	9.822	9.862	9.837	9.852	9.868	9.898	9.928
19	0	9.845	9.860	9.901	9.876	9.892	9.907	9.939	9.970
20	0	9.663	9.675	9.705	9.686	9.698	9.710	9.733	9.756
21	0	10.342	10.359	10.404	10.376	10.393	10.410	10.445	10.479
22	0	10.687	10.707	10.759	10.727	10.747	10.767	10.807	10.846
23	0	11.277	11.297	11.349	11.317	11.337	11.357	11.397	11.436
24	0	11.182	11.199	11.244	11.216	11.233	11.250	11.285	11.319
25	0	11.977	11.997	12.049	12.017	12.037	12.057	12.097	12.136

Table 6-2. Long wave model responses for no breach condition for Year 0 (continued)

		Station ID							
Event ID	Breach	9	10	11	12	13	14	15	16
1	0	7.271	7.269	7.261	7.176	3.556	3.637	3.596	3.597
2	0	7.828	7.826	7.816	7.723	3.600	3.692	3.646	3.647
3	0	8.022	8.020	8.009	7.903	3.614	3.711	3.662	3.663
4	0	8.183	8.180	8.171	8.077	3.628	3.728	3.677	3.679
5	0	8.693	8.690	8.679	8.562	3.667	3.777	3.722	3.723
6	0	8.755	8.752	8.740	8.620	3.672	3.783	3.727	3.728
7	0	8.915	8.912	8.900	8.775	3.684	3.799	3.741	3.742
8	0	8.930	8.927	8.917	8.808	3.687	3.802	3.744	3.745
9	0	9.134	9.131	9.119	8.998	3.702	3.821	3.761	3.762
10	0	9.068	9.066	9.056	8.963	3.699	3.816	3.757	3.758
11	0	9.408	9.405	9.393	9.276	3.724	3.849	3.786	3.787
12	0	9.543	9.540	9.527	9.400	3.734	3.862	3.797	3.799
13	0	9.772	9.769	9.755	9.614	3.751	3.884	3.817	3.818
14	0	9.961	9.957	9.942	9.789	3.765	3.902	3.833	3.835
15	0	9.816	9.812	9.799	9.662	3.755	3.888	3.821	3.823
16	0	10.156	10.152	10.137	9.984	3.781	3.921	3.850	3.852
17	0	10.326	10.322	10.306	10.147	3.794	3.938	3.865	3.867
18	0	9.944	9.941	9.928	9.807	3.767	3.902	3.834	3.835
19	0	9.985	9.982	9.970	9.845	3.770	3.906	3.837	3.839
20	0	9.768	9.766	9.756	9.663	3.755	3.886	3.820	3.821
21	0	10.496	10.492	10.479	10.342	3.810	3.956	3.882	3.884
22	0	10.866	10.862	10.846	10.687	3.837	3.992	3.914	3.916
23	0	11.456	11.452	11.436	11.277	3.885	4.051	3.967	3.969
24	0	11.336	11.332	11.319	11.182	3.877	4.040	3.958	3.959
25	0	12.156	12.152	12.136	11.977	3.941	4.121	4.030	4.032

Table 6-2. Long wave model responses for no breach condition for Year 0 (continued)

Event ID	Breach	Station ID							
		17	18	19	20	21	22	23	24
1	0	3.638	3.618	3.480	3.440	7.040	7.092	7.134	7.081
2	0	3.693	3.670	3.513	3.468	7.565	7.629	7.676	7.618
3	0	3.712	3.688	3.525	3.477	7.745	7.797	7.850	7.784
4	0	3.728	3.704	3.534	3.485	7.902	7.983	8.030	7.971
5	0	3.778	3.751	3.565	3.510	8.379	8.446	8.504	8.431
6	0	3.784	3.757	3.568	3.514	8.437	8.500	8.560	8.485
7	0	3.800	3.772	3.578	3.521	8.587	8.649	8.712	8.634
8	0	3.802	3.774	3.579	3.522	8.607	8.700	8.754	8.686
9	0	3.822	3.793	3.591	3.532	8.797	8.878	8.938	8.863
10	0	3.817	3.788	3.588	3.530	8.743	8.869	8.916	8.858
11	0	3.849	3.819	3.607	3.546	9.058	9.160	9.218	9.145
12	0	3.862	3.831	3.615	3.553	9.183	9.272	9.336	9.256
13	0	3.884	3.852	3.629	3.564	9.396	9.474	9.544	9.456
14	0	3.903	3.869	3.640	3.573	9.570	9.635	9.712	9.616
15	0	3.889	3.857	3.631	3.566	9.438	9.526	9.594	9.509
16	0	3.922	3.888	3.652	3.583	9.756	9.832	9.908	9.813
17	0	3.939	3.904	3.662	3.591	9.915	9.989	10.068	9.969
18	0	3.903	3.870	3.639	3.573	9.565	9.685	9.746	9.670
19	0	3.907	3.873	3.642	3.575	9.604	9.719	9.782	9.704
20	0	3.887	3.855	3.630	3.565	9.408	9.569	9.616	9.558
21	0	3.957	3.921	3.672	3.600	10.084	10.206	10.274	10.189
22	0	3.993	3.955	3.694	3.618	10.428	10.529	10.608	10.509
23	0	4.052	4.011	3.729	3.648	10.989	11.119	11.198	11.099
24	0	4.041	4.001	3.723	3.642	10.882	11.046	11.114	11.029
25	0	4.122	4.078	3.771	3.683	11.654	11.819	11.898	11.799

Table 6-2. Long wave model responses for no breach condition for Year 0 (continued)

		Station ID							
Event ID	Breach	25	26	27	28	29	30	31	32
1	0	7.081	7.071	3.673	7.155	3.634	3.435	3.827	3.722
2	0	7.618	7.606	3.733	7.699	3.688	3.462	3.909	3.789
3	0	7.784	7.771	3.753	7.877	3.706	3.471	3.935	3.812
4	0	7.971	7.960	3.772	8.054	3.724	3.480	3.962	3.832
5	0	8.431	8.417	3.825	8.533	3.772	3.503	4.034	3.893
6	0	8.485	8.470	3.832	8.590	3.778	3.506	4.043	3.900
7	0	8.634	8.618	3.849	8.743	3.793	3.514	4.065	3.919
8	0	8.686	8.673	3.853	8.781	3.797	3.516	4.071	3.921
9	0	8.863	8.847	3.873	8.968	3.816	3.525	4.099	3.946
10	0	8.858	8.846	3.870	8.939	3.812	3.524	4.095	3.938
11	0	9.145	9.130	3.904	9.247	3.844	3.539	4.141	3.978
12	0	9.256	9.240	3.918	9.368	3.856	3.545	4.159	3.994
13	0	9.456	9.439	3.941	9.579	3.877	3.555	4.191	4.022
14	0	9.616	9.597	3.960	9.750	3.895	3.564	4.217	4.044
15	0	9.509	9.492	3.946	9.628	3.882	3.558	4.198	4.027
16	0	9.813	9.793	3.982	9.946	3.914	3.573	4.246	4.068
17	0	9.969	9.949	4.000	10.108	3.931	3.581	4.270	4.088
18	0	9.670	9.655	3.962	9.776	3.897	3.565	4.220	4.043
19	0	9.704	9.688	3.967	9.813	3.900	3.567	4.226	4.048
20	0	9.558	9.546	3.947	9.639	3.882	3.559	4.200	4.022
21	0	10.189	10.172	4.021	10.308	3.950	3.592	4.300	4.109
22	0	10.509	10.489	4.059	10.648	3.985	3.608	4.351	4.153
23	0	11.099	11.079	4.124	11.238	4.044	3.638	4.440	4.224
24	0	11.029	11.012	4.114	11.148	4.034	3.634	4.426	4.209
25	0	11.799	11.779	4.201	11.938	4.114	3.673	4.545	4.308

Table 6-2. Long wave model responses for no breach condition for Year 0 (concluded)

Event ID	Breach	Station ID								
		33	34	35	36	37	38	39	40	41
1	0	3.632	7.218	3.397	7.092	7.071	7.092	3.634		
2	0	3.686	7.770	3.418	7.629	7.606	7.629	3.688		
3	0	3.704	7.956	3.425	7.797	7.771	7.797	3.706		
4	0	3.721	8.124	3.433	7.983	7.960	7.983	3.724		
5	0	3.769	8.620	3.452	8.446	8.417	8.446	3.772		
6	0	3.775	8.680	3.454	8.500	8.470	8.500	3.778		
7	0	3.790	8.837	3.460	8.649	8.618	8.649	3.793		
8	0	3.794	8.862	3.462	8.700	8.673	8.700	3.797		
9	0	3.813	9.059	3.469	8.878	8.847	8.878	3.816		
10	0	3.810	9.010	3.468	8.869	8.846	8.869	3.812		
11	0	3.841	9.335	3.480	9.160	9.130	9.160	3.844		
12	0	3.853	9.464	3.485	9.272	9.240	9.272	3.856		
13	0	3.874	9.684	3.494	9.474	9.439	9.474	3.877		
14	0	3.891	9.865	3.500	9.635	9.597	9.635	3.895		
15	0	3.879	9.730	3.496	9.526	9.492	9.526	3.882		
16	0	3.911	10.061	3.508	9.832	9.793	9.832	3.914		
17	0	3.927	10.227	3.515	9.989	9.949	9.989	3.931		
18	0	3.894	9.868	3.501	9.685	9.655	9.685	3.897		
19	0	3.897	9.907	3.503	9.719	9.688	9.719	3.900		
20	0	3.880	9.710	3.496	9.569	9.546	9.569	3.882		
21	0	3.947	10.410	3.523	10.206	10.172	10.206	3.950		
22	0	3.981	10.767	3.536	10.529	10.489	10.529	3.985		
23	0	4.040	11.357	3.560	11.119	11.079	11.119	4.044		
24	0	4.031	11.250	3.556	11.046	11.012	11.046	4.034		
25	0	4.110	12.057	3.588	11.819	11.779	11.819	4.114		

Table 6-3. Long wave model responses for with breach condition for Year 0

Event ID	Breach	Station ID							
		1	2	3	4	5	6	7	8
26	1	7.176	7.187	7.214	7.197	7.208	7.218	7.240	7.261
27	1	7.723	7.735	7.765	7.746	7.758	7.770	7.793	7.816
28	1	7.903	7.916	7.951	7.930	7.943	7.956	7.983	8.009
29	1	8.077	8.089	8.119	8.101	8.112	8.124	8.148	8.171
30	1	8.562	8.577	8.615	8.591	8.606	8.620	8.650	8.679
31	1	8.620	8.635	8.674	8.650	8.665	8.680	8.710	8.740
32	1	8.775	8.790	8.831	8.806	8.822	8.837	8.869	8.900
33	1	8.808	8.822	8.857	8.835	8.849	8.862	8.890	8.917
34	1	8.998	9.014	9.053	9.029	9.044	9.059	9.089	9.119
35	1	8.963	8.975	9.005	8.986	8.998	9.010	9.033	9.056
36	1	9.276	9.291	9.329	9.306	9.320	9.335	9.364	9.393
37	1	9.400	9.416	9.457	9.432	9.448	9.464	9.496	9.527
38	1	9.614	9.632	9.677	9.649	9.667	9.684	9.720	9.755
39	1	9.789	9.808	9.858	9.827	9.846	9.865	9.904	9.942
40	1	9.662	9.679	9.724	9.696	9.713	9.730	9.765	9.799
41	1	9.984	10.004	10.053	10.023	10.042	10.061	10.099	10.137
42	1	10.147	10.167	10.219	10.187	10.207	10.227	10.267	10.306
43	1	9.807	9.822	9.862	9.837	9.852	9.868	9.898	9.928
44	1	9.845	9.860	9.901	9.876	9.892	9.907	9.939	9.970
45	1	9.663	9.675	9.705	9.686	9.698	9.710	9.733	9.756
46	1	10.342	10.359	10.404	10.376	10.393	10.410	10.445	10.479
47	1	10.687	10.707	10.759	10.727	10.747	10.767	10.807	10.846
48	1	11.277	11.297	11.349	11.317	11.337	11.357	11.397	11.436
49	1	11.182	11.199	11.244	11.216	11.233	11.250	11.285	11.319
50	1	11.977	11.997	12.049	12.017	12.037	12.057	12.097	12.136

Table 6-3. Long wave model responses for with breach condition for Year 0 (continued)

		Station ID							
Event ID	Breach	9	10	11	12	13	14	15	16
26	1	7.271	7.269	7.261	7.176	6.595	6.817	6.643	6.573
27	1	7.828	7.826	7.816	7.723	7.060	7.312	7.115	7.035
28	1	8.022	8.020	8.009	7.903	7.215	7.480	7.273	7.190
29	1	8.183	8.180	8.171	8.077	7.361	7.631	7.420	7.333
30	1	8.693	8.690	8.679	8.562	7.776	8.077	7.842	7.747
31	1	8.755	8.752	8.740	8.620	7.826	8.131	7.893	7.797
32	1	8.915	8.912	8.900	8.775	7.958	8.272	8.027	7.929
33	1	8.930	8.927	8.917	8.808	7.984	8.295	8.052	7.951
34	1	9.134	9.131	9.119	8.998	8.147	8.471	8.218	8.115
35	1	9.068	9.066	9.056	8.963	8.114	8.428	8.182	8.077
36	1	9.408	9.405	9.393	9.276	8.383	8.720	8.456	8.347
37	1	9.543	9.540	9.527	9.400	8.489	8.835	8.565	8.454
38	1	9.772	9.769	9.755	9.614	8.673	9.034	8.752	8.639
39	1	9.961	9.957	9.942	9.789	8.823	9.196	8.905	8.789
40	1	9.816	9.812	9.799	9.662	8.713	9.075	8.792	8.678
41	1	10.156	10.152	10.137	9.984	8.989	9.372	9.073	8.953
42	1	10.326	10.322	10.306	10.147	9.128	9.521	9.215	9.092
43	1	9.944	9.941	9.928	9.807	8.835	9.199	8.914	8.794
44	1	9.985	9.982	9.970	9.845	8.867	9.235	8.947	8.827
45	1	9.768	9.766	9.756	9.663	8.709	9.058	8.784	8.665
46	1	10.496	10.492	10.479	10.342	9.291	9.687	9.377	9.249
47	1	10.866	10.862	10.846	10.687	9.587	10.007	9.679	9.546
48	1	11.456	11.452	11.436	11.277	10.089	10.538	10.186	10.041
49	1	11.336	11.332	11.319	11.182	10.005	10.443	10.100	9.954
50	1	12.156	12.152	12.136	11.977	10.684	11.168	10.788	10.629

Table 6-3. Long wave model responses for with breach condition for Year 0 (continued)

		Station ID							
Event ID	Breach	17	18	19	20	21	22	23	24
26	1	6.582	6.622	6.560	6.520	11.654	11.819	11.898	11.799
27	1	7.045	7.090	7.019	6.973	7.040	7.092	7.134	7.081
28	1	7.201	7.249	7.176	7.129	7.565	7.629	7.676	7.618
29	1	7.343	7.391	7.313	7.264	7.745	7.797	7.850	7.784
30	1	7.760	7.813	7.730	7.676	7.902	7.983	8.030	7.971
31	1	7.810	7.864	7.780	7.725	8.379	8.446	8.504	8.431
32	1	7.942	7.998	7.912	7.855	8.437	8.500	8.560	8.485
33	1	7.963	8.019	7.929	7.873	8.587	8.649	8.712	8.634
34	1	8.128	8.186	8.095	8.036	8.607	8.700	8.754	8.686
35	1	8.086	8.144	8.048	7.990	8.797	8.878	8.938	8.863
36	1	8.360	8.421	8.323	8.262	8.743	8.869	8.916	8.858
37	1	8.468	8.530	8.432	8.370	9.058	9.160	9.218	9.145
38	1	8.653	8.718	8.618	8.553	9.183	9.272	9.336	9.256
39	1	8.805	8.871	8.771	8.704	9.396	9.474	9.544	9.456
40	1	8.692	8.757	8.655	8.590	9.570	9.635	9.712	9.616
41	1	8.969	9.038	8.933	8.864	9.438	9.526	9.594	9.509
42	1	9.109	9.179	9.072	9.002	9.756	9.832	9.908	9.813
43	1	8.807	8.873	8.766	8.700	9.915	9.989	10.068	9.969
44	1	8.840	8.907	8.800	8.733	9.565	9.685	9.746	9.670
45	1	8.674	8.739	8.629	8.564	9.604	9.719	9.782	9.704
46	1	9.263	9.335	9.220	9.148	9.408	9.569	9.616	9.558
47	1	9.563	9.638	9.520	9.445	10.084	10.206	10.274	10.189
48	1	10.058	10.139	10.010	9.928	10.428	10.529	10.608	10.509
49	1	9.969	10.049	9.917	9.836	10.989	11.119	11.198	11.099
50	1	10.646	10.734	10.591	10.502	10.882	11.046	11.114	11.029

Table 6-3. Long wave model responses for with breach condition for Year 0 (continued)

		Station ID							
Event ID	Breach	25	26	27	28	29	30	31	32
26	1	11.799	11.779	4.201	11.938	4.114	3.673	4.545	4.308
27	1	7.081	7.071	6.586	7.155	6.546	6.472	6.568	6.859
28	1	7.618	7.606	7.050	7.699	7.006	6.922	7.030	7.359
29	1	7.784	7.771	7.204	7.877	7.157	7.066	7.181	7.532
30	1	7.971	7.960	7.351	8.054	7.303	7.216	7.331	7.678
31	1	8.431	8.417	7.764	8.533	7.711	7.609	7.739	8.135
32	1	8.485	8.470	7.813	8.590	7.759	7.656	7.788	8.190
33	1	8.634	8.618	7.944	8.743	7.889	7.782	7.918	8.334
34	1	8.686	8.673	7.973	8.781	7.917	7.817	7.950	8.349
35	1	8.863	8.847	8.135	8.968	8.077	7.969	8.109	8.531
36	1	8.858	8.846	8.104	8.939	8.047	7.951	8.084	8.475
37	1	9.145	9.130	8.371	9.247	8.311	8.202	8.346	8.778
38	1	9.256	9.240	8.476	9.368	8.414	8.300	8.449	8.899
39	1	9.456	9.439	8.658	9.579	8.594	8.472	8.628	9.103
40	1	9.616	9.597	8.806	9.750	8.741	8.612	8.774	9.272
41	1	9.509	9.492	8.699	9.628	8.635	8.514	8.670	9.143
42	1	9.813	9.793	8.973	9.946	8.905	8.774	8.940	9.447
43	1	9.969	9.949	9.111	10.108	9.042	8.907	9.078	9.600
44	1	9.670	9.655	8.822	9.776	8.756	8.640	8.796	9.260
45	1	9.704	9.688	8.854	9.813	8.788	8.670	8.827	9.297
46	1	9.558	9.546	8.699	9.639	8.635	8.532	8.679	9.105
47	1	10.189	10.172	9.277	10.308	9.206	9.078	9.248	9.755
48	1	10.509	10.489	9.570	10.648	9.496	9.355	9.537	10.086
49	1	11.099	11.079	10.072	11.238	9.991	9.845	10.038	10.617
50	1	11.029	11.012	9.991	11.148	9.911	9.775	9.962	10.511

Table 6-3. Long wave model responses for with breach condition for Year 0 (concluded)

Event ID	Breach	Station ID								
		33	34	35	36	37	38	39	40	41
26	1	6.450	7.218	6.372	7.092	7.071	7.092	6.625	7.094	6.420
27	1	6.897	7.770	6.808	7.629	7.606	7.629	7.095	7.632	6.862
28	1	7.042	7.956	6.949	7.797	7.771	7.797	7.250	7.800	7.006
29	1	7.187	8.124	7.091	7.983	7.960	7.983	7.400	7.985	7.148
30	1	7.580	8.620	7.474	8.446	8.417	8.446	7.817	8.449	7.539
31	1	7.627	8.680	7.520	8.500	8.470	8.500	7.867	8.503	7.586
32	1	7.753	8.837	7.643	8.649	8.618	8.649	8.000	8.653	7.710
33	1	7.784	8.862	7.673	8.700	8.673	8.700	8.029	8.703	7.739
34	1	7.937	9.059	7.823	8.878	8.847	8.878	8.192	8.881	7.892
35	1	7.914	9.010	7.800	8.869	8.846	8.869	8.162	8.872	7.866
36	1	8.166	9.335	8.046	9.160	9.130	9.160	8.431	9.163	8.118
37	1	8.265	9.464	8.142	9.272	9.240	9.272	8.537	9.275	8.217
38	1	8.438	9.684	8.311	9.474	9.439	9.474	8.722	9.477	8.389
39	1	8.578	9.865	8.448	9.635	9.597	9.635	8.872	9.639	8.529
40	1	8.478	9.730	8.350	9.526	9.492	9.526	8.763	9.529	8.428
41	1	8.739	10.061	8.605	9.832	9.793	9.832	9.040	9.835	8.687
42	1	8.872	10.227	8.734	9.989	9.949	9.989	9.180	9.993	8.819
43	1	8.600	9.868	8.469	9.685	9.655	9.685	8.887	9.688	8.547
44	1	8.630	9.907	8.499	9.719	9.688	9.719	8.920	9.723	8.577
45	1	8.488	9.710	8.360	9.569	9.546	9.569	8.764	9.572	8.433
46	1	9.036	10.410	8.894	10.206	10.172	10.206	9.348	10.209	8.979
47	1	9.314	10.767	9.166	10.529	10.489	10.529	9.645	10.533	9.256
48	1	9.798	11.357	9.638	11.119	11.079	11.119	10.152	11.123	9.734
49	1	9.725	11.250	9.566	11.046	11.012	11.046	10.070	11.049	9.659
50	1	10.372	12.057	10.198	11.819	11.779	11.819	10.754	11.823	10.301

7 Year 50 Results

Year 50 NRC curve I Response Database

Model simulations for the Year 0 conditions were performed with two primary revisions to the model simulations performed for Year 0. First, the bathymetry was updated based on the sediment transport modeling of Brown (2010) to reflect the changes in bathymetry associated with a sea level change using the NRC curve I (see Figure 7-1). Secondly, all of the tidal boundary conditions used in the model simulations (see Table 5-1) were raised by the differential sea level between Year 0 and Year 50 for the NRC curve I (0.72 ft).

The simulation results for Year 50 bathymetry were also analyzed for peak flood levels at the same specific locations selected for Year 0 for the statistical uncertainty analysis. Those locations were presented in Figure 6-1. The locations of those analysis stations used for the characterization of the long wave model results were presented in Table 6-1. The data base of responses for the events listed in Table 5-1, with the associated increase in sea level, are presented in Tables 7-1 and 7-2 for simulations without and with breaches, respectively, for the Year 50 simulations. The event numbers are 1 through 25 for the no-breach conditions and 26 through 50, sequentially for the with beach conditions.

Sensitivity of Year 50 Long Wave Model to Bathymetric Projection

The bathymetric differences from Year 0 through Year 50 were developed using the assumption that sea level rise would be at the rate of the NRC curve I (NRC, 1987). The changes in bathymetry were based on numerical sediment model simulations (Brown, 2010) that evaluated the sediment supply requirements t maintain plan form equilibrium of the local bathymetry in far South Bay relative to a rising mean sea level. Based on the estimated sediment budget for the system it was determined that for up to the NRC curve I that plan form equilibrium is a reasonable assumption.

However, if the sea level rise proceeds more rapidly, e.g. at the NRC curve III rates, then the assumption of adequate sediment supply may break down. Brown (2010) evaluated this possibility and developed an alternate bathymetry projection for NRC curve III that does not have adequate sediment supply (see Figure 7-2).

In order to evaluate the sensitivity of the projected flood levels at Year 50 to the projected bathymetric condition, a series of sensitivity simulations in the long wave model were performed. Each of the sensitivity simulations were made for the January 1983 storm of record. Three simulations were used in this sensitivity analysis, summarized in Table 7-3. The first simulation was the one that was used in the Year 50 response database, using the NRC curve I sea level rise for both the bathymetry estimate (Figure 7-1) and the mean water level for the tidal boundary conditions. The two additional simulations both used the NRC curve III bathymetry (Figure 7-2). The test ID B3T1 used the tidal mean water level at the NRC curve I level and B3T3 used the NRC curve III mean tide level at Year 50.

The time series results of the three simulations at the Presidio, Dumbarton Bridge and Pond A2 are shown in Figures 7-3 through 7 5, respectively. Also include in the plots are the differences between the B3T1 and B1T1 and between B3T3 and B1T1. The adjusted difference between B3T3 and B1T1 for the differential mean water level is also plotted. These figures show the largest differences at mid tide level and the smallest differences near the peak water levels for each tidal high water. The differences at the Presidio are very small. The differences at Pond A2 outboard levee are relatively large at low water, showing the effects of the bathymetric changes in shallow water. However, the differences at the peak water level re relatively small.

Test B3T1 serves to identify the effects of the change in bathymetry for the same tidal condition. Table 7-4 presents a summary of the results of the sensitivity simulations on the peak water levels at five locations. The conditions at the ocean boundary condition series to clarify the conditions of each simulation. The results at the Presidio provide some measure of the overall sensitivity of the bathymetry to the global San Francisco Bay. The results at Dumbarton Bridge, the outboard levee at Pond A2 and the mouth of Coyote Creek serve to quantify the effects on the project area.

Included in Table 7-4 are the adjusted results of test B3T3 by subtracting the differential sea level (2.13-0.72=1.41) to see how linear the response is to sea level change. At the Presidio the shifted response for B3T3 is within 0.01 ft of the B3T1 peak and 0.02 ft of B1T1 peak. The levels are also within 0.02 ft for Dumbarton Bridge and Pond A2. At the mouth of Coyote Creek the nonlinearity of the system raised the water level for B3T3 0.1 ft above B3T1.

In order to more clearly identify the uncertainty of these results on the Monte Carlo analysis (Letter, 2010) the specific period of record storm was processed

by the Monte Carlo interpolation routine for the increased sea level associated with NRC curve III. These results are also included in Table 7-4. The entry Test ID of MC-B1T1 is based on the full long wave model response database developed for Year 50, using the NRC curve I bathymetry and mean tidal levels. The Test ID MC-B0T0 is the Year 0 response database.

The peak level entered at the Presidio is simply the defined event for the Monte Carlo interpolation and not an output. The Monte Carlo interpolated response at Dumbarton Bridge gives the same peak water level (12.16 ft NAVD) using either the Year 0 or the Year 50 database. The mouth of Coyote Creek results show that the Year 0 database overpredicts the response by only 0.03 ft compared to the Year 50 database. Both of the Monte Carlo estimates are within 0.2 ft of the B3T3 simulation using the NRC curve III bathymetry and mean tide level.

Table 7-4 summarizes the evaluation by computing an average and standard deviation of these estimates of the response for each of the period of record storms at both NRC curves I and III mean sea levels for year 50. At all stations the standard deviations are less than 0.1 ft.

Table 7-1. Long wave model responses for no breach condition for Year 50

		Station ID							
Event ID	Breach	1	2	3	4	5	6	7	8
1	0	8.014	8.025	8.053	8.036	8.047	8.058	8.079	8.101
2	0	8.577	8.589	8.621	8.601	8.613	8.625	8.650	8.674
3	0	8.763	8.777	8.812	8.790	8.804	8.817	8.845	8.872
4	0	8.942	8.954	8.986	8.966	8.978	8.991	9.015	9.039
5	0	9.442	9.457	9.496	9.472	9.487	9.502	9.532	9.562
6	0	9.501	9.517	9.557	9.532	9.548	9.563	9.594	9.625
7	0	9.661	9.677	9.719	9.693	9.709	9.725	9.757	9.790
8	0	9.695	9.709	9.745	9.723	9.737	9.751	9.779	9.807
9	0	9.891	9.907	9.947	9.922	9.938	9.953	9.984	10.016
10	0	9.854	9.867	9.898	9.879	9.891	9.903	9.927	9.951
11	0	10.177	10.193	10.232	10.208	10.223	10.238	10.268	10.298
12	0	10.305	10.321	10.364	10.337	10.354	10.370	10.403	10.436
13	0	10.525	10.544	10.591	10.562	10.580	10.598	10.634	10.670
14	0	10.705	10.725	10.776	10.745	10.764	10.784	10.823	10.863
15	0	10.575	10.592	10.638	10.610	10.628	10.645	10.680	10.715
16	0	10.907	10.926	10.978	10.946	10.966	10.985	11.025	11.064
17	0	11.075	11.095	11.148	11.116	11.136	11.156	11.197	11.238
18	0	10.724	10.739	10.780	10.755	10.771	10.786	10.818	10.849
19	0	10.763	10.779	10.821	10.795	10.811	10.827	10.859	10.892
20	0	10.575	10.588	10.619	10.600	10.612	10.624	10.648	10.672
21	0	11.275	11.293	11.338	11.310	11.328	11.346	11.381	11.416
22	0	11.631	11.651	11.704	11.672	11.692	11.713	11.753	11.794
23	0	12.239	12.259	12.312	12.279	12.300	12.320	12.361	12.402
24	0	12.140	12.158	12.204	12.176	12.193	12.211	12.246	12.281
25	0	12.960	12.980	13.033	13.000	13.021	13.041	13.082	13.123

Table 7-1. Long wave model responses for no breach condition for Year 50 (continued)

Event ID	Breach	Station ID							
		9	10	11	12	13	14	15	16
1	0	8.112	8.110	8.101	8.014	4.285	4.369	4.327	4.328
2	0	8.686	8.683	8.674	8.577	4.330	4.426	4.378	4.379
3	0	8.886	8.883	8.872	8.763	4.345	4.445	4.395	4.396
4	0	9.051	9.049	9.039	8.942	4.360	4.463	4.411	4.412
5	0	9.577	9.574	9.562	9.442	4.400	4.514	4.456	4.457
6	0	9.640	9.637	9.625	9.501	4.405	4.520	4.462	4.463
7	0	9.806	9.802	9.790	9.661	4.417	4.536	4.476	4.477
8	0	9.821	9.818	9.807	9.695	4.420	4.539	4.479	4.480
9	0	10.031	10.028	10.016	9.891	4.436	4.559	4.497	4.498
10	0	9.963	9.961	9.951	9.854	4.433	4.554	4.493	4.494
11	0	10.313	10.310	10.298	10.177	4.459	4.587	4.522	4.524
12	0	10.452	10.449	10.436	10.305	4.469	4.600	4.534	4.535
13	0	10.688	10.684	10.670	10.525	4.487	4.623	4.554	4.556
14	0	10.883	10.879	10.863	10.705	4.501	4.642	4.571	4.572
15	0	10.733	10.729	10.715	10.575	4.491	4.628	4.558	4.560
16	0	11.084	11.080	11.064	10.907	4.517	4.662	4.589	4.591
17	0	11.259	11.255	11.238	11.075	4.531	4.679	4.604	4.606
18	0	10.865	10.862	10.849	10.724	4.502	4.642	4.572	4.573
19	0	10.908	10.905	10.892	10.763	4.506	4.646	4.575	4.577
20	0	10.684	10.682	10.672	10.575	4.490	4.626	4.558	4.559
21	0	11.433	11.430	11.416	11.275	4.547	4.698	4.622	4.623
22	0	11.815	11.811	11.794	11.631	4.575	4.734	4.654	4.656
23	0	12.423	12.418	12.402	12.239	4.624	4.795	4.709	4.711
24	0	12.299	12.295	12.281	12.140	4.616	4.784	4.699	4.701
25	0	13.144	13.139	13.123	12.960	4.682	4.867	4.774	4.775

Table 7-1. Long wave model responses for no breach condition for Year 50 (continued)

		Station ID							
Event ID	Breach	17	18	19	20	21	22	23	24
1	0	4.370	4.349	4.207	4.166	7.874	7.927	7.971	7.916
2	0	4.427	4.403	4.241	4.194	8.415	8.481	8.529	8.469
3	0	4.446	4.421	4.253	4.204	8.601	8.654	8.708	8.640
4	0	4.463	4.438	4.263	4.213	8.762	8.845	8.894	8.833
5	0	4.514	4.486	4.294	4.239	9.253	9.322	9.382	9.307
6	0	4.520	4.492	4.298	4.242	9.312	9.378	9.440	9.362
7	0	4.537	4.508	4.308	4.250	9.467	9.532	9.596	9.516
8	0	4.539	4.510	4.309	4.251	9.488	9.584	9.639	9.570
9	0	4.559	4.529	4.321	4.261	9.683	9.767	9.829	9.751
10	0	4.554	4.525	4.318	4.258	9.628	9.758	9.806	9.746
11	0	4.588	4.556	4.338	4.275	9.952	10.057	10.117	10.042
12	0	4.601	4.569	4.347	4.282	10.081	10.173	10.239	10.157
13	0	4.624	4.591	4.360	4.294	10.300	10.381	10.453	10.363
14	0	4.642	4.608	4.372	4.303	10.480	10.547	10.626	10.528
15	0	4.629	4.595	4.363	4.296	10.344	10.434	10.505	10.417
16	0	4.663	4.627	4.384	4.313	10.672	10.749	10.828	10.730
17	0	4.680	4.644	4.394	4.322	10.835	10.911	10.993	10.891
18	0	4.643	4.609	4.371	4.303	10.475	10.599	10.661	10.583
19	0	4.647	4.612	4.374	4.305	10.514	10.634	10.698	10.618
20	0	4.626	4.593	4.361	4.294	10.313	10.479	10.527	10.467
21	0	4.699	4.662	4.405	4.331	11.010	11.135	11.205	11.117
22	0	4.735	4.696	4.428	4.350	11.364	11.467	11.549	11.447
23	0	4.796	4.754	4.464	4.380	11.941	12.075	12.157	12.055
24	0	4.785	4.744	4.457	4.374	11.832	12.000	12.070	11.982
25	0	4.868	4.823	4.507	4.416	12.626	12.796	12.878	12.776

Table 7-1. Long wave model responses for no breach condition for Year 50 (continued)

Event ID	Breach	Station ID 25	26	27	28	29	30	31	32
1	0	7.916	7.906	4.406	7.993	4.365	4.161	4.565	4.457
2	0	8.469	8.457	4.468	8.553	4.422	4.188	4.649	4.526
3	0	8.640	8.626	4.488	8.736	4.440	4.197	4.676	4.549
4	0	8.833	8.821	4.508	8.918	4.458	4.207	4.704	4.569
5	0	9.307	9.292	4.563	9.412	4.508	4.231	4.778	4.632
6	0	9.362	9.347	4.570	9.471	4.514	4.234	4.787	4.640
7	0	9.516	9.499	4.587	9.628	4.530	4.242	4.810	4.660
8	0	9.570	9.556	4.591	9.667	4.534	4.244	4.816	4.662
9	0	9.751	9.736	4.612	9.860	4.553	4.253	4.845	4.687
10	0	9.746	9.734	4.608	9.830	4.549	4.252	4.841	4.679
11	0	10.042	10.027	4.644	10.147	4.582	4.268	4.888	4.721
12	0	10.157	10.140	4.658	10.272	4.594	4.274	4.907	4.737
13	0	10.363	10.345	4.682	10.489	4.617	4.285	4.939	4.765
14	0	10.528	10.508	4.702	10.666	4.635	4.293	4.966	4.788
15	0	10.417	10.399	4.688	10.540	4.621	4.287	4.947	4.771
16	0	10.730	10.710	4.724	10.867	4.655	4.303	4.996	4.812
17	0	10.891	10.870	4.743	11.034	4.671	4.312	5.021	4.833
18	0	10.583	10.567	4.704	10.692	4.636	4.295	4.970	4.787
19	0	10.618	10.602	4.708	10.730	4.640	4.297	4.976	4.792
20	0	10.467	10.455	4.688	10.551	4.622	4.288	4.949	4.765
21	0	11.117	11.100	4.765	11.240	4.692	4.322	5.052	4.855
22	0	11.447	11.426	4.804	11.590	4.727	4.339	5.104	4.900
23	0	12.055	12.034	4.871	12.198	4.788	4.370	5.196	4.973
24	0	11.982	11.965	4.860	12.105	4.778	4.366	5.182	4.959
25	0	12.776	12.755	4.950	12.919	4.860	4.406	5.304	5.060

Table 7-1. Long wave model responses for no breach condition for Year 50 (concluded)

Event ID	Breach	Station ID								
		33	34	35	36	37	38	39	40	41
1	0	4.363	8.058	4.121	7.927	7.906	7.092	3.634	7.930	4.081
2	0	4.419	8.625	4.144	8.481	8.457	7.629	3.688	8.483	4.098
3	0	4.438	8.817	4.151	8.654	8.626	7.797	3.706	8.656	4.104
4	0	4.456	8.991	4.158	8.845	8.821	7.983	3.724	8.848	4.109
5	0	4.505	9.502	4.178	9.322	9.292	8.446	3.772	9.325	4.124
6	0	4.511	9.563	4.180	9.378	9.347	8.500	3.778	9.381	4.126
7	0	4.527	9.725	4.187	9.532	9.499	8.649	3.793	9.535	4.131
8	0	4.531	9.751	4.188	9.584	9.556	8.700	3.797	9.586	4.132
9	0	4.550	9.953	4.196	9.767	9.736	8.878	3.816	9.770	4.137
10	0	4.547	9.903	4.195	9.758	9.734	8.869	3.812	9.760	4.136
11	0	4.579	10.238	4.207	10.057	10.027	9.160	3.844	10.060	4.146
12	0	4.591	10.370	4.212	10.173	10.140	9.272	3.856	10.176	4.150
13	0	4.613	10.598	4.221	10.381	10.345	9.474	3.877	10.384	4.156
14	0	4.631	10.784	4.228	10.547	10.508	9.635	3.895	10.551	4.162
15	0	4.618	10.645	4.223	10.434	10.399	9.526	3.882	10.438	4.158
16	0	4.651	10.985	4.236	10.749	10.710	9.832	3.914	10.753	4.168
17	0	4.667	11.156	4.243	10.911	10.870	9.989	3.931	10.915	4.173
18	0	4.633	10.786	4.229	10.599	10.567	9.685	3.897	10.602	4.162
19	0	4.637	10.827	4.231	10.634	10.602	9.719	3.900	10.637	4.164
20	0	4.619	10.624	4.224	10.479	10.455	9.569	3.882	10.481	4.158
21	0	4.688	11.346	4.251	11.135	11.100	10.206	3.950	11.138	4.179
22	0	4.723	11.713	4.265	11.467	11.426	10.529	3.985	11.471	4.190
23	0	4.784	12.320	4.290	12.075	12.034	11.119	4.044	12.079	4.208
24	0	4.775	12.211	4.286	12.000	11.965	11.046	4.034	12.003	4.205
25	0	4.856	13.041	4.318	12.796	12.755	11.819	4.114	12.800	4.229

Table 7-2. Long wave model responses for with breach condition for Year 50

		Station ID							
Event ID	Breach	1	2	3	4	5	6	7	8
26	1	8.014	8.025	8.053	8.036	8.047	8.058	8.079	8.101
27	1	8.577	8.589	8.621	8.601	8.613	8.625	8.650	8.674
28	1	8.763	8.777	8.812	8.790	8.804	8.817	8.845	8.872
29	1	8.942	8.954	8.986	8.966	8.978	8.991	9.015	9.039
30	1	9.442	9.457	9.496	9.472	9.487	9.502	9.532	9.562
31	1	9.501	9.517	9.557	9.532	9.548	9.563	9.594	9.625
32	1	9.661	9.677	9.719	9.693	9.709	9.725	9.757	9.790
33	1	9.695	9.709	9.745	9.723	9.737	9.751	9.779	9.807
34	1	9.891	9.907	9.947	9.922	9.938	9.953	9.984	10.016
35	1	9.854	9.867	9.898	9.879	9.891	9.903	9.927	9.951
36	1	10.177	10.193	10.232	10.208	10.223	10.238	10.268	10.298
37	1	10.305	10.321	10.364	10.337	10.354	10.370	10.403	10.436
38	1	10.525	10.544	10.591	10.562	10.580	10.598	10.634	10.670
39	1	10.705	10.725	10.776	10.745	10.764	10.784	10.823	10.863
40	1	10.575	10.592	10.638	10.610	10.628	10.645	10.680	10.715
41	1	10.907	10.926	10.978	10.946	10.966	10.985	11.025	11.064
42	1	11.075	11.095	11.148	11.116	11.136	11.156	11.197	11.238
43	1	10.724	10.739	10.780	10.755	10.771	10.786	10.818	10.849
44	1	10.763	10.779	10.821	10.795	10.811	10.827	10.859	10.892
45	1	10.575	10.588	10.619	10.600	10.612	10.624	10.648	10.672
46	1	11.275	11.293	11.338	11.310	11.328	11.346	11.381	11.416
47	1	11.631	11.651	11.704	11.672	11.692	11.713	11.753	11.794
48	1	12.239	12.259	12.312	12.279	12.300	12.320	12.361	12.402
49	1	12.140	12.158	12.204	12.176	12.193	12.211	12.246	12.281
50	1	12.960	12.980	13.033	13.000	13.021	13.041	13.082	13.123

Table 7-2. Long wave model responses for with breach condition for Year 50 (continued)

		Station ID							
Event ID	Breach	9	10	11	12	13	14	15	16
26	1	8.112	8.110	8.101	8.014	7.415	7.644	7.465	7.393
27	1	8.686	8.683	8.674	8.577	7.895	8.155	7.952	7.869
28	1	8.886	8.883	8.872	8.763	8.054	8.327	8.114	8.029
29	1	9.051	9.049	9.039	8.942	8.205	8.483	8.265	8.175
30	1	9.577	9.574	9.562	9.442	8.632	8.942	8.700	8.603
31	1	9.640	9.637	9.625	9.501	8.683	8.997	8.752	8.654
32	1	9.806	9.802	9.790	9.661	8.819	9.143	8.890	8.789
33	1	9.821	9.818	9.807	9.695	8.847	9.167	8.916	8.813
34	1	10.031	10.028	10.016	9.891	9.015	9.348	9.088	8.981
35	1	9.963	9.961	9.951	9.854	8.981	9.304	9.050	8.942
36	1	10.313	10.310	10.298	10.177	9.258	9.604	9.333	9.221
37	1	10.452	10.449	10.436	10.305	9.367	9.723	9.445	9.331
38	1	10.688	10.684	10.670	10.525	9.556	9.927	9.637	9.521
39	1	10.883	10.879	10.863	10.705	9.710	10.094	9.795	9.676
40	1	10.733	10.729	10.715	10.575	9.598	9.970	9.679	9.561
41	1	11.084	11.080	11.064	10.907	9.881	10.276	9.968	9.845
42	1	11.259	11.255	11.238	11.075	10.025	10.429	10.114	9.988
43	1	10.865	10.862	10.849	10.724	9.723	10.098	9.804	9.681
44	1	10.908	10.905	10.892	10.763	9.756	10.135	9.838	9.715
45	1	10.684	10.682	10.672	10.575	9.593	9.953	9.670	9.547
46	1	11.433	11.430	11.416	11.275	10.193	10.601	10.281	10.149
47	1	11.815	11.811	11.794	11.631	10.498	10.930	10.592	10.455
48	1	12.423	12.418	12.402	12.239	11.014	11.477	11.115	10.965
49	1	12.299	12.295	12.281	12.140	10.928	11.379	11.025	10.876
50	1	13.144	13.139	13.123	12.960	11.627	12.126	11.735	11.571

Table 7-2. Long wave model responses for with breach condition for Year 50 (continued)

Event ID	Breach	Station ID							
		17	18	19	20	21	22	23	24
26	1	7.402	7.443	7.379	7.338	7.874	7.927	7.971	7.916
27	1	7.879	7.926	7.852	7.805	8.415	8.481	8.529	8.469
28	1	8.040	8.089	8.014	7.966	8.601	8.654	8.708	8.640
29	1	8.186	8.236	8.155	8.105	8.762	8.845	8.894	8.833
30	1	8.615	8.671	8.585	8.529	9.253	9.322	9.382	9.307
31	1	8.667	8.723	8.636	8.580	9.312	9.378	9.440	9.362
32	1	8.803	8.860	8.772	8.714	9.467	9.532	9.596	9.516
33	1	8.825	8.882	8.790	8.732	9.488	9.584	9.639	9.570
34	1	8.994	9.054	8.960	8.900	9.683	9.767	9.829	9.751
35	1	8.952	9.011	8.912	8.853	9.628	9.758	9.806	9.746
36	1	9.233	9.296	9.195	9.132	9.952	10.057	10.117	10.042
37	1	9.345	9.409	9.308	9.243	10.081	10.173	10.239	10.157
38	1	9.536	9.602	9.499	9.433	10.300	10.381	10.453	10.363
39	1	9.692	9.760	9.657	9.588	10.480	10.547	10.626	10.528
40	1	9.575	9.642	9.538	9.471	10.344	10.434	10.505	10.417
41	1	9.861	9.932	9.824	9.753	10.672	10.749	10.828	10.730
42	1	10.005	10.077	9.967	9.895	10.835	10.911	10.993	10.891
43	1	9.694	9.762	9.652	9.583	10.475	10.599	10.661	10.583
44	1	9.728	9.797	9.687	9.618	10.514	10.634	10.698	10.618
45	1	9.557	9.624	9.511	9.444	10.313	10.479	10.527	10.467
46	1	10.164	10.238	10.119	10.045	11.010	11.135	11.205	11.117
47	1	10.472	10.550	10.429	10.351	11.364	11.467	11.549	11.447
48	1	10.983	11.066	10.933	10.849	11.941	12.075	12.157	12.055
49	1	10.891	10.973	10.837	10.754	11.832	12.000	12.070	11.982
50	1	11.588	11.679	11.531	11.440	12.626	12.796	12.878	12.776

Table 7-2. Long wave model responses for with breach condition for Year 50 (continued)

		Station ID							
Event ID	Breach	25	26	27	28	29	30	31	32
26	1	7.916	7.906	7.406	7.993	7.366	7.289	7.388	7.687
27	1	8.469	8.457	7.885	8.553	7.839	7.752	7.864	8.202
28	1	8.640	8.626	8.042	8.736	7.994	7.901	8.019	8.381
29	1	8.833	8.821	8.195	8.918	8.145	8.055	8.174	8.531
30	1	9.307	9.292	8.620	9.412	8.565	8.460	8.594	9.002
31	1	9.362	9.347	8.670	9.471	8.615	8.508	8.644	9.059
32	1	9.516	9.499	8.806	9.628	8.749	8.638	8.778	9.207
33	1	9.570	9.556	8.835	9.667	8.778	8.674	8.811	9.222
34	1	9.751	9.736	9.001	9.860	8.942	8.831	8.975	9.410
35	1	9.746	9.734	8.970	9.830	8.911	8.812	8.950	9.352
36	1	10.042	10.027	9.245	10.147	9.183	9.071	9.219	9.664
37	1	10.157	10.140	9.353	10.272	9.289	9.171	9.325	9.788
38	1	10.363	10.345	9.541	10.489	9.475	9.349	9.510	9.999
39	1	10.528	10.508	9.693	10.666	9.626	9.493	9.660	10.173
40	1	10.417	10.399	9.583	10.540	9.516	9.392	9.553	10.040
41	1	10.730	10.710	9.865	10.867	9.795	9.660	9.831	10.354
42	1	10.891	10.870	10.007	11.034	9.936	9.797	9.973	10.510
43	1	10.583	10.567	9.709	10.692	9.642	9.522	9.683	10.160
44	1	10.618	10.602	9.742	10.730	9.674	9.553	9.715	10.199
45	1	10.467	10.455	9.583	10.551	9.517	9.411	9.563	10.001
46	1	11.117	11.100	10.178	11.240	10.105	9.973	10.148	10.670
47	1	11.447	11.426	10.480	11.590	10.403	10.259	10.445	11.011
48	1	12.055	12.034	10.997	12.198	10.914	10.763	10.962	11.558
49	1	11.982	11.965	10.913	12.105	10.832	10.691	10.884	11.449
50	1	12.776	12.755	11.610	12.919	11.520	11.362	11.575	12.207

Table 7-2. Long wave model responses for with breach condition for Year 50 (concluded)

		Station ID						
Event ID	Breach	33	34	35	36	37	38	39
26	1	7.267	8.058	7.186	7.927	7.906	7.092	6.625
27	1	7.726	8.625	7.635	8.481	8.457	7.629	7.095
28	1	7.876	8.817	7.780	8.654	8.626	7.797	7.250
29	1	8.025	8.991	7.926	8.845	8.821	7.983	7.400
30	1	8.431	9.502	8.322	9.322	9.292	8.446	7.817
31	1	8.479	9.563	8.368	9.378	9.347	8.500	7.867
32	1	8.608	9.725	8.495	9.532	9.499	8.649	8.000
33	1	8.640	9.751	8.526	9.584	9.556	8.700	8.029
34	1	8.798	9.953	8.680	9.767	9.736	8.878	8.192
35	1	8.774	9.903	8.656	9.758	9.734	8.869	8.162
36	1	9.034	10.238	8.910	10.057	10.027	9.160	8.431
37	1	9.136	10.370	9.009	10.173	10.140	9.272	8.537
38	1	9.314	10.598	9.183	10.381	10.345	9.474	8.722
39	1	9.459	10.784	9.324	10.547	10.508	9.635	8.872
40	1	9.355	10.645	9.224	10.434	10.399	9.526	8.763
41	1	9.624	10.985	9.486	10.749	10.710	9.832	9.040
42	1	9.760	11.156	9.619	10.911	10.870	9.989	9.180
43	1	9.481	10.786	9.346	10.599	10.567	9.685	8.887
44	1	9.512	10.827	9.376	10.634	10.602	9.719	8.920
45	1	9.365	10.624	9.233	10.479	10.455	9.569	8.764
46	1	9.930	11.346	9.784	11.135	11.100	10.206	9.348
47	1	10.217	11.713	10.064	11.467	11.426	10.529	9.645
48	1	10.715	12.320	10.550	12.075	12.034	11.119	10.152
49	1	10.639	12.211	10.476	12.000	11.965	11.046	10.070
50	1	11.306	13.041	11.127	12.796	12.755	11.819	10.754

Table 7-2. Long wave model responses for with breach condition for Year 50 (concluded)

Event ID	Breach	Station ID								
		33	34	35	36	37	38	39	40	41
26	1	7.267	8.058	7.186	7.927	7.906	7.927	7.447	7.930	7.235
27	1	7.726	8.625	7.635	8.481	8.457	8.481	7.931	8.483	7.690
28	1	7.876	8.817	7.780	8.654	8.626	8.654	8.090	8.656	7.839
29	1	8.025	8.991	7.926	8.845	8.821	8.845	8.245	8.848	7.986
30	1	8.431	9.502	8.322	9.322	9.292	9.322	8.674	9.325	8.388
31	1	8.479	9.563	8.368	9.378	9.347	9.378	8.726	9.381	8.436
32	1	8.608	9.725	8.495	9.532	9.499	9.532	8.863	9.535	8.564
33	1	8.640	9.751	8.526	9.584	9.556	9.584	8.892	9.586	8.594
34	1	8.798	9.953	8.680	9.767	9.736	9.767	9.061	9.770	8.752
35	1	8.774	9.903	8.656	9.758	9.734	9.758	9.029	9.760	8.725
36	1	9.034	10.238	8.910	10.057	10.027	10.057	9.307	10.060	8.984
37	1	9.136	10.370	9.009	10.173	10.140	10.173	9.416	10.176	9.086
38	1	9.314	10.598	9.183	10.381	10.345	10.381	9.606	10.384	9.263
39	1	9.459	10.784	9.324	10.547	10.508	10.547	9.761	10.551	9.408
40	1	9.355	10.645	9.224	10.434	10.399	10.434	9.649	10.438	9.304
41	1	9.624	10.985	9.486	10.749	10.710	10.749	9.934	10.753	9.571
42	1	9.760	11.156	9.619	10.911	10.870	10.911	10.079	10.915	9.706
43	1	9.481	10.786	9.346	10.599	10.567	10.599	9.777	10.602	9.426
44	1	9.512	10.827	9.376	10.634	10.602	10.634	9.810	10.637	9.457
45	1	9.365	10.624	9.233	10.479	10.455	10.479	9.649	10.481	9.309
46	1	9.930	11.346	9.784	11.135	11.100	11.135	10.251	11.138	9.871
47	1	10.217	11.713	10.064	11.467	11.426	11.467	10.557	11.471	10.157
48	1	10.715	12.320	10.550	12.075	12.034	12.075	11.080	12.079	10.649
49	1	10.639	12.211	10.476	12.000	11.965	12.000	10.995	12.003	10.572
50	1	11.306	13.041	11.127	12.796	12.755	12.796	11.700	12.800	11.233

Table 7-3. Conditions in Year 50 Bathymetry sensitivity long wave model simulations

Test ID	Year 50 Bathymetry	Tidal BC Mean water level relative to Year 0 (ft)
B1T1	Based on NRC curve I (Figure 7-1)	0.72
B3T1	Based on NRC curve III (Figure 7-2)	0.72
B3T3	Based on NRC curve III (Figure 7-2)	2.13

Table 7-4 Sensitivity of Peak Elevations to Bathymetry and Analysis Method

Test ID	Year 50 Bathymetry	Tidal BC	Location				
			Ocean BC	Presidio	Dumbarton Bridge	Pond A2 outboard	Mouth Coyote Creek
B1T1	NRC I	NRC I	8.9	9.14	10.62	10.78	10.62
B3T1	NRC III	NRC I	8.9	9.15	10.59	10.73	10.67
B3T3	NRC III	NRC III	10.31	10.58	12.02	12.13	12.18
B3T3-1.41	NRC III	NRC III	8.9	9.17	10.61	10.72	10.77
MC-B1T1	NRC I	NRC I	n/a	10.5	12.16	12.2	12.32
MC-B0T0	Year 0	Year 0	n/a	10.5	12.16	12.2	12.35
Average NRC I				9.15	10.61	10.74	10.69
Std Dev NRC I				0.02	0.02	0.03	0.08
Average NRC III				10.53	12.11	12.18	12.28
Std Dev NRC III				0.05	0.08	0.04	0.09

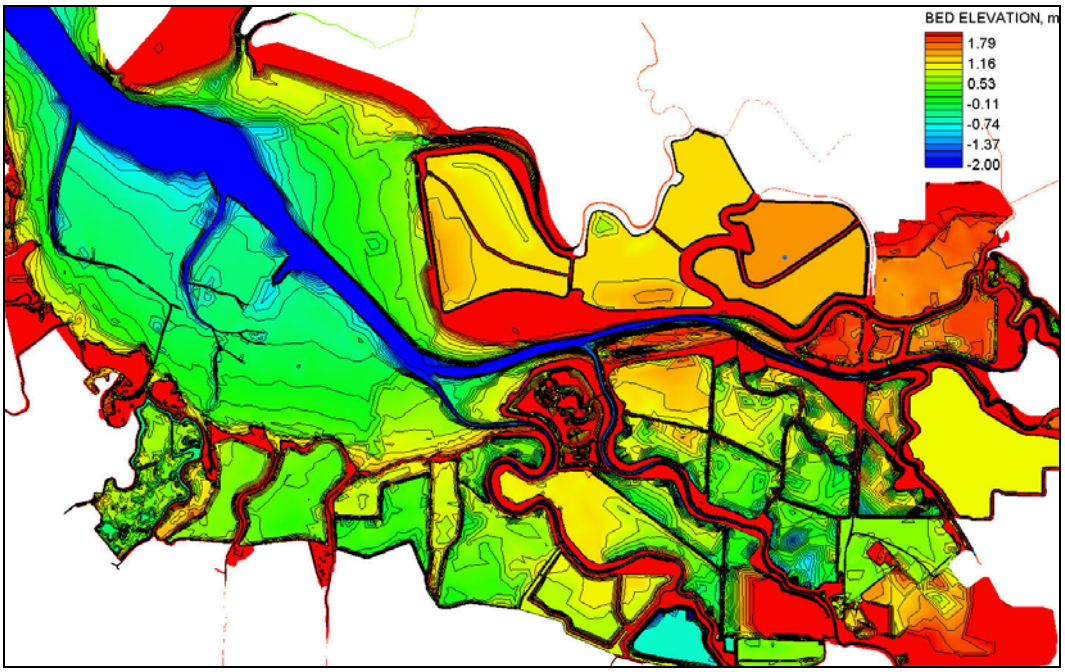

Figure 7-1. Year 50 bathymetry based on NRC curve I for sea level rise (from Brown, 2010).

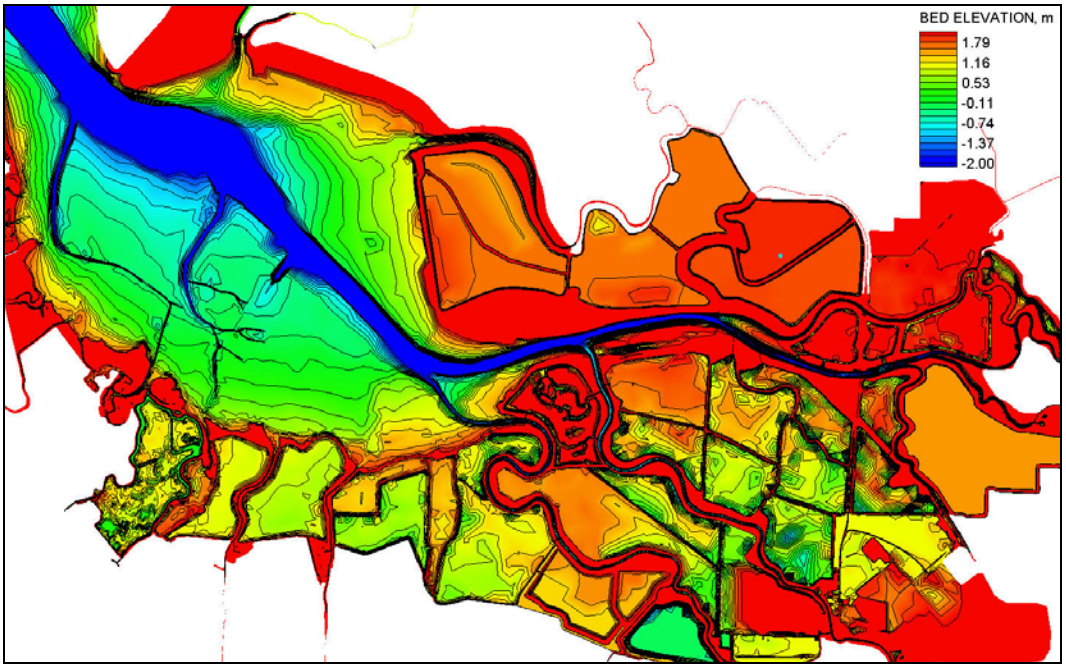

Figure 7-2. Year 50 bathymetry based on NRC curve III for sea level rise (from Brown, 2010).

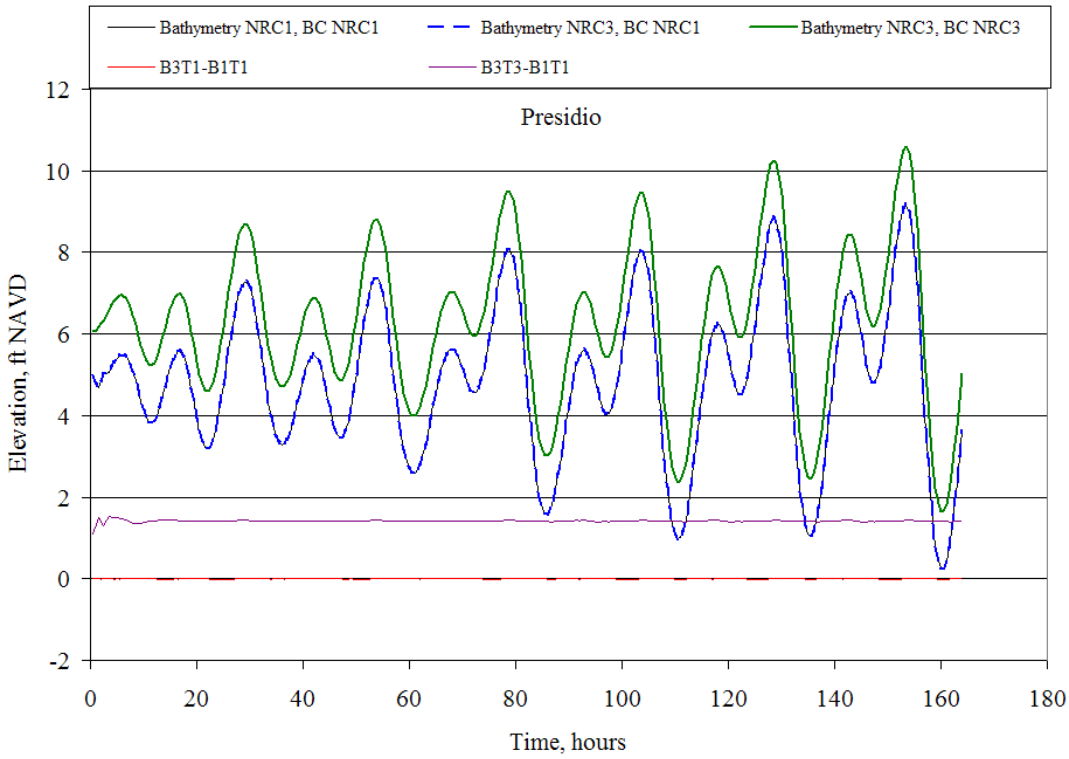

Figure 7-3. Effects of bathymetric sensitivity test with NRC curve III on flood event of January 1983 at the Presidio.

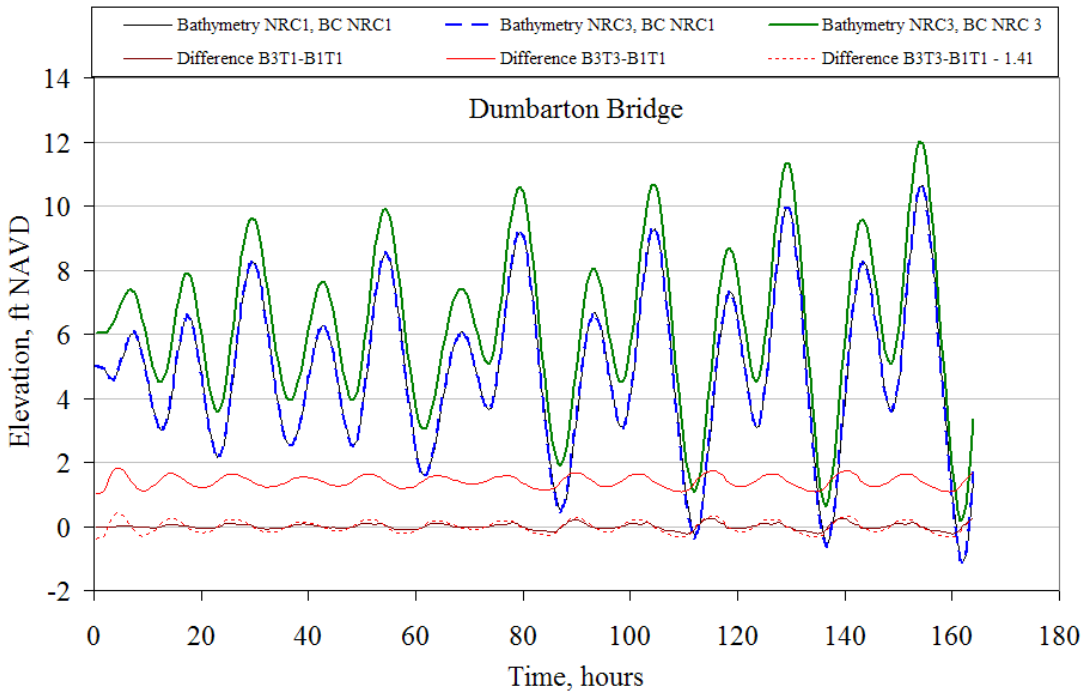

Figure 7-4. Effects of bathymetric sensitivity test with NRC curve III on flood event of January 1983 at Dumbarton Bridge.

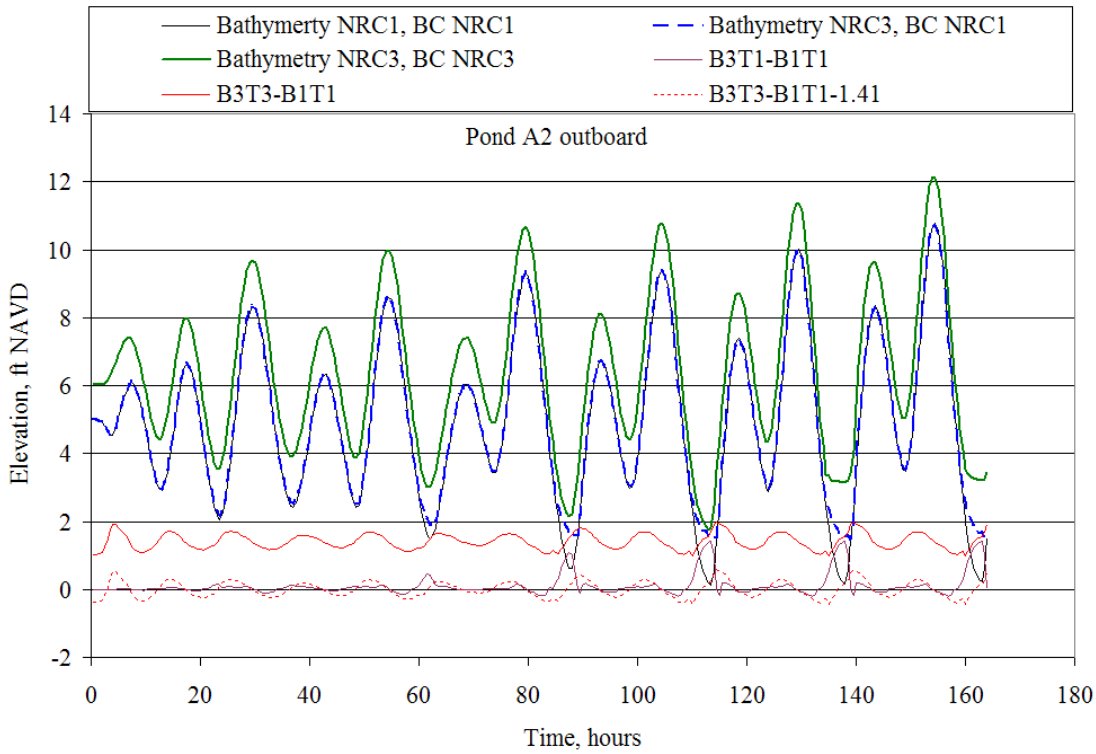

Figure 7-5. Effects of bathymetric sensitivity test with NRC curve III on flood event of January 1983 at bay side of Pond A2 outboard levee.

9 Summary

The long wave model developed for the SSFBSS supports the project goals of determining the statistical uncertainties of predicted flood potential by generating a database of simulations that can be flexible in allowing for an interpolated response for random storm parameters from the database.

The sensitivity analysis of the effects of projected Year 50 bathymetry suggests that the uncertainty in water levels for the period of record storm (January 1983) are within 0.1 ft throughout the project area. This finding validates the use of the NRC curve I sea level rise in estimating the bathymetry for Year 50 as a reasonable approach.

References

Brown, G. L., 2010 (in preparation), "Sediment Analysis and Modeling for the South San Francisco Bay Shoreline Study," U.S. Army ERDC, Vicksburg, MS.

CEERDC, September 2006, "South San Francisco Bay Shoreline Study (SSFBSS) Technical Approach and Scope of Work."

Collins, J. Ian, Robert Dean, and David Divoky, October 2006, "South San Francisco Bay Shoreline Study; Review of Proposed Technical Approach," Review comments by board of consultants.

Christensen, B. A. (1970) Manning's n For Cast-In-Place Concrete Pipe; Discussions by Bent A. Christensen, and R. Sakthivadivel, S. Seetharaman and M.V. Somasundaram, Journal of the Hydraulics Division, Proceedings of the American Society of Civil Engineers, Vol. 96, No. HY3.

Choy, Steve (SCVWD). Email to Anne K. Sturm dated 6 March 2007. Subject: Need Permanente Creek data.

Chung, Christy (SCVWD). Email to Eric Zhang dated 20 November 2006. Subject: Alviso Slough.

Donnell, Barbara P., Letter, Joseph V., McAnally, W. H., and others, "Users Guide for RMA2 Version 4.5," [09 May] 2008, [http://chl.wes.army.mil/software/tabs/docs.htp].

Dyer, Beth (SCVWD). October 2006. CD-R and DVD w/ Guadalupe River contour map and profile in vicinity of Gold St. Bridge.

Environmental Data Solutions. February 2007. Cross-section survey data for Inner and Outer Charleston Slough. Survey performed for City of Mountain View.

Foxgrover, A.C. and Jaffe, B.E., 2005, South San Francisco Bay 2004 topographic lidar survey: Data overview and preliminary quality assessment, U.S. Geological Survey Open-File Report OFR-2005-1284 [URL: http://pubs.usgs.gov/of/2005/1284/]

Foxgrover, A.C., Jaffe, B.E., Hovis, G.T., Martin, C.A., Hubbard, J.R., Samant, M.R., and Sullivan, S.M., 2007, 2005 Hydrographic Survey of South San Francisco Bay, California, U.S. Geological Survey Open-File Report 2007-1169, 113 p. [URL: http://pubs.usgs.gov/of/2007/1169]

Knuuti, Kevin, May 1995, "Extreme Tide Prediction for San Francisco Bay," Hydraulic Engineering Laboratory, University of California, Berkley, CA.

Kulpa, James (Environmental Data Solutions). Email to Anne K. Sturm dated 3 Aug 2006. Subject: SBSP2004DataCollection.

Letter, J. V., Jr., 2010 (in preparation), "Coastal Flooding Uncertainty Analysis for South San Francisco Bay Shoreline Study: without Project Conditions," U.S. Army ERDC, Vicksburg, MS.

Mark Thomas & Company, Inc. 16 September 2005. As-built Plans (Electronic CAD format) for Matadero Creek PAFB to Alma Street. Prepared for SCVWD.

Moffatt & Nichol Engineers, March 2004, Urban Levee Flood Management Requirements - South Bay Salt Pond Restoration Project, prepared for California State Coastal Conservancy

Moffatt & Nichol Engineers, February 2005, Summary of South San Francisco Bay Winter-Spring 2004 Interim Monitoring Data - South Bay Salt Pond Restoration Project, prepared for California State Coastal Conservancy.

National Resources Council (1987) "Responding to Changes in Sea-Level: Engineering Implications" National Academy Press, Washington.

Philip Williams and Associates, Ltd, Memorandum dated October 25, 2006, Subject: Bair Island Survey Data, from Jeremy Lowe.

Philip Williams and Associates, Ltd. 30 June 2000. Bair Island Restoration and Management Plan: Existing Hydrologic Conditions Assessment. Prepared for H.T. Harvey & Associates.

Wu, Frank and John Cheng, Memorandum for Record, "Tidal Analysis ..." in preparation.

Roig, Lisa C., (1995) "Mathematical Theory and Numerical Methods for the Modeling of Wetland Hydraulics", in Water Resources Engineering, Proceedings of the 1995 First International Conference San Antonio, Texas, August 14 - 18, 1995, ASCE, New York, pp. 249-253.

Santa Clara Valley Water District (SCVWD), 20 January 2000. MS Word file projinfo.doc: Project name: Palo Alto Flood Basin / Baylands. Job number 1028.

Santa Clara Valley Water District (SCVWD), plot date 7 December 2004. Guadalupe River Post Construction X-sections. Hard copy CAD drawings, cross-sections 7+050 to 8+880.

Santa Clara Valley Water District (SCVWD), plot date 26 January 2005. Guadalupe River Post Construction X-sections. Hard copy CAD drawings, cross-sections 8+820 to 14+430.

Santa Clara Valley Water District (SCVWD), plot date 17 February 2005. Guadalupe River Post Construction X-sections. Hard copy CAD drawings, cross-sections 6+570 to 6+780.

Santa Clara Valley Water District (SCVWD), plot date 3 March 2005. Guadalupe River Post Construction X-sections. Hard copy CAD drawings, cross-sections 14+460 to 17+430.

Schaaf & Wheeler Consulting Civil Engineers. 18 October 2002. SCVWD Matadero/Barron Creeks Long-Term Remediation Planning Study Final Engineer's Report. Project No. 102109. Prepared for SCVWD.

Siegel, Stuart and Roger Leventhal. Memorandum dated January 9, 2006, Subject: Update to Pond Bottom Elevations and Tide Heights Based on District December 2005 Confirmation Survey, Island Ponds Restoration Project. Memo to: Ngoc Nguyen and Clyde Morris.

Smagorinsky, J., "General Circulation Experiments with the Primitive Equations", Monthly Weather Review, Vol. 93, 1963, pp. 99-165

Takekawa, J. Y., A. K. Miles, D. H. Schoellhamer, B. Jaffe, N. D. Athearn, S. E. Spring, G. G. Shellenbarger, M.K. Saiki, F. Mejia, and M. A. Lionberger, South Bay Salt Ponds Restoration Project, Short-term Data Needs, 2003-2005 Final Report,

Towill, Inc. 1999. Electronic CAD File: "Topographic Map of Palo Alto Tidal Basin for MacKay & Somps." Photogrammetric survey, date of photography: 2 April 1999.

Tucker, Thomas (Tucker & Associates). 3 August 2006. Teleconference: 2004 Moffatt & Nichol Engineers Channel Transect survey.

Tucker & Associates. 27 July 2004. Moffatt Nichol-Coastal Conservancy South Bay Salt Pond Restoration Project Survey Report.

U.S. Army Corps of Engineers District, San Francisco. October 1984, “San Francisco Bay: Tidal Stage and Frequency Study, “San Francisco, CA.

U.S. Army Corps of Engineers, 2006, “Planning: Risk Analysis for Flood Damage Reduction Studies,” Engineer Regulation 1105-2-101, U.S. Army Corps of Engineers, Washington, D.C.

U. S. Fish & Wildlife Service (USFWS), Don Edwards National Wildlife Refuge, and Santa Clara Valley Water District. 2006. Restoration and Mitigation Monitoring Plan for the Island Ponds Restoration Project.

Appendix A: The TABS-MDS System

TABS-MDS is a collection of generalized computer programs and utility codes integrated into a numerical modeling system. TABS-MDS is capable of one-, two-, and/or three-dimensional computations; however, only the one- and two-dimensional vertically averaged capability will be discussed in this summary. The system is used for studying hydrodynamics, sedimentation, and transport problems in rivers, reservoirs, bays, and estuaries. A schematic representation of the system is shown in Figure A1. It can be used either as a stand-alone solution technique or as a step in the hybrid modeling approach. The basic concept is to calculate water-surface elevations, current patterns, sediment erosion, transport and deposition, the resulting bed surface elevations, and the feedback to hydraulics. Existing and proposed geometry can be analyzed to determine the impact on sedimentation of project designs and to determine the impact of project designs on salinity and on the stream system. The system is described in detail by Thomas and McAnally (1985).

The three basic 2D depth-averaged components of the system are as follows:

a. "A Two-Dimensional Model for Free Surface Flows," RMA2.
b. "Sediment Transport in Unsteady 2-Dimensional Flows, Horizontal Plane," SED2D.
c. "Two-Dimensional Finite Element Program for Water Quality," RMA4.

The U.S. Army Engineer Research and Development Center, Coastal and Hydraulics Laboratory, developed and maintains the TABS-MDS system.

RMA2 is a finite element solution of the Reynolds form of the Navier-Stokes equations for turbulent flows. Friction is calculated with Manning's equation and eddy viscosity coefficients are used to define the turbulent exchanges. A velocity form of the basic equation is used with side boundaries treated as either slip or static. The model has a marsh porosity option as well as the ability to automatically perform wetting and drying. Boundary conditions may be water-surface elevations, velocities, discharges, or tidal radiation.

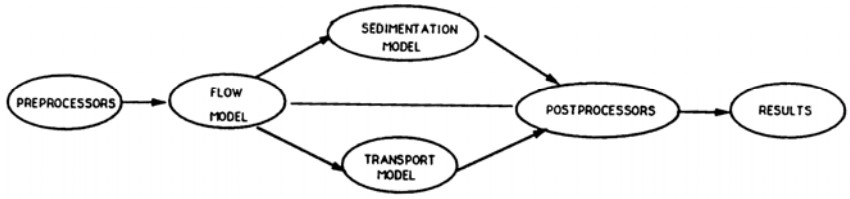

Figure A1. TABS-MD schematic

The sedimentation model, SED2D, solves the convection-diffusion equation with bed source-sink terms. These terms are structured for either sand or cohesive sediments. The Ackers-White (1973) procedure is used to calculate a sediment transport potential for the sands from which the actual transport is calculated based on availability. Clay erosion is based on work by Partheniades (1962) and Ariathurai and the deposition of clay used Krone's equations (Ariathurai, MacArthur, and Krone 1977). Deposited material forms layers and bookkeeping allows up to 10 layers at each node for maintaining separate material types, deposit thickness, and age. The code uses the same mesh as RMA2.

Consistent transport calculations including salinity are made under RMA4 using a form of the convective-diffusion equation which has general source-sink terms. Up to six conservative substances or substances requiring a decay term can be routed. The code uses the same mesh as RMA2. The model accommodates a mixing zone outside of the model boundaries for estimation of reentrainment.

Pre- and Post Processing and Analysis of TABS-MDS Models

The Surface Water Modeling System (SMS) is a comprehensive graphical user environment for performing model conceptualizations; mesh generator, statistical interpretation, and visual examination of surface water model simulations.

SMS is a pre- and post-processor for surface water modeling and analysis in shallow open water areas such as rivers, bays, and estuaries. It includes two-dimensional finite element, two-dimensional finite difference, three-dimensional finite element and one-dimensional step backwater modeling tools. Interfaces specifically designed to facilitate the utilization of several numerical models comprise the modules of SMS. Supported models include

the USACE-WES supported TABS-MD (GFGEN, RMA2, RMA4, RMA10, SED2D-WES).

Each TABS-MDS model is designed to address a specific class of problem. RMA2 calculate hydrodynamic data such as water surface elevations and flow velocities. RMA4 tracks contaminant migration, and SED20 calculates suspended sediment concentrations, erosion and deposition. The models support both steady-state and dynamic analyses.

The finite element mesh or cross section entities, along with associated boundary conditions necessary for analysis, are created within SMS and then saved to model-specific files. These files are used as input to the hydrodynamic, contaminant migration, and sediment transport analysis engines. The numerical models create solution files that contain the water surface elevations, flow velocities, contaminant concentrations, sediment concentrations or other functional data at each node, cell, or section.

These files are then used to perform the analyses. Resulting solution files can be read into SMS to generate vector plots, color-shaded contour plots, time-history diagrams, and solution animation sequences.

Finite Element Modeling

The TABS-MDS numerical models employ the finite element method to solve the governing equations. To help those who are unfamiliar with the method to better understand the system, a brief description of the method is given here.

The finite element method approximates a solution to governing equations by dividing the area of interest into smaller sub areas, which are called elements. The dependent variables (e.g., water-surface elevations or sediment concentrations) are approximated over each element by continuous functions which interpolate based on unknown point (node) values of the variables. An error, defined as the deviation of the governing equations using the approximate solution from the equation using the correct solution, is minimized. Then, when boundary conditions are imposed, a set of solvable simultaneous equations is created. The solution is continuous over the area of interest.

In one-dimensional problems, elements are line segments. In two-dimensional problems, the elements are polygons, either triangles or quadrilaterals. Nodes are located on the edges of elements and occasionally inside the elements. The interpolating functions may be linear or higher order polynomials. Figure A2 illustrates a quadrilateral element with eight nodes and a linear solution surface where F is the interpolating function.

Most water resource applications of the finite element method use the Galerkin method of weighted residuals to minimize error. In this method the residual, the local error in the equations use of the approximate and solution, is weighted by a function that is identical to the interpolating function and then minimized. Minimization results in a set of simultaneous equations in terms of nodal values of the dependent variable (e.g. water-surface elevations or sediment concentration). The time portion of time-dependent problems can be solved by the finite element method, but it is generally more efficient to express derivatives with respect to time in finite difference form.

The Hydrodynamic Model, RMA2

Applications

RMA-2 is designed for far-field problems in which vertical accelerations are negligible and the velocity vectors at a node generally point in the same directions over the entire depth of the water column at any instant of time. It expects a vertically homogeneous fluid with a free surface. The model will define the response to a specified horizontally inhomogeneous fluid. Both steady and unsteady state problems can be analyzed. A surface wind stress can be imposed and the effects of the earth's rotation (Coriolis effect) can be included.

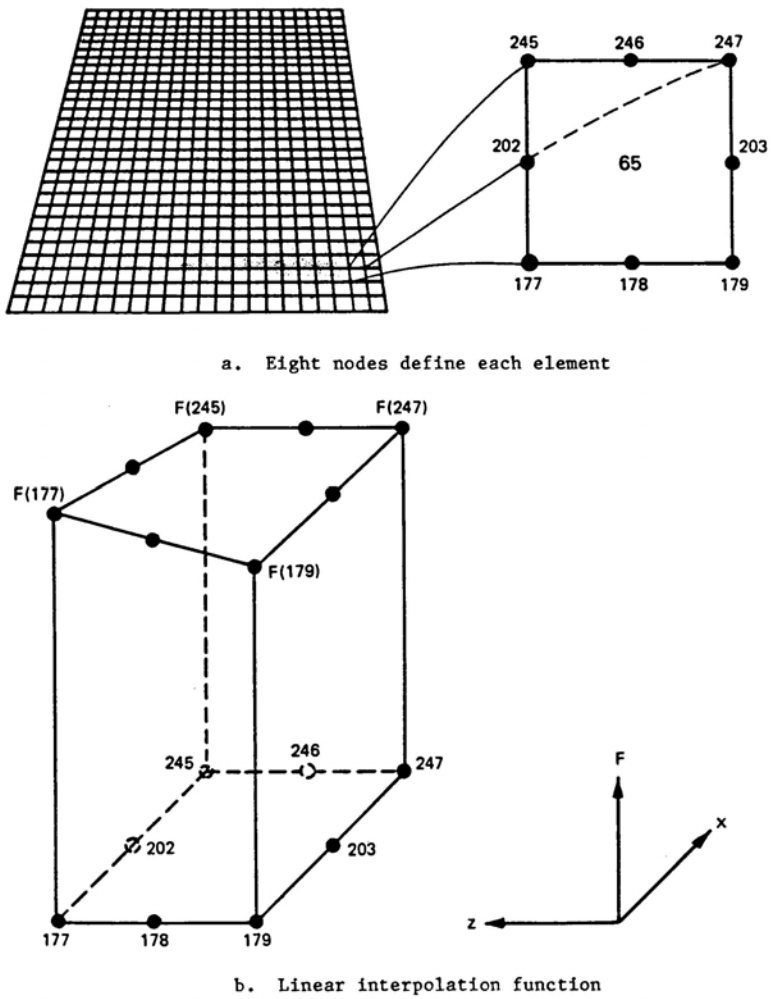

Figure A2. Two-dimensional finite element mesh

RMA2 has been applied to calculate water levels and flow distribution around islands; flow at bridges having one or more relief openings, in contracting and expanding reaches, into and out of off-channel hydropower plants, at river junctions, and into and out of pumping plant channels; circulation and transport in water-bodies with wetlands; and general water levels and flow patterns in rivers, reservoirs, and estuaries.

Limitations

RMA2 is not designed for near-field problems where flow structure interactions (such as vortices, vibrations, or vertical accelerations) are of

interest. Areas of vertically stratified flow are beyond this program's capability unless it is used in a hybrid modeling approach. It is two-dimensional in the horizontal plane, and zones where the bottom current is in a different direction from the surface current must be analyzed with considerable subjective judgment. It is a free-surface calculation for sub critical flow problems.

Governing equations

The generalized computer program RMA2 solves the depth-integrated equations of fluid mass and momentum conservation in two horizontal directions. The form of the solved equations is

$$h\frac{\partial u}{\partial t} + hu\frac{\partial u}{\partial x} + hv\frac{\partial u}{\partial y} - \frac{h}{\rho}\left(\varepsilon_{xx}\frac{\partial^2 u}{\partial x^2} + \varepsilon_{xy}\frac{\partial^2 u}{\partial_y{}^2}\right) + gh\left(\frac{\partial a}{\partial x} + \frac{\partial h}{\partial x}\right) + \frac{gun^2}{\left(1.486h^{1/6}\right)^2}\left(u^2 + v^2\right)^{1/2} - \zeta\, V_a^2 \cos\psi - 2h\omega v \sin\phi = 0 \qquad (A1)$$

$$h\frac{\partial v}{\partial t} + hu\frac{\partial v}{\partial x} + hv\frac{\partial v}{\partial y} - \frac{h}{\rho}\left(\varepsilon_{yx}\frac{\partial^2 v}{\partial x^2} + \varepsilon_{yy}\frac{\partial^2 v}{\partial y^2}\right) + gh\left(\frac{\partial a}{\partial y} + \frac{\partial h}{\partial y}\right) + \frac{gvn^2}{\left(1.486h^{1/6}\right)^2}\left(u^2 + v^2\right)^{1/2} - \zeta\, V_a^2 \sin\psi + 2\omega\, hu \sin\phi + 0 \qquad (A2)$$

$$\frac{\partial h}{\partial t} + h\left(\frac{\partial u}{\partial x} + \frac{\partial v}{\partial y}\right) + u\frac{\partial h}{\partial x} + v\frac{\partial h}{\partial y} = 0 \qquad (A3)$$

where

h	=	depth
u,v	=	x and y direction velocities, respectively
x,y,t	=	Cartesian coordinates and time
ρ	=	density of fluid
ε	=	eddy viscosity coefficient, for xx = normal direction on x-axis surface; yy= normal direction on y-axis surface; xy and yx = shear direction on each surface
g	=	acceleration due to gravity
a	=	elevation of bottom

n	=	Manning's n value
1.486	=	conversion from SI (metric) to non-SI units
ζ	=	empirical wind shear coefficient
V_a	=	wind speed
ψ	=	wind direction
ω	=	rate of earth's angular rotation
ϕ	=	local latitude

Equations A1, A2, and A3 are solved by the finite element method using Galerkin weighted residuals. The elements may be one-dimensional lines or two-dimensional quadrilaterals or triangles and may have curved (parabolic) sides. The shape functions are quadratic for velocity and linear for depth. Integration in space is performed by Gaussian integration. Derivatives in time are replaced by a nonlinear finite difference approximation. Variables are assumed to vary over each time interval in the form

$$f(t) = f(0) + at + bt^c \quad t_o \leq t \angle t_0 + \Delta t \qquad (A4)$$

which is differentiated with respect to time, and cast in finite difference form. Letters a, b, and c are constants. It has been found by experiment that the best value for c is 1.5 (Norton and King 1977).

The solution is fully implicit and the set of simultaneous equations is solved by Newton-Raphson nonlinear iteration.

References

Ackers, P., and White, W. R. 1973. (Nov). Sediment Transport: New Approach and Analysis," *Journal, Hydraulics Division, American Society of Civil Engineers*, Vol 99, No. HY-11, pp 2041-2060.

Ariathurai, R., MacArthur, R. D., and Krone, R. C. 1977 (Oct). "Mathematical Model of Estuarial Sediment Transport," Technical Report D-77-12, U.S. Army Engineer Waterways Experiment Station, Vicksburg, MS.

King, Ian P., and Richard Rachiele, 1989. "Program Documentation: A Two Dimensional Water Quality Model; Version 3.0", Resource Management Associates, Laffayette, CA.

Krone, R. B. 1962. "Flume Studies of Transport of Sediment in Estuarial Shoaling Processes," Final Report, Hydraulics Engineering Research Laboratory, University of California, Berkeley, CA.

Norton, W. R., and King, I. P. 1977 (Feb). "Operating Instructions for the Computer Program," Resource Management Associates, Lafayette, CA.

Partheniades, E. 1962. "A Study of Erosion and Deposition of Cohesive Soils in Salt Water," Ph.D. Dissertation, University of California, Berkeley, CA.

Smagorinsky, J., "General Circulation Experiments with the Primitive Equations", Monthly Weather Review, Vol. 93, 1963, pp. 99-165

Swart, D. H. 1976 (Sep). "Coastal Sediment Transport, Computation of Longshore Transport," R968, Part 1, Delft Hydraulics Laboratory, The Netherlands.

Thomas, W. A., and McAnally, W. H., Jr. 1985 (Aug). "User's Manual for the Generalized Computer Program System; Open-Channel Flow and Sedimentation, Main Text and Appendices A through O," Instruction Report, U.S. Army Engineer Waterways Experiment Station, Vicksburg, MS.

White, W. R., Milli, H., and Crabbe, A. D. 1975. "Sediment Transport Theories: An Appraisal of Available Methods," Report Int 119, Vols 1 and 2, Hydraulics Research Station, Wallingford, England.

NOTE: An annotated Bibliography of selected TABS-MD applications is available at:

HPPT://CHL.WES.ARMY.MIL/SOFTWARE/TABS/DOCS.HLP.